The Consultative Committee for Space Data Systems

Draft Report Concerning
Space Data System Standards

SCCC—SUMMARY OF DEFINITION AND PERFORMANCE

DRAFT INFORMATIONAL REPORT

CCSDS 130.11-G-1.1

DRAFT GREEN BOOK

January 2023

AUTHORITY

Issue:	Draft Green Book, Issue 1.1
Date:	January 2023
Location:	Not Applicable

(WHEN THIS INFORMATIONAL REPORT IS FINALIZED, IT WILL CONTAIN THE FOLLOWING STATEMENT OF AUTHORITY:)

This document has been approved for publication by the Management Council of the Consultative Committee for Space Data Systems (CCSDS) and reflects the consensus of technical working group experts from CCSDS Member Agencies. The procedure for review and authorization of CCSDS Reports is detailed in *Organization and Processes for the Consultative Committee for Space Data Systems* (CCSDS A02.1-Y-4).

This document is published and maintained by:

CCSDS Secretariat
National Aeronautics and Space Administration
Washington, DC, USA
E-mail: secretariat@mailman.ccsds.org

FOREWORD

Through the process of normal evolution, it is expected that expansion, deletion, or modification of this document may occur. This Report is therefore subject to CCSDS document management and change control procedures, which are defined in *Organization and Processes for the Consultative Committee for Space Data Systems* (CCSDS A02.1-Y-4). Current versions of CCSDS documents are maintained at the CCSDS Web site:

http://www.ccsds.org/

Questions relating to the contents or status of this document should be sent to the CCSDS Secretariat at the e-mail address indicated on page i.

At time of publication, the active Member and Observer Agencies of the CCSDS were:

Member Agencies

- Agenzia Spaziale Italiana (ASI)/Italy.
- Canadian Space Agency (CSA)/Canada.
- Centre National d'Etudes Spatiales (CNES)/France.
- China National Space Administration (CNSA)/People's Republic of China.
- Deutsches Zentrum für Luft- und Raumfahrt (DLR)/Germany.
- European Space Agency (ESA)/Europe.
- Federal Space Agency (FSA)/Russian Federation.
- Instituto Nacional de Pesquisas Espaciais (INPE)/Brazil.
- Japan Aerospace Exploration Agency (JAXA)/Japan.
- National Aeronautics and Space Administration (NASA)/USA.
- UK Space Agency/United Kingdom.

Observer Agencies

- Austrian Space Agency (ASA)/Austria.
- Belgian Federal Science Policy Office (BFSPO)/Belgium.
- Central Research Institute of Machine Building (TsNIIMash)/Russian Federation.
- China Satellite Launch and Tracking Control General, Beijing Institute of Tracking and Telecommunications Technology (CLTC/BITTT)/China.
- Chinese Academy of Sciences (CAS)/China.
- China Academy of Space Technology (CAST)/China.
- Commonwealth Scientific and Industrial Research Organization (CSIRO)/Australia.
- Danish National Space Center (DNSC)/Denmark.
- Departamento de Ciência e Tecnologia Aeroespacial (DCTA)/Brazil.
- Electronics and Telecommunications Research Institute (ETRI)/Korea.
- European Organization for the Exploitation of Meteorological Satellites (EUMETSAT)/Europe.
- European Telecommunications Satellite Organization (EUTELSAT)/Europe.
- Geo-Informatics and Space Technology Development Agency (GISTDA)/Thailand.
- Hellenic National Space Committee (HNSC)/Greece.
- Hellenic Space Agency (HSA)/Greece.
- Indian Space Research Organization (ISRO)/India.
- Institute of Space Research (IKI)/Russian Federation.
- Korea Aerospace Research Institute (KARI)/Korea.
- Ministry of Communications (MOC)/Israel.
- Mohammed Bin Rashid Space Centre (MBRSC)/United Arab Emirates.
- National Institute of Information and Communications Technology (NICT)/Japan.
- National Oceanic and Atmospheric Administration (NOAA)/USA.
- National Space Agency of the Republic of Kazakhstan (NSARK)/Kazakhstan.
- National Space Organization (NSPO)/Chinese Taipei.
- Naval Center for Space Technology (NCST)/USA.
- Research Institute for Particle & Nuclear Physics (KFKI)/Hungary.
- Scientific and Technological Research Council of Turkey (TUBITAK)/Turkey.
- South African National Space Agency (SANSA)/Republic of South Africa.
- Space and Upper Atmosphere Research Commission (SUPARCO)/Pakistan.
- Swedish Space Corporation (SSC)/Sweden.
- Swiss Space Office (SSO)/Switzerland.
- United States Geological Survey (USGS)/USA.

DOCUMENT CONTROL

Document	Title	Date	Status
CCSDS 130.11-G-1	SCCC—Summary of Definition and Performance, Informational Report, Issue 1	April 2019	Original issue
CCSDS 130.11-G-1.1	SCCC—Summary of Definition and Performance, Draft Informational Report, Issue 1.1	January 2023	Current draft

CONTENTS

CONTENTS (continued)

Section Page

Figure

CONTENTS (continued)

Figure Page

CONTENTS (continued)

Figure Page

CONTENTS (continued)

Figure Page

CONTENTS (continued)

Figure Page

Table

1 INTRODUCTION

1.1 PURPOSE AND SCOPE

It is expected that a number of Earth Exploration Satellite Service (EESS) missions will carry payloads producing substantial data rates, that is, starting from a few hundred Mb/s. Such missions would benefit from employing transmitters using a state-of-the-art air interface that exploits link adaption, that is, achieves high spectral efficiency by adjusting the modulation and coding to the link budget. For this reason, the Consultative Committee for Space Data Systems (CCSDS) developed a flexible advanced coding and modulation scheme for high rate telemetry applications (reference [1] that offers precisely such benefits by means of powerful Serially Concatenated Convolutional Codes (SCCCs) with modulations belonging to the family of Phase Shift Keying (PSK) and Amplitude PSK (APSK), providing efficiencies up to 5.39 bits per channel symbol.

The goal of this document is to provide additional informative material for reference [1]. Namely, this Green Book includes a tutorial overview of CCSDS specification in reference [1] (aimed at helping first-time readers understand the recommendation) together with performance information supported by illustrations.

This Report is not intended to provide all necessary knowledge for successfully designing telemetry communication links; it provides supporting and descriptive material only: this document is a CCSDS informational report and is therefore not to be taken as a CCSDS Recommended Standard. The actual Recommended Standard is in reference [1]. In the event of any conflict between reference [1] and the material presented herein, the Recommended Standard (reference [1]) is the controlling specification.

In no event will CCSDS or its members be liable for any incidental, consequential, or indirect damages, including any lost profits, lost savings, or loss of data, or for any claim by another party related to errors or omissions in this Report.

This term “PL Frame” (Physical Layer Frame) should be spelled out and introduced here. It’s the first place where it shows up in the text.

1.2 ORGANIZATION

The remainder of this Report is organized as follows: section 2 covers a tutorial overview of CCSDS specification in reference [1] (aimed at helping first-time readers to understand the recommendation), describing its main functions and parameters with a focus on the encoding function, constellations and mapping, PL frame and pilot insertion, and baseband filtering. Section 3 shows the performance of the recommended codes and modulations by means of error rate curves on the linear AWGN channel assuming ideal synchronization. Section 4, then, provides the performance on a nonlinear channel that models nonlinear distortions due to amplification. Section 5 focuses on the synchronization chain and provides a possible reference receiver with details on its performance on the AWGN channel with phase noise and Doppler. In sections 6 and 7, end-to-end performance is provided, and in section 8, conclusions are drawn.

1.3 TERMINOLOGY

The terminology adopted here tries to comply with that adopted in reference [1], but for the reader's convenience, some of the most important terms and symbols are reported here with the aim of avoiding confusion with other meanings sometimes adopted in other documents.

Recommended Standard: Reference to CCSDS Blue Book, CCSDS 131.2-B-1, for which this Green Book provides additional informative material.

information bit: Bit at the input interface of the SCCC encoding block coming from the ACM Mode adaptation (see figure 2-1 in section 2).

encoded bit: Bit at the output interface of the SCCC encoding block and at the input of the PL Framing (see figure 2-1 in section 2).

channel symbol: Modulated symbol at the output of the constellation mapping.

efficiency: Number of information bits per channel symbol, excluding Physical Layer (PL) signaling and pilot insertion. It is not to be confused with the classical spectral efficiency denoting the information rate per Hz of bandwidth adopted, although it is proportional to it.

ModCod: Modulation and coding format.

$\boldsymbol{E_s/N_0}$: Signal-to-noise ratio defined as energy per channel symbol over noise power spectral density.

$\boldsymbol{E_b/N_0}$: Signal-to-noise ratio defined as energy per information bit over noise power spectral density.

$\mathbf{R_{chs}}$: Channel symbol rate, measured in MBaud.

1.4 MATHEMATICAL NOTATION

x	Scalar value (real or complex)
x^*	Complex conjugated
$\mathcal{R}(x)$	Real part
$\lvert x \rvert$	Absolute value
$\angle x$, angle(x)	Phase angle
x_k	Indexed scalar value (e.g., for indexing of signal samples)
$\{x_k\}$	Sequence of the indexed values
$x(t)$	Analog signal (as function of time)
$\oplus$	Sum modulo 2 (XOR)
$E\{\cdot\}$	Expected value

1.5 REFERENCES

The following documents are referenced in this Report. At the time of publication, the editions indicated were valid. All documents are subject to revision, and users of this Report are encouraged to investigate the possibility of applying the most recent editions of the documents indicated below. The CCSDS Secretariat maintains a register of currently valid CCSDS documents.

[1] *Flexible Advanced Coding and Modulation Scheme for High Rate Telemetry Applications*. Issue 1. Recommendation for Space Data System Standards (Blue Book), CCSDS 131.2-B-1. Washington, D.C.: CCSDS, March 2012.

[2] William Ryan and Shu Lin. *Channel Codes: Classical and Modern*. New York: Cambridge UP, 2009.

[3] G. Karam and H. Sari. "A Data Predistortion Technique with Memory for QAM Radio Systems." *IEEE Transactions on Communications* 39, no. 22 (1991): 336–344.

[4] Lei Ding, et al. "A Robust Digital Baseband Predistorter Constructed Using Memory Polynomials." *IEEE Transactions on Communications* 52, no. 1 (2004): 159–165.

[5] F. Gardner. "A BPSK/QPSK Timing-Error Detector for Sampled Receivers." *IEEE Transactions on Communications* 34, no. 5 (1986): 423–429.

[6] R. Scholtz. "Frame Synchronization Techniques." *IEEE Transactions on Communications* 28, no. 8 (1980): 1204–1213.

[7] *Radio Frequency and Modulation Systems—Part 1: Earth Stations and Spacecraft*. Issue 32. Recommendations for Space Data System Standards (Blue Book), CCSDS 401.0-B-32. Washington, D.C.: CCSDS, October 2021.

[8] S. Cioni, G.E. Corazza, and M. Bousquet. "An Analytical Characterization of Maximum Likelihood Signal-to-Noise Ratio Estimation." In *Proceedings of the 2nd International Symposium on Wireless Communication Systems (5–7 September 2005, Siena, Italy)*, 827–830. Piscataway, New Jersey: IEEE, 2005.

[9] Floyd M. Gardner. *Phaselock Techniques*. Hoboken, New Jersey: Wiley, 2005.

[10] E. Casini, R. De Gaudenzi, and A. Ginesi. "DVB-S2 Modem Algorithms Design and Performance over Typical Satellite Channels." *International Journal of Satellite Communications and Networking* 22, no. 3 (16 June 2004): 281–318.

[11] *FleXLink: Multi-Gigabit Data Downlink End-to-End Chain*. White Paper: Maximizing Throughput in Satellite to Ground Transmissions. Backnang, Germany and Tromsø, Norway: Tesat-Spacecom and Kongsberg Spacetec, June 2017.

2 OVERVIEW

2.1 INTRODUCTION

This section provides a quick overview of the coding and modulation scheme of the Recommended Standard. In particular, it aims at providing additional informative material for an easier understanding of the Recommended Standard (reference [1]) and of the results shown later in this report.

This section is not meant to provide a full description of the functions needed at the sending end; it only provides a preliminary overview of some functions. Reference [1] provides the full and detailed description.

2.2 FLEXIBLE ADVANCED CODING AND MODULATION SCHEME

2.2.1 GENERAL

The *Flexible Advanced Coding and Modulation Scheme for High Rate Telemetry Applications* (reference [1]) is designed for space communications links, primarily between spacecraft and ground elements, and is based on SCCCs (see reference [2]) able to support a wide range of spectral efficiency values based on a single coding structure. The frame structure deployed by this standard is agnostic as to the protocol used at higher layer (e.g., AOS or TM) while providing support for maintaining synchronization during transition from one ModCod to another.

An overview of the functional blocks of the architecture at the sending end is shown in figure 2-1.[1] At its input, the system accepts *transfer frames* (from the Data Link protocol sublayer), performs the functions illustrated, and delivers a continuous stream of channel symbols to the PL.

The use of the term “frame” is confusing, since “frames” in CCSDS are link layer artifacts. This is really Physical Layer (PL) frame data structure.

You probably ought to add USLP to AOS & TM, since USLP can support the higher data rates this is aimed at.

MODCOD is used without being introduced as a concept.

[1] Figures 2-1 and 2-2 are taken from reference [1], which should be referred to for normative purposes, and they are copied here for readers’ convenience only.

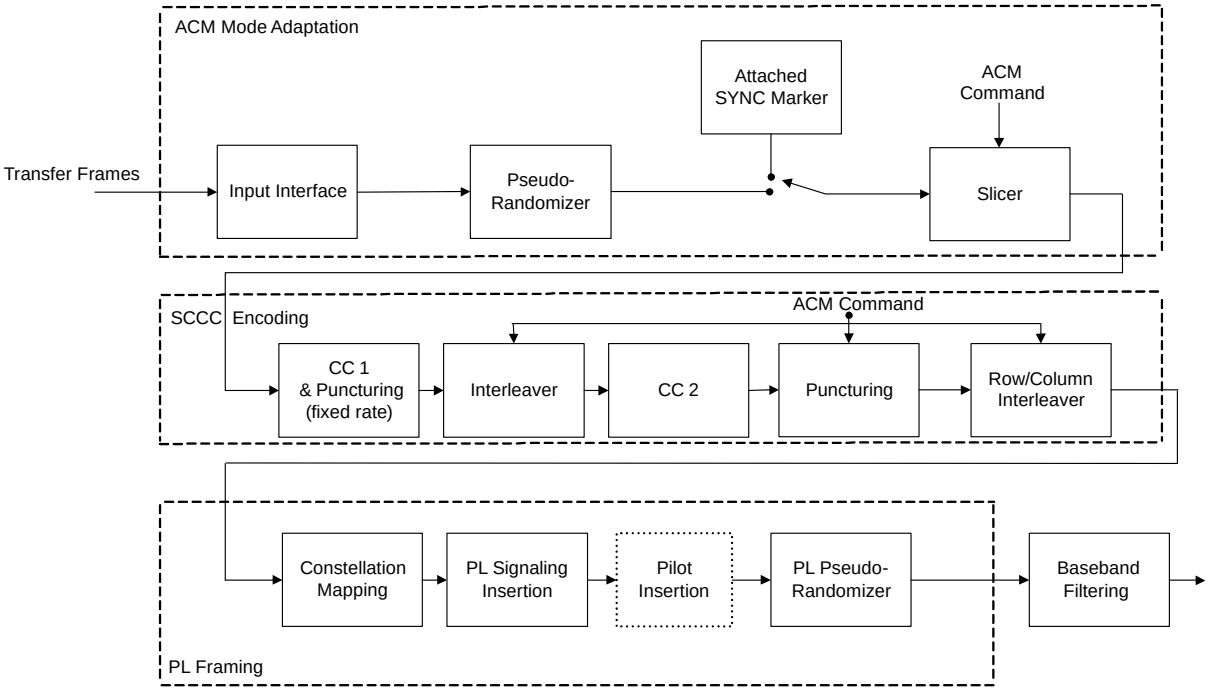

Figure 2-1: Functional Diagram at Sending End[1]

The stream format at different stages of processing is shown in figure 2-2. Attached SYNC Markers (ASMs) are inserted between transfer frames, generating a stream of SMTFs, prior to the slicer block. Then, the stream of SMTFs is sliced into *information blocks* of K bits that are fed to the SCCC encoding function that provides as output *encoded blocks* of N bits. Afterwards, constellation mapping is performed and its output stream is a block of e*ncoded (channel) symbols* belonging to a PSK or APSK modulation, and with block length always equal to 8100 symbols. Finally, PL signaling and (optional) pilot insertion is done, followed by PL pseudo-randomization.

I may be missing something, but I do not see either SMTF in fig 2-1. Where do they appear?

The term "Slicer Block" is a little confusing. Isn't it the "slicer function" and not a "block" of any kind?

How does "ACM format" relate to fig 2-1 or 2-2? They mention "ACM Mode" and "ACM command", but not "ACM Format".

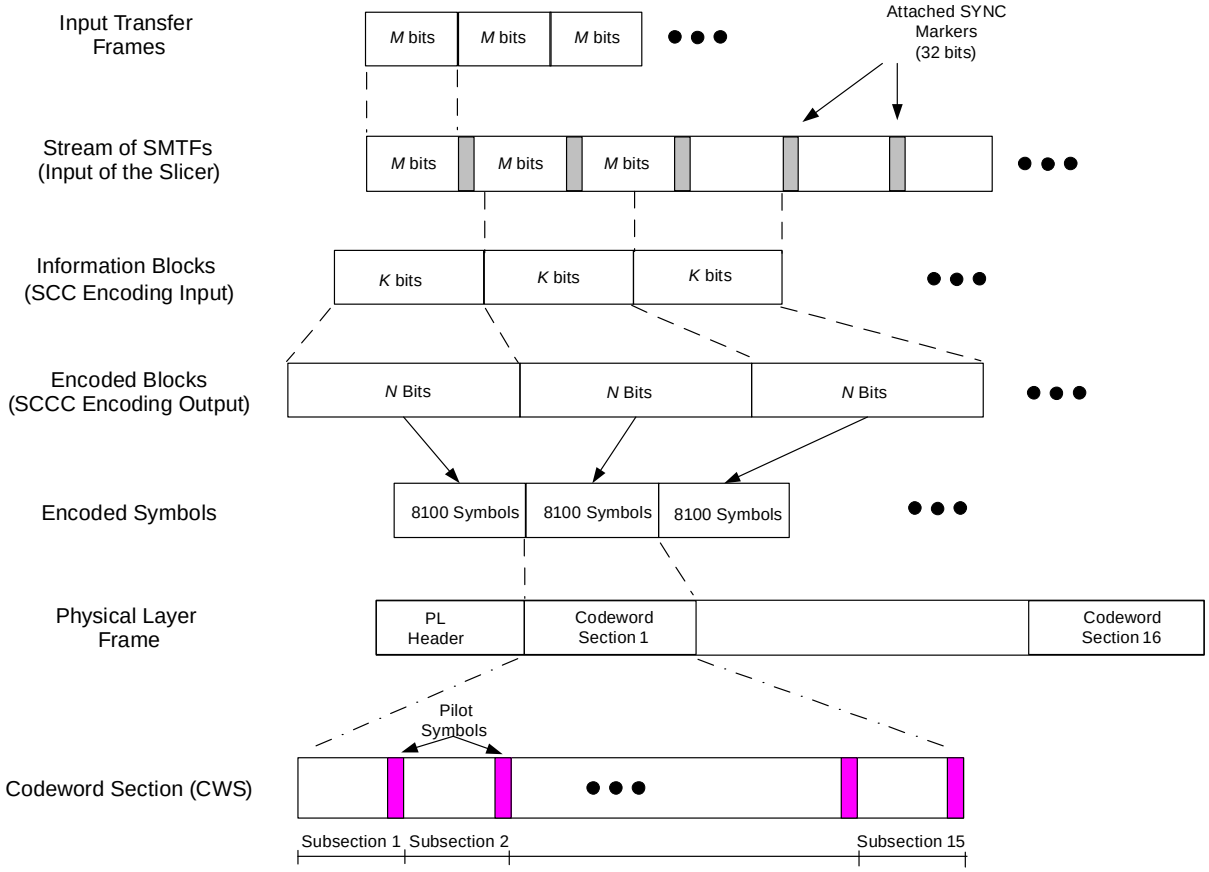

Figure 2-2: Stream Format at Different Stages of Processing[1]

The configuration of all functional blocks is performed by means of a list of *managed parameters*, for which full list and description can be found in section 9 of reference [1]. Among these, the *ACM format* can be seen as the main parameter, and it is identified with an integer number ranging from 1 to 27. By changing the ACM format parameter, the modulation and coding format changes, and thus the spectral efficiency can be selected as required. The ACM format is the only parameter that supports reconfiguration during operation, meaning that it can be changed without interruption or significant delay in data transmission.

Table 2-1[2] shows how the ACM format selection varies some of the main figures of the modulation and encoding scheme. In particular, it varies the constellation cardinality m (number of encoded bits per channel symbol), the length of the information block K, the length of the encoded block N, the *coding rate* defined as K / N (i.e., information bits per encoded bit), and the *efficiency* defined as Km / N (i.e., information bit per channel symbol). It can be seen that the ACM allows one to select five different constellations mappings ranging from 2 to 6 bits per channel symbol. It also allows one to select several coding rates for each constellation; hence the efficiency can change from a minimum of 0.71 bit/channel symbol, to a maximum of 5.39 bit/channel symbol.

[2] As with figures 2-1 and 2-2, table 2-1 is copied from reference [1].

Table 2-1: Modulation Cardinality, Information Block Length, Encoded Block Length, Coding Rate, and Efficiency As Functions of the ACM Format

	ACM	*m*	*K*	*N*	*K*/*N*	Efficiency
QPSK	1	2	5758	16200	0.36	0.71
	2		6958		0.43	0.86
	3		8398		0.52	1.04
	4		9838		0.61	1.21
	5		11278		0.70	1.39
	6		13198		0.81	1.63
8PSK	7	3	11278	24300	0.46	1.39
	8		13198		0.54	1.63
	9		14878		0.61	1.84
	10		17038		0.70	2.10
	11		19198		0.79	2.37
	12		21358		0.88	2.64
16APSK	13	4	19198	32400	0.59	2.37
	14		21358		0.66	2.64
	15		23518		0.73	2.90
	16		25918		0.80	3.20
	17		28318		0.87	3.50
32APSK	18	5	25918	40500	0.64	3.20
	19		28318		0.70	3.50
	20		30958		0.76	3.82
	21		33358		0.82	4.12
	22		35998		0.89	4.44
64APSK	23	6	33358	48600	0.69	4.12
	24		35998		0.74	4.44
	25		38638		0.80	4.77
	26		41038		0.84	5.06
	27		43678		0.90	5.39

For the functional blocks in figure 2-1 (i.e., SCCC encoding, constellation, bit mapping, pseudo-randomization, and baseband filter), the reader should refer to reference [1], in which the normative description for each element is provided. The rest of this section provides additional explanatory details on the PL signaling (as specified in reference [1]).

2.2.2 PL SIGNALING, PILOT INSERTION, AND PSEUDO-RANDOMIZATION

As explained in reference [1] and shown in figure 2-3, 16 *encoded blocks* of 8100 symbols, each of them representing a codeword, are collected into a PL frame structure, to which a header is prepended, with pilot groups inserted periodically (see reference [1] for details).

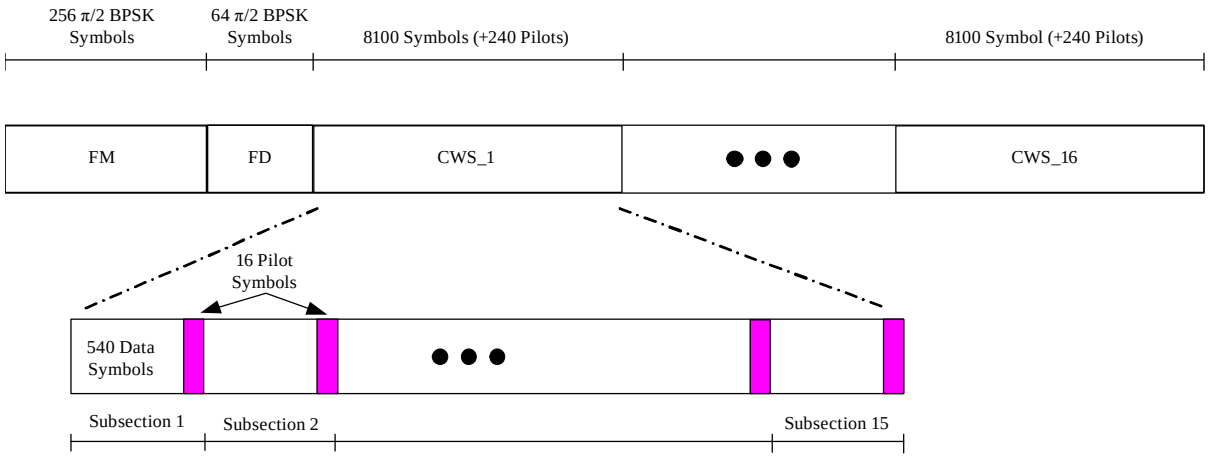

Figure 2-3: PL Frame Structure[3]

The header is composed of a Frame Marker (FM) and a Frame Descriptor (FD), which are mapped to π/2-BPSK symbols, as shown in figure 2-4. The π/2-BPSK transmits on the I and III quadrants bisector for odd bit positions (first, third, etc.) and on the II and IV quadrants bisector for even bit positions. Mathematically, for all bits b_i, i = 1, …, 320 of the FM and FD, the I and Q components of the transmitted channel symbol are

$$I_i = Q_i = \frac{1}{\sqrt{2}}(1 - 2b_i), \qquad \text{if } i = 1,3,5,\ldots$$
$$I_i = -Q_i = -\frac{1}{\sqrt{2}}(1 - 2b_i), \qquad \text{if } i = 2,4,6,\ldots ,$$

which is exactly the same mathematical expression of equation (5) in the Recommended Standard (reference [1]).

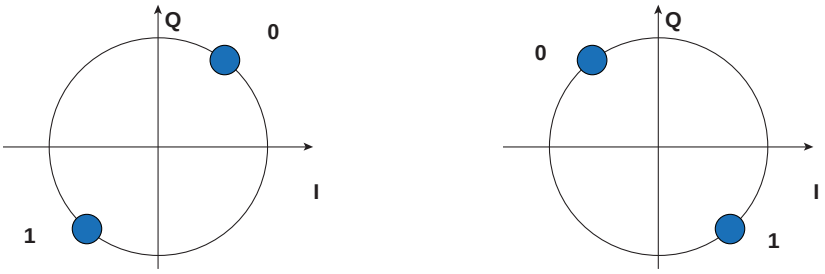

Figure 2-4: π/2-BPSK Constellation at Odd Bit Position (Left) and Even Bit Position (Right)

In case pilots are used (signaled by the proper field in the FD, as described in reference [1]), they are un-modulated QPSK symbols, with I and Q components

$$I_i = Q_i = \frac{1}{\sqrt{2}} .$$

[3] From reference [1].

The overhead of PL signaling is less than 1 percent, and increases up to ~3 percent when pilot insertion is performed.

The resulting frame is finally randomized by means of the PL pseudo-randomization process described in annex C of reference [1]. The randomization process is done by means of a complex multiplication of the channel symbol with a randomization sequence that is uniquely identified by a *code number*, denoted in reference [1] as *n*.

3 PERFORMANCE OF THE RECOMMENDED CODES AND MODULATIONS ON THE AWGN CHANNEL WITH IDEAL SYNCHRONIZATION

3.1 INTRODUCTION

This section reports the performance of the recommended codes and modulations over the linear channel affected by Additive White Gaussian Noise (AWGN). In particular, 3.2 describes the channel model adopted, while 3.3 shows the numerical results derived by means of computer simulations.

3.2 CHANNEL MODEL

The baseband model of the transmitted signal by the sending end is

$$x(t) = \sum_k x_k p(t - kT) \,, \tag{1}$$

where x_k are the transmitted channel symbols at the output of the PL framing function (described in section 2), $p(t)$ is the shaping pulse, and T is the channel symbol duration. The constellation of symbols is properly normalized such that $E\{|x_k|^2\} = E_s$, where E_s denotes the energy per symbol. The shaping pulse is SRRC; hence in ideal conditions it satisfies the intersymbol-interference free condition (the so-called Nyquist condition), that is,

$$\int_{-\infty}^{\infty} p(t)p(t - kT)dt = \begin{cases} 1, & k = 0 \\ 0, & k \neq 0 \end{cases}.$$

The channel is considered affected only by AWGN; hence the baseband model of the received signal is given by

$$y(t) = \sum_k x_k p(t - kT) \; + w(t),$$

where $w(t)$ is white complex Gaussian noise with power spectral density N_0. A sufficient statistic for the computation of the Log-Likelihood Ratios (LLR) is sampled at the output of a matched filter. The received samples after the matched filter read

$$y_k = x_k + w_k \,, \tag{2}$$

where w_k are independent Gaussian random variables with variance equal to N_0. For this discrete-time received signal, the Signal-to-Noise Ratio (SNR) can be expressed as E_s/N_0 or E_b/N_0, where E_b is the energy per information bit. The E_b/N_0 is related to the E_s/N_0 by

$$\frac{E_b}{N_0}\left(\frac{K}{N}\right)m = \frac{E_s}{N_0} \,, \tag{3}$$

where m and K/N are the modulation order (number of bits per channel symbol) and the coding rate, respectively (as defined in section 2).

3.3 NUMERICAL RESULTS

The performance results of the Recommended Standard's modulation and coding scheme has been evaluated over the AWGN channel described in 3.2 by means of computer simulations and under the assumption of ideal synchronization. Clearly, with the AWGN channel model, results are independent of the channel symbol rate and roll-off.

As first results, figures 3-1 and 3-2 show the measured Bit Error Rate (BER) as a function of the E_s/N_0 for all PSK/APSK constellations that are adopted by the various ACM formats in absence of SCCC turbo coding (uncoded). It can be observed that for ACM formats using 16APSK (from 13 to 17) and 32APSK (from 18 to 22), constellations have different performance even when the cardinality is the same, because of the different radii (see table 5-1 of reference [1]).

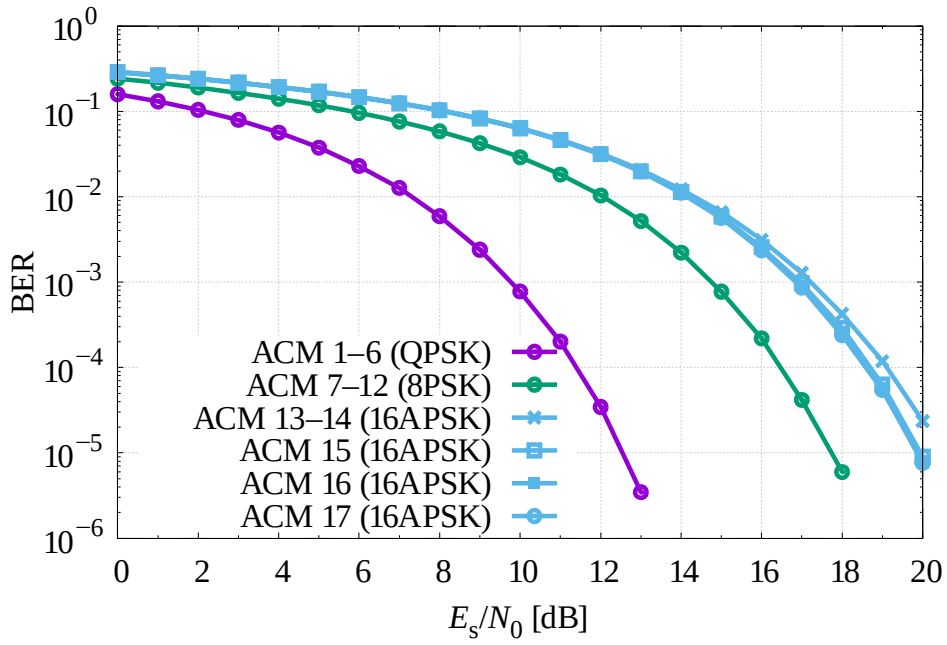

Figure 3-1: BER on Linear AWGN Channel for PSK/APSK Constellations Adopted by the ACM Formats (Uncoded BER)

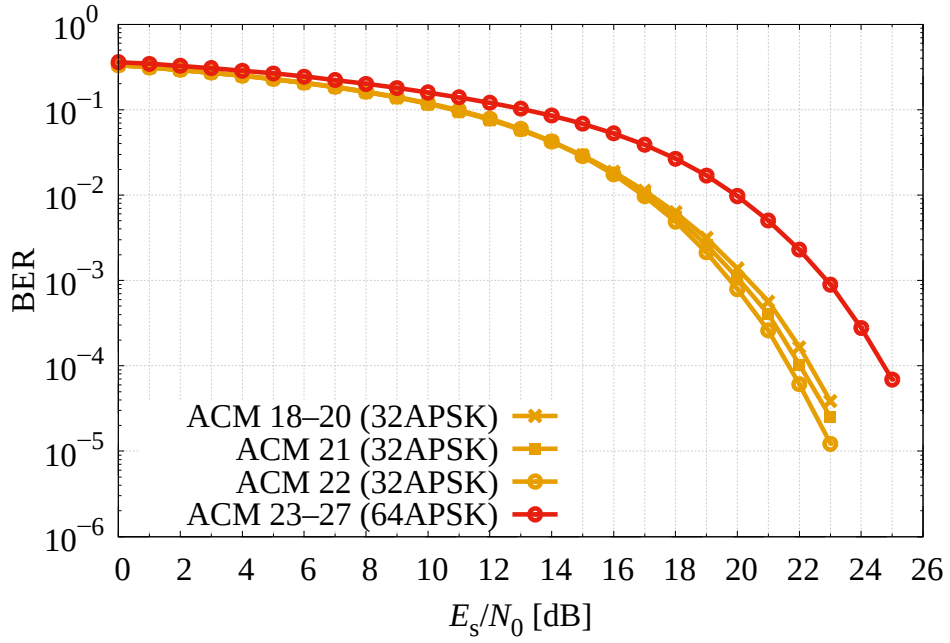

Figure 3-2: BER on Linear AWGN Channel for APSK Constellations Adopted by the ACM Formats (Uncoded BER)

Figures 3-3 to 3-6 show the BER and Codeword Error Rate (CER) as functions of the E_b/N_0 for all 27 ACM formats, when 10 iterations of the SCCC turbo decoder are performed.

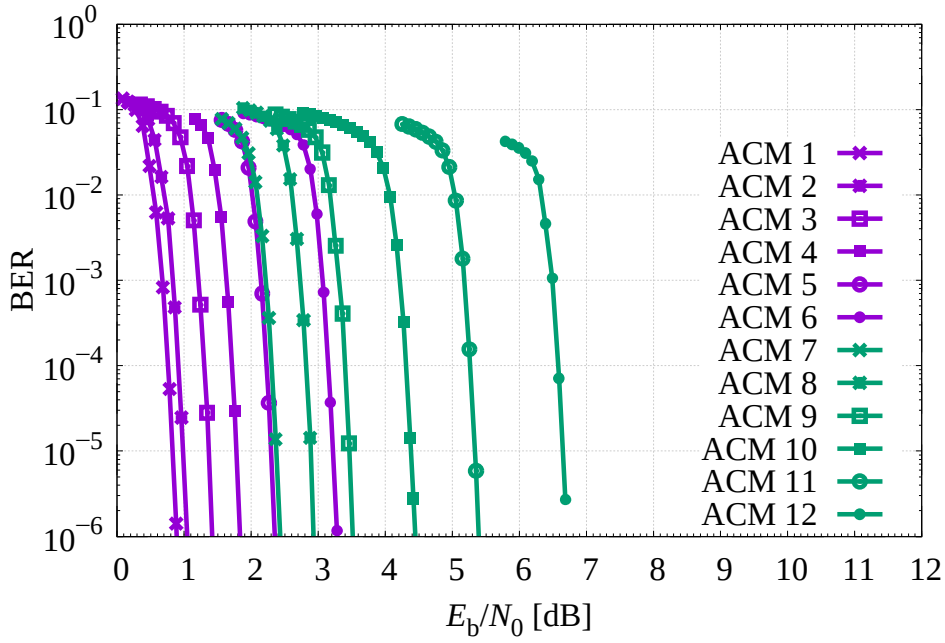

Figure 3-3: BER on Linear AWGN Channel for ACM Formats from 1 to 12 (PSK Modulations)

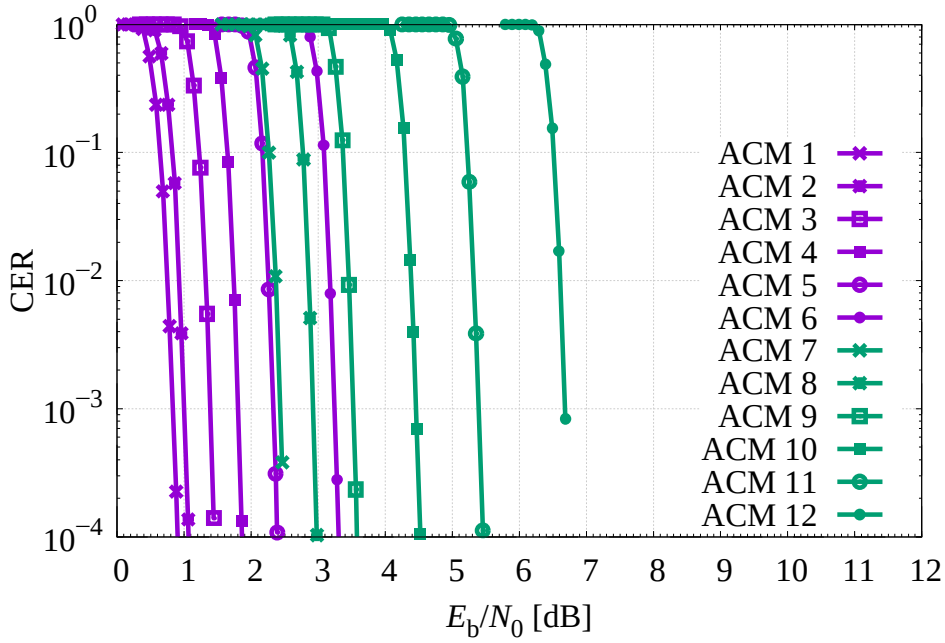

Figure 3-4: CER on Linear AWGN Channel for ACM Formats from 1 to 12 (PSK Modulations)

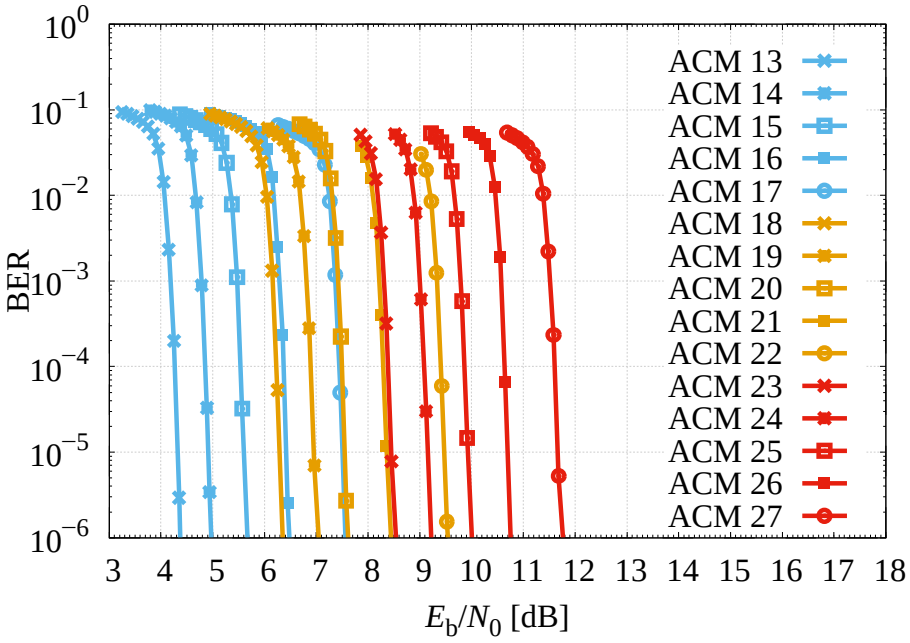

Figure 3-5: BER on Linear AWGN Channel for ACM Formats from 13 to 27 (APSK Modulations)

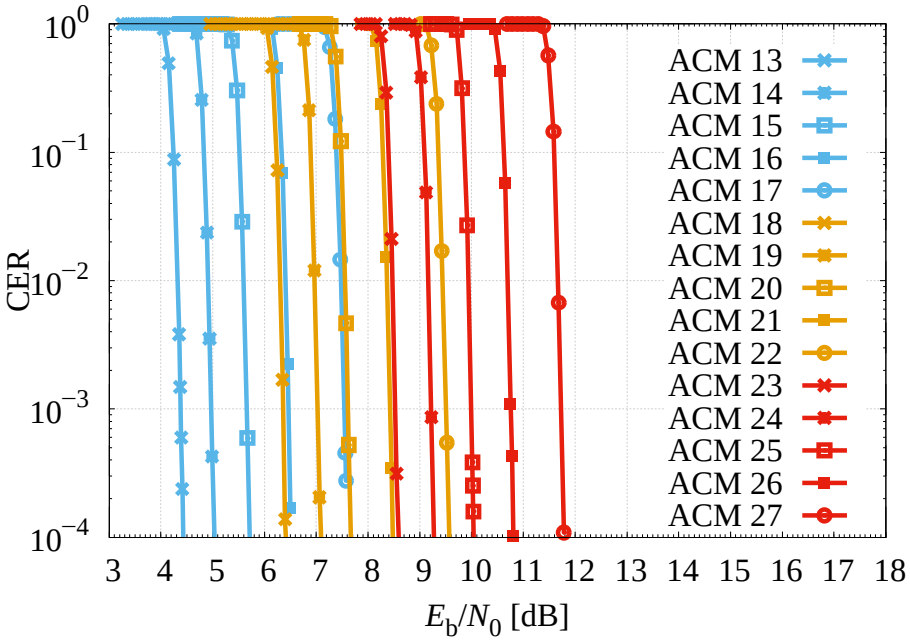

Figure 3-6: CER on Linear AWGN Channel for ACM Formats from 13 to 27 (APSK Modulations)

Table 3-1 shows the required SNR (in terms of both E_s/N_0 and E_b/N_0) for achieving a target CER of 10^{-4}, and the corresponding efficiency in terms of bits per transmitted channel symbol. These values can be shown also in a plane with the efficiency versus E_b/N_0, as shown in figure 3-7. For comparison, the AWGN capacity (*Shannon limit*, reference [2]) is also shown.

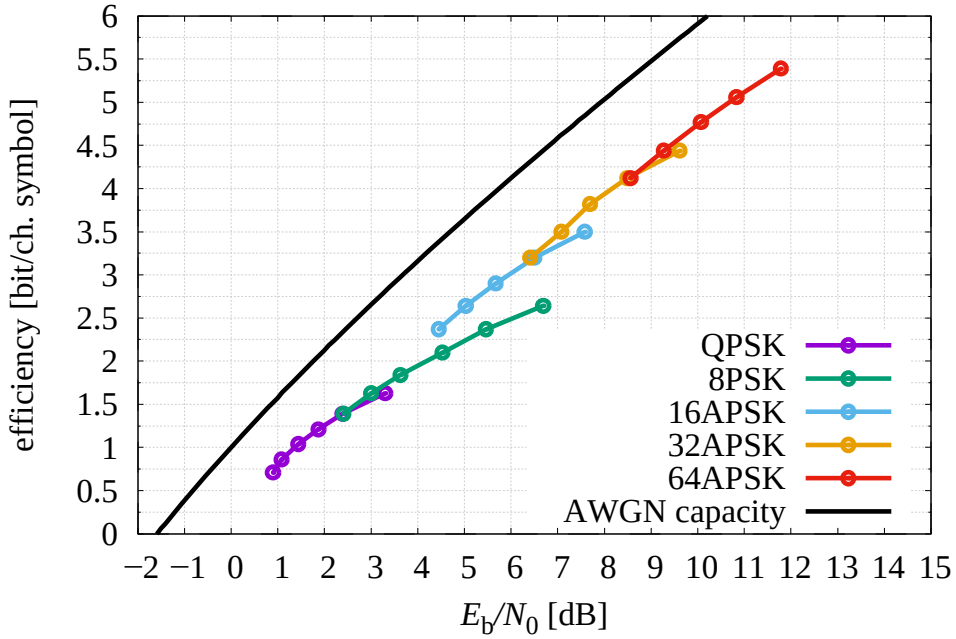

Figure 3-7: Efficiency of the Recommended ACM Formats on the Linear AWGN Channel with Respect to Channel Capacity

Table 3-1: SNR Thresholds for CER=1e−4, Achieved on the AWGN Channel by the ACM Formats

	ACM	E_s/N_0 [dB]	E_b/N_0 [dB]	Efficiency
QPSK	1	-0.58	0.90	0.71
	2	0.42	1.08	0.86
	3	1.60	1.44	1.04
	4	2.71	1.87	1.21
	5	3.83	2.39	1.39
	6	5.42	3.30	1.63
8PSK	7	3.91	2.41	1.39
	8	5.10	3.00	1.63
	9	6.25	3.63	1.84
	10	7.75	4.53	2.10
	11	9.21	5.46	2.37
	12	10.90	6.69	2.64
16APSK	13	8.18	4.45	2.37
	14	9.24	5.03	2.64
	15	10.34	5.67	2.90
	16	11.55	6.50	3.20
	17	13.02	7.58	3.50
32APSK	18	11.46	6.41	3.20
	19	12.52	7.08	3.50
	20	13.49	7.69	3.82
	21	14.62	8.49	4.12
	22	16.04	9.61	4.44
64APSK	23	14.73	8.56	4.12
	24	15.74	9.27	4.44
	25	16.83	10.07	4.77
	26	17.85	10.83	5.06
	27	19.10	11.78	5.39

4 PERFORMANCE OF THE RECOMMENDED CODES AND MODULATIONS ON NONLINEAR CHANNELS WITH IDEAL SYNCHRONIZATION

4.1 INTRODUCTION

This section focuses on the performance of the Recommended Standard's codes and modulations over a nonlinear channel model with ideal synchronization. In particular, 4.2 provides a channel model that includes nonlinear distortions typically due to a Traveling Wave Tube Amplifier (TWTA), an output filter (aimed at mitigating spectral regrowth), and AWGN. Starting from this channel model, 4.3 describes how to optimize the Input and Output Back-Off (IBO/OBO) by means of the Total Degradation (TD). Finally, 4.4 shows the numerical results for the recommended codes and modulations, in particular, their TD, BER/FER curves, and the bandwidth expansion after the nonlinearity (due to spectral regrowth). It will also be shown how pre-distortion can improve the performance, especially for ACMs 13-17 (based on APSK modulations).

4.2 NONLINEAR CHANNEL MODEL

The linearly modulated signal of equation (1) is applied to the nonlinear channel (as shown in figure 4-1), which includes a TWTA and an RF output filter (mitigating spectral regrowth). The distorted signal is then further corrupted by AWGN.

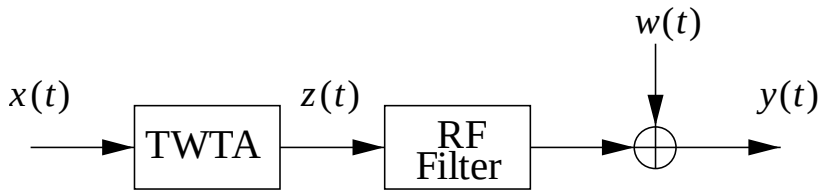

Figure 4-1: Block Diagram of the Overall Channel Model Considered in Simulations

The TWTA was modelled by means of the input/output relationship

$$z(t) = f_{\mathrm{AM}}(|x(t)|)e^{j\angle x(t)+f_{\mathrm{PM}}(|x(t)|)},$$

where $f_{\mathrm{AM}}(|x(t)|)$ and $f_{\mathrm{PM}}(|x(t)|)$ are the AM/AM and AM/PM characteristics, respectively.

For all simulations, a channel symbol rate of 100 MBaud and SRRC with roll-off 0.35 were assumed (unless differently specified), while at the receiver, a symbol-by-symbol detector was adopted for computing the soft information (the LLRs) that is the input of the decoder. A maximum of 10 decoding SCCC turbo iterations was assumed for the simulations. The specific AM/AM and AM/PM characteristics adopted for simulations (modelling a typical TWTA operating in the 25.5-27 GHz band) are as shown in figure 4-2, while the output filter is a 5th order Elliptical filter with frequency response as shown in figure 4-3, having ripple 0.1 dB, and passband and stopband 75 MHz and 93.75 MHz, respectively.

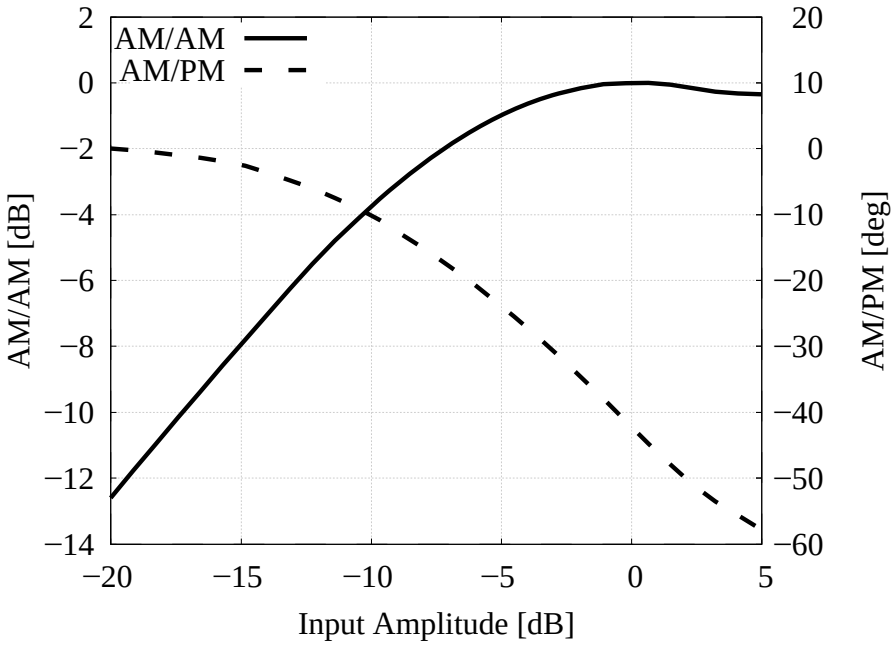

Figure 4-2: AM/AM and AM/PM Nonlinear Transfer Characteristics Adopted for Simulations

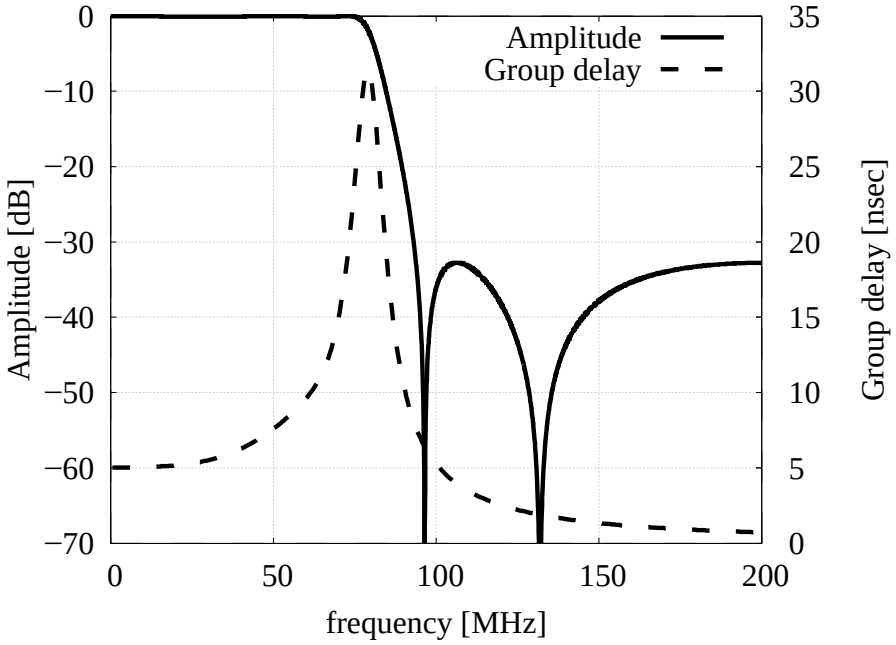

Figure 4-3: RF Filter Frequency Response

4.3 IBO/OBO OPTIMIZATION BY MEANS OF TOTAL DEGRADATION

A useful figure of merit for optimizing the operating point is the total degradation, defined as

$$TD = \left(\frac{E_b}{N_0} + \mathrm{OBO}\right) - \left(\frac{E_b}{N_0}\right)_{\mathrm{AWGN}} \qquad [\mathrm{dB}],$$

where $\left(\frac{E_b}{N_0} + \mathrm{OBO}\right)$ is the SNR and OBO values required for obtaining a specific target CER with the channel model assumed. The value $\left(\frac{E_b}{N_0}\right)_{\mathrm{AWGN}}$ represents instead the SNR required on the ideal AWGN channel to achieve the same target CER (and reported in table 2-1). With this definition, TD provides a useful representation of the overall losses experienced by the link, both in term of distortion and as reduced available power (due to the back-off). In this report, a target CER equal to 10^{-4} has been adopted for the optimization of the operating point.

To achieve operating point optimization, CER curves must be computed for different IBOs,[4] and the total degradation is derived as loss between each of the curves, with respect to the AWGN curve at CER = 10^{-4}. Finally, the resulting TD values are reported as functions of the IBO. An example of this process is shown in figures 4-4 and 4-5 for ACM format 15. In the first figure, all CER curves are shown down to CER = 10^{-4}, and the total degradation is measured as loss from the AWGN curve. In the second figure, the loss is reported as function of the IBO, and it can be seen that the optimal IBO is around 5 dB.

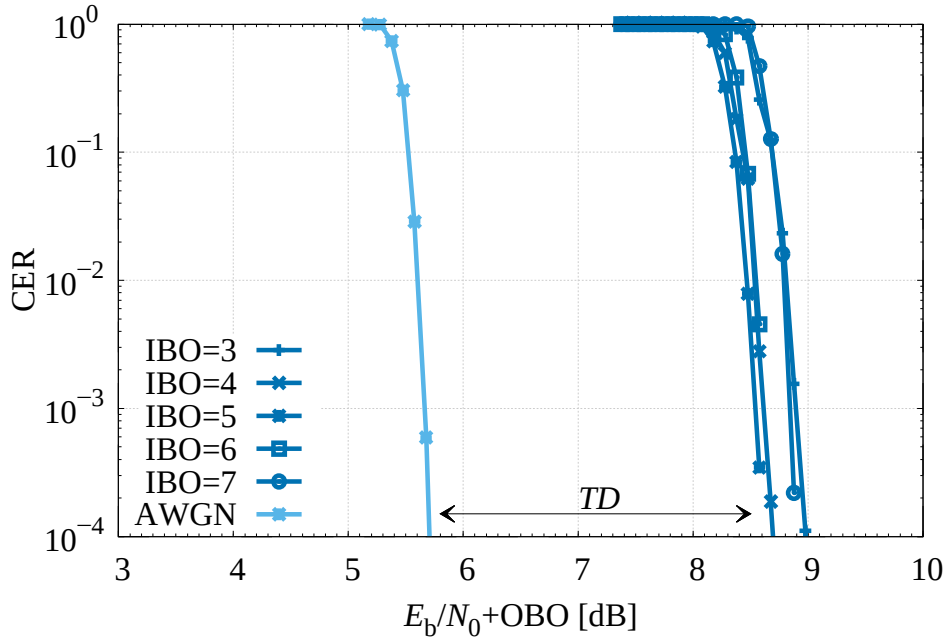

Figure 4-4: CER for Different IBO for ACM 15 on Nonlinear AWGN Channel

[4] While IBO is an input parameter, the OBO is measured at the output of the amplifier and cannot be directly derived, for the modulated signal, by the AM/AM curve of figure 4-2 (that is valid for an unmodulated carrier).

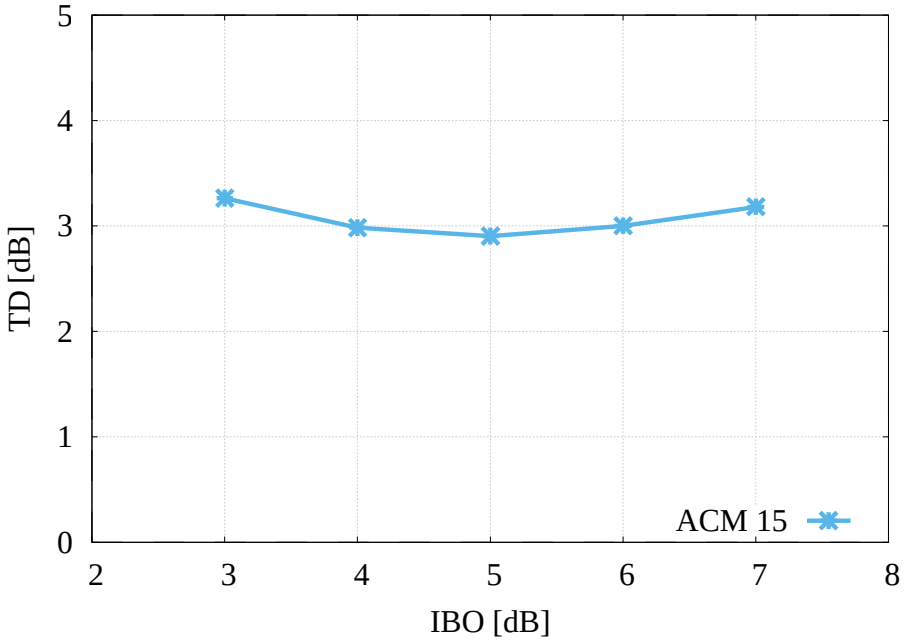

Figure 4-5: Total Degradation for ACM Format 15

4.4 NUMERICAL RESULTS

4.4.1 TOTAL DEGRADATION AND ERROR RATE CURVES

Numerical simulations have been carried out with the channel model described in the previous section in order to assess the impact of the TWTA together with the RF filter.

Figures 4-6 and 4-7 show the total degradation for all the ACM formats as a function of the IBO. It can be observed that the optimal IBO and the minimum total degradation tend to increase with the modulation order. In particular, the optimal IBO for PSK modulations is between 0 and 1 dB and the total degradation ranges from 0.6 to 1.3 dB, whereas the optimal IBO for APSK modulations can range from 4 to 12 dB, with corresponding total degradation from 2 to 8 dB.

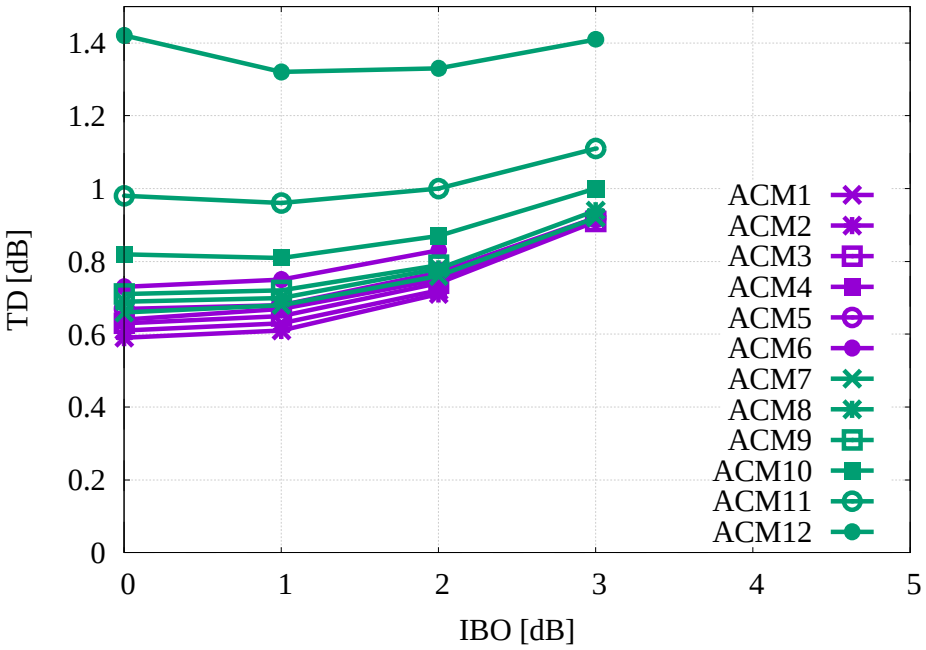

Figure 4-6: Total Degradation for ACM Formats from 1 to 12 (PSK Modulations)

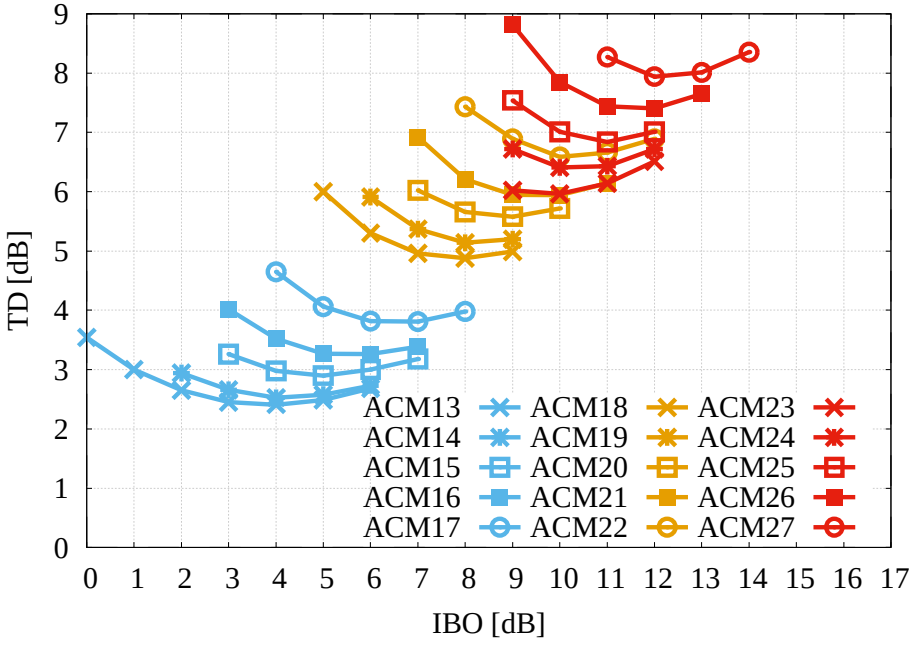

Figure 4-7: Total Degradation for ACM Formats from 13 to 27 (APSK Modulations)

Figures 4-8 to 4-11 show the BER and CER for all possible ACM formats using the optimal IBO found by means of the total degradation analysis. The corresponding SNR thresholds for CER equal 10^{-4}, and OBO for each individual ACM mode (to be taken into account when performing system level design) can be found in table 4-1.

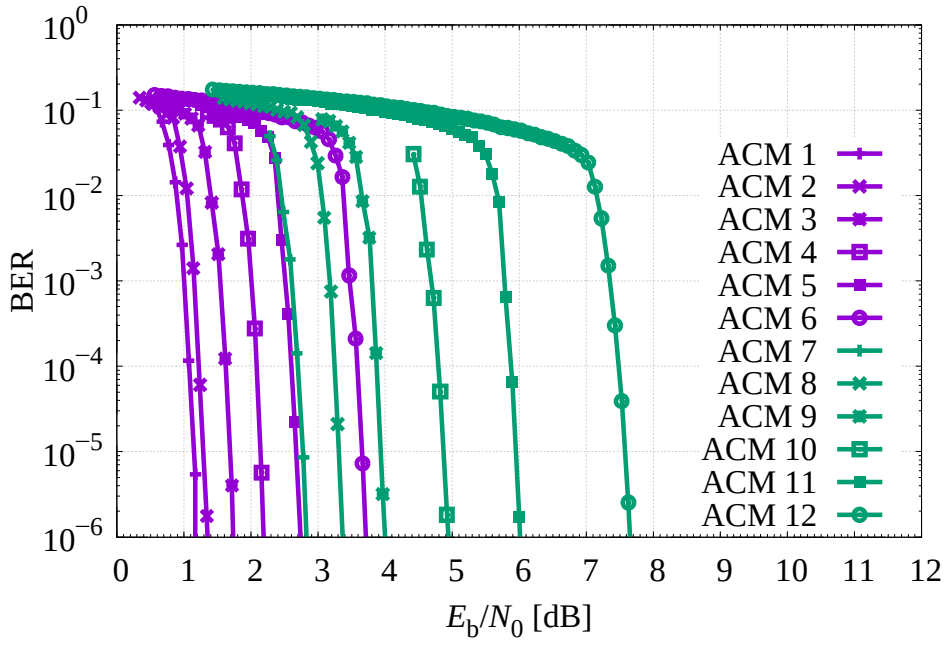

Figure 4-8: BER on Nonlinear AWGN Channel for ACM Formats from 1 to 12 (PSK Modulations) with the Optimal IBO

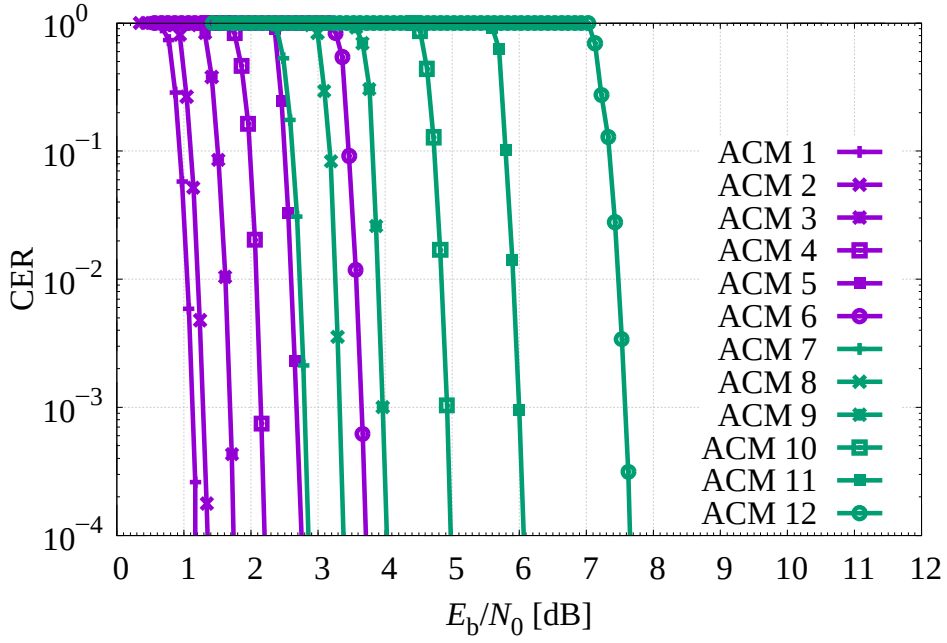

Figure 4-9: CER on Nonlinear AWGN Channel for ACM Formats from 1 to 12 (PSK Modulations) with the Optimal IBO

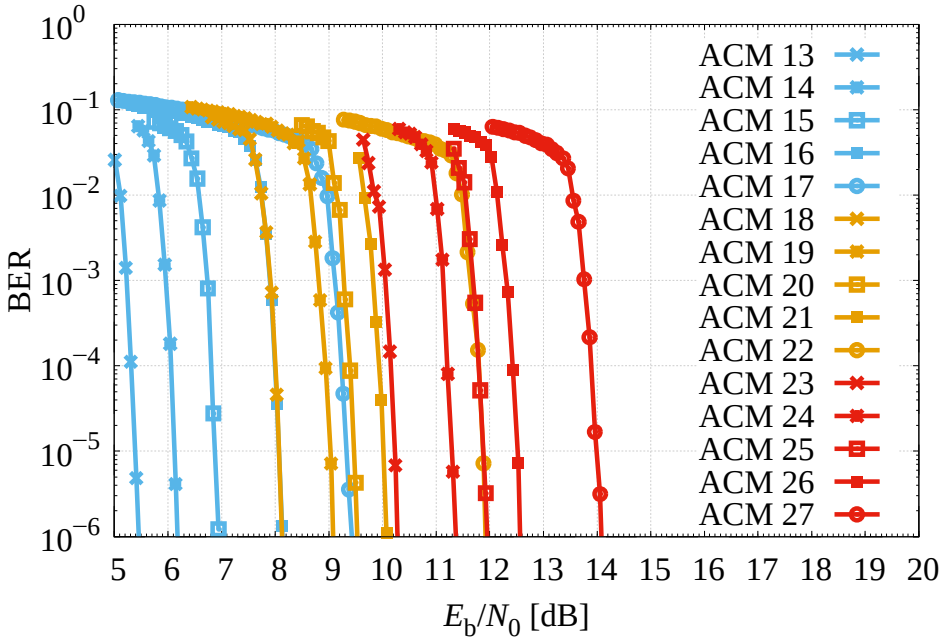

Figure 4-10: BER on Nonlinear AWGN Channel for ACM Formats from 13 to 27 (APSK Modulations) with the Optimal IBO

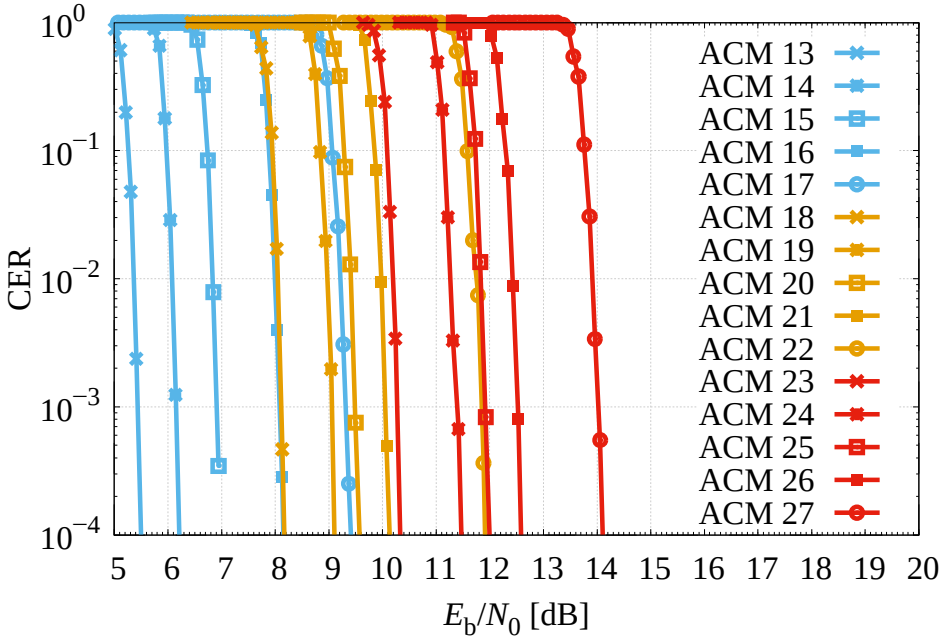

Figure 4-11: CER on Nonlinear AWGN Channel for ACM Formats from 13 to 27 (APSK Modulations) with the Optimal IBO

Table 4-1: SNR Thresholds for CER=1e−4, and Corresponding OBO and TD, Achieved by the Recommended ACM Formats on the Nonlinear AWGN Channel without Pre-Distortion

	ACM	E_s/N_0 [dB]	E_b/N_0 [dB]	OBO [dB]	TD [dB]	Efficiency
QPSK	1	-0.28	1.20	0.32	0.61	0.71
	2	0.70	1.35	0.32	0.59	0.86
	3	1.91	1.74	0.32	0.63	1.04
	4	3.03	2.20	0.32	0.64	1.21
	5	4.18	2.75	0.32	0.67	1.39
	6	5.84	3.72	0.32	0.73	1.63
8PSK	7	4.29	2.86	0.29	0.66	1.39
	8	5.50	3.38	0.29	0.69	1.63
	9	6.67	4.02	0.29	0.71	1.84
	10	8.20	4.98	0.36	0.81	2.10
	11	9.82	6.07	0.36	0.96	2.37
	12	11.87	7.65	0.36	1.32	2.64
16APSK	13	9.25	5.50	1.34	2.41	2.37
	14	10.43	6.21	1.34	2.53	2.64
	15	11.61	6.99	1.63	2.90	2.90
	16	13.19	8.14	1.63	3.27	3.20
	17	14.85	9.41	1.99	3.82	3.50
32APSK	18	13.22	8.17	3.12	4.88	3.20
	19	14.54	9.09	3.12	5.14	3.50
	20	15.39	9.57	3.68	5.58	3.82
	21	16.29	10.14	4.27	5.94	4.12
	22	18.37	11.88	4.27	6.59	4.44
64APSK	23	16.48	10.33	4.21	5.96	4.12
	24	17.94	11.47	4.21	6.41	4.44
	25	18.78	12.00	4.89	6.84	4.77
	26	19.63	12.59	5.62	7.40	5.06
	27	21.42	14.10	5.62	7.94	5.39

4.4.2 STATIC PRE-DISTORTION

The total degradation can be effectively decreased by means of pre-distortion. A static data pre-distorter (at the transmitter), such as the one in reference [3], was assumed for the simulations presented in this section. Such pre-distortion is basically a simple look-up table that transmits the constellation symbols with a fixed correction of the radii amplitudes and phases (computed off-line).

Figures 4-12 to 4-14 show the total degradation as a function of IBO for ACM formats using 16APSK, 32APSK, and 64APSK. For comparison, the total degradation without pre-distortion (as in 4.4.1) is also shown. It can be seen how, already with this simple pre-distorter, a performance gain of more than 0.5 dB is possible with 16APSK, and more than 2 dB with 32APSK and 64APSK.

On the other hand, in case of PSK modulations, there are no performance gains since the constellation has a constant amplitude. Figure 4-15 shows the total degradation for some ACM formats having 8PSK modulation, and it can be seen that the static pre-distorter does not provide any improvement.

It is pointed out that the pre-distortion algorithm adopted here is just a reference, and it is not be considered to be optimal. For instance, it is expected that pre-distortion based on a more complex model, for example, a polynomial representation of the amplifier (see reference [4]), can provide a performance gain of up to 5 dB for 64APSK, in addition to reducing the spectral occupation.

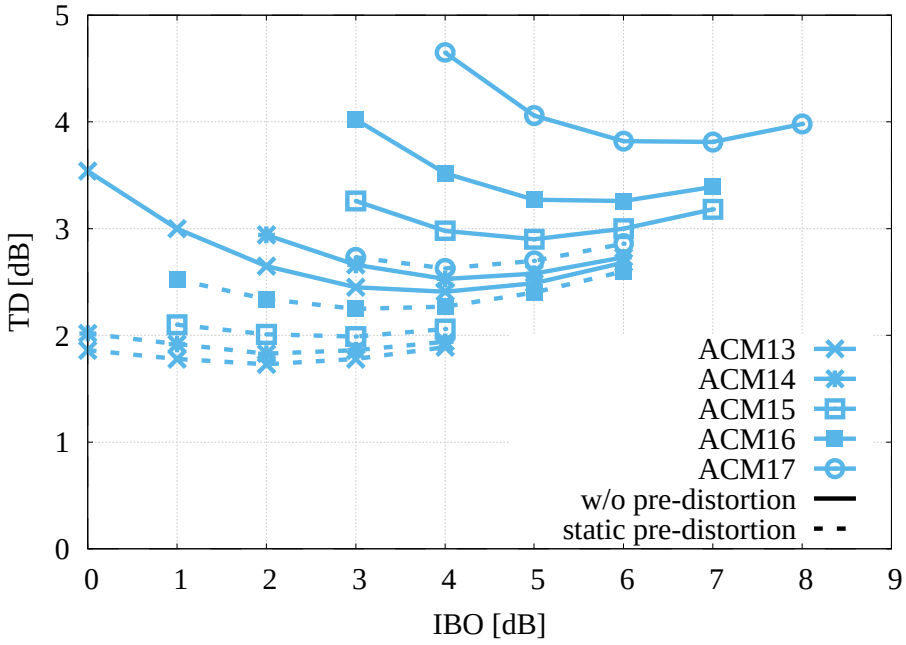

Figure 4-12: Total Degradation for ACM Formats from 13 to 17 (16APSK) with and without Pre-Distortion

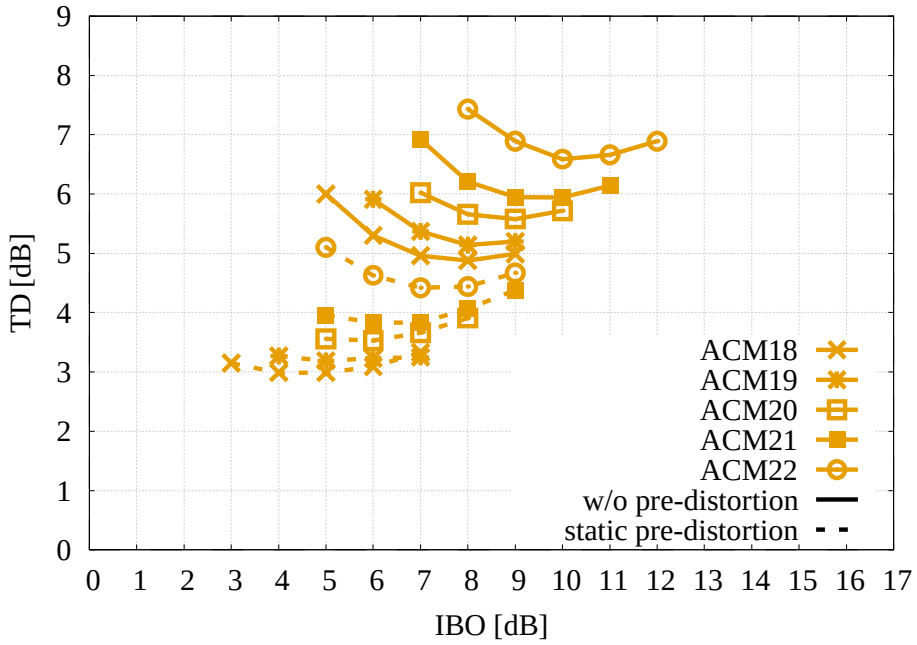

Figure 4-13: Total Degradation for AMC Formats from 18 to 22 (32APSK) with and without Pre-Distortion

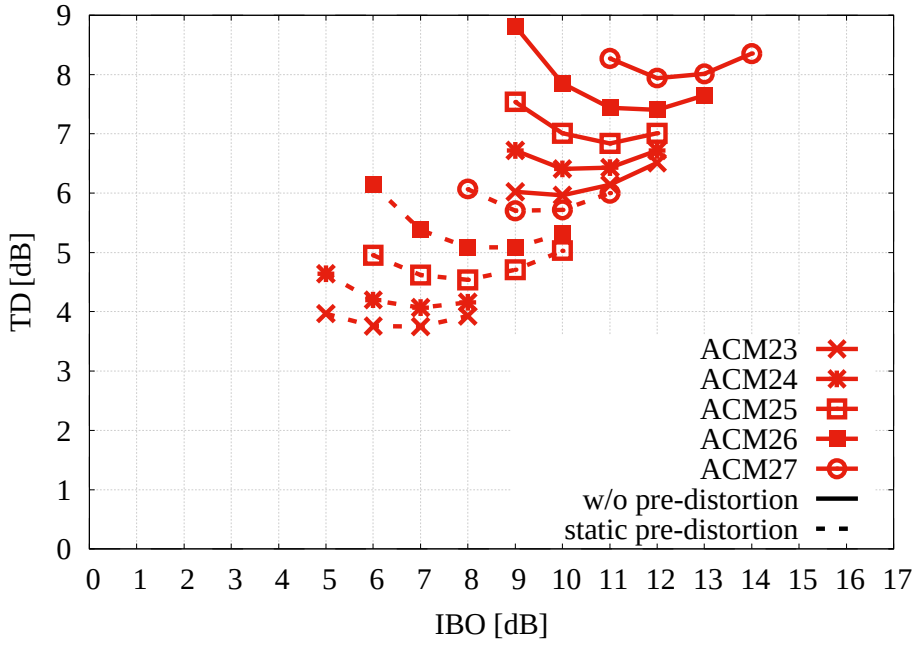

Figure 4-14: Total Degradation for ACM Formats from 23 to 27 (64APSK) with and without Pre-Distortion

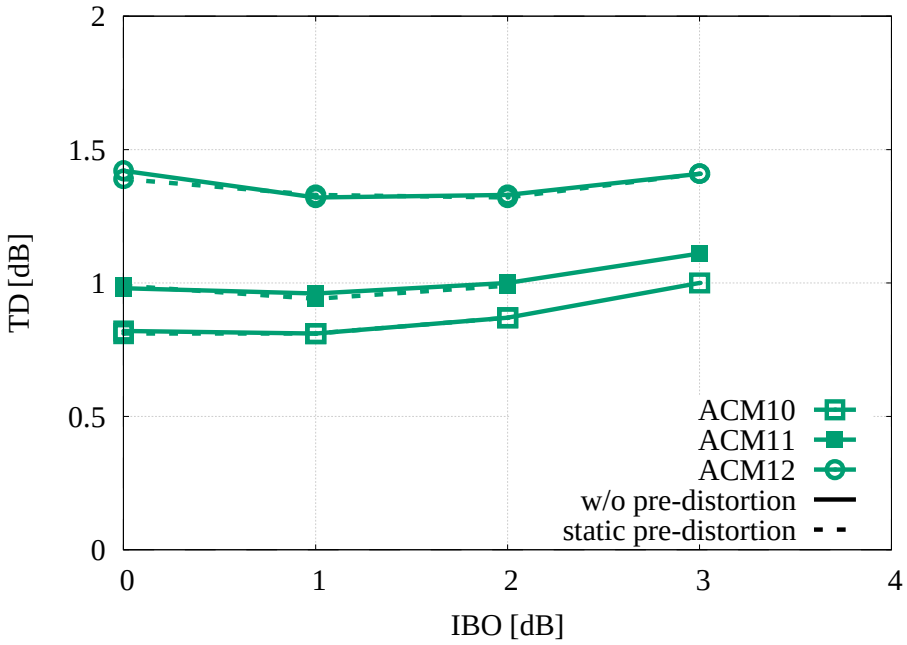

Figure 4-15: Total Degradation for ACM Formats from 10 to 12 (8PSK) with and without Pre-Distortion

The SNR values for APSK modulations that allow a CER equal to 10^{-4} when static pre-distortion is adopted are summarized in table 4-2. In the table, the corresponding OBO, total degradation TD, and its gain with respect to the scenario without pre-distortion (see table 4-1) are also reported. The total degradation gain can also be seen in a SNR plane as the one in figure 4-16, where the E_b/N_0 + OBO is shown for each E_b/N_0 threshold for the AWGN channel, and the distance from the bisector is the total degradation.

Table 4-2: SNR Thresholds for CER=1e−4, and Corresponding OBO and TD, Achieved by the Recommended ACM Formats with Pre-Distortion

	ACM	E_s/N_0 [dB]	E_b/N_0 [dB]	OBO [dB]	TD [dB]	TD Gain [dB]
16APSK	13	8.91	5.16	1.00	1.73	0.68
	14	10.07	5.86	1.00	1.83	0.70
	15	11.18	6.55	1.14	1.99	0.91
	16	12.26	7.61	1.15	2.25	1.02
	17	14.30	8.86	1.35	2.63	1.19
32APSK	18	12.42	7.37	2.03	2.99	1.89
	19	13.68	8.24	2.03	3.19	1.95
	20	14.68	8.86	2.34	3.53	2.05
	21	16.10	9.95	2.35	3.83	2.11
	22	17.79	11.31	2.67	4.42	2.17
64APSK	23	16.29	10.13	2.20	3.76	2.20
	24	17.19	10.71	2.62	4.07	2.34
	25	18.27	11.48	3.10	4.54	2.30
	26	19.29	12.25	3.65	5.09	2.31
	27	21.15	13.83	3.65	5.70	2.24

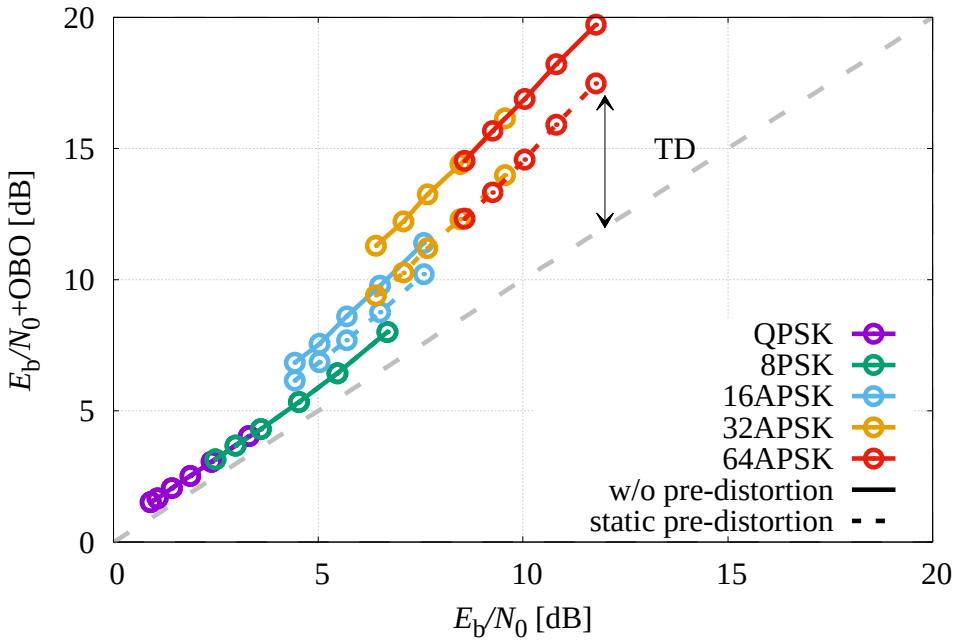

Figure 4-16: SNR Threshold Plane for All the ACM Formats

4.4.3 OCCUPIED BANDWIDTH

The bandwidth *W*, defined as the bandwidth containing 99 percent of the signal power, has been computed after the nonlinearity for roll-off 0.2 and 0.35. Figures 4-17 and 4-18 show *W* before a post-amplifier RF Filter and normalized to the channel symbol rate R_{chs} as a function of OBO. Since 16APSK and 32APSK have circumference radii that depend on the actual ModCod, it is shown that only ACM13 and ACM18 that have the highest peak-to-average ratio of their set. It can be seen that for OBO greater than 4 dB, a bandwidth equal to the one in linear regime is reached; that is, all the modulations have bandwidths $1.07R_{chs}$ and $1.17R_{chs}$ for roll-off 0.2 and 0.35, respectively. Additionally, it can be seen that 32APSK has the largest bandwidth occupancy. This results from its peak-to-average ratio, which can be demonstrated to be higher than those for 16APSK and 64APSK.

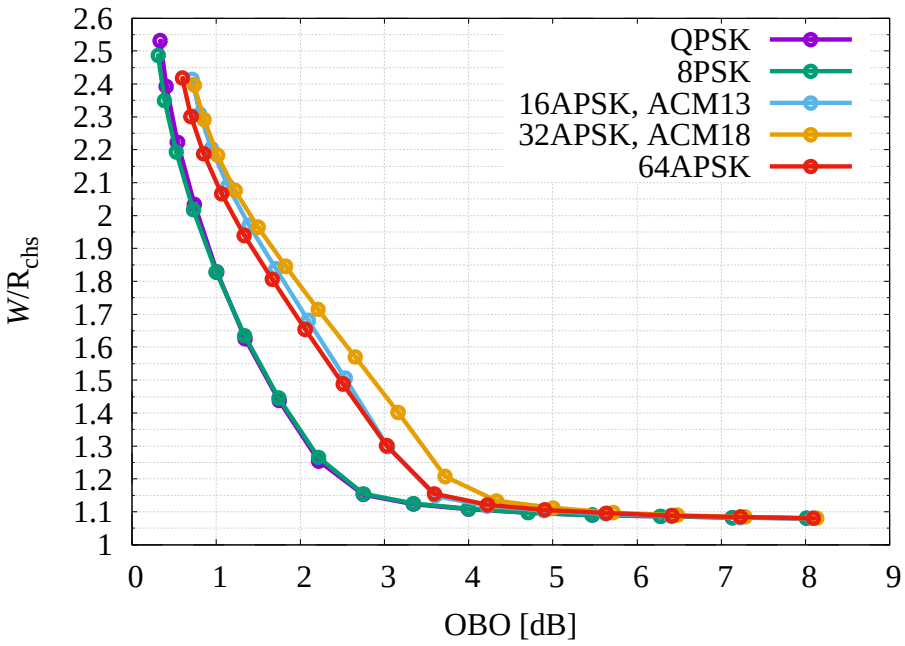

Figure 4-17: Bandwidth Normalized to the Channel Symbol Rate as a Function of the OBO (SRRC with Roll-Off 0.20)

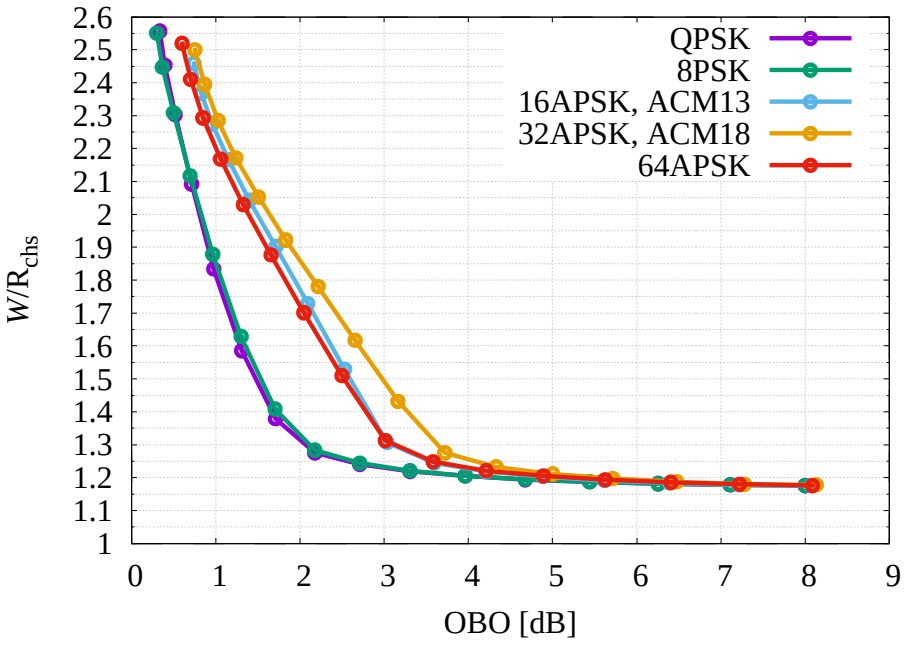

Figure 4-18: Bandwidth Normalized to the Channel Symbol Rate as a Function of the OBO (SRRC with Roll-Off 0.35)

The RF filter aims to minimize the spectral regrowth outside the signal bandwidth. Figures 4-19 and 4-20 show the bandwidth for all the modulations after the filter. It can be seen that in all cases, the bandwidth is always less than $1.4R_{chs}$.

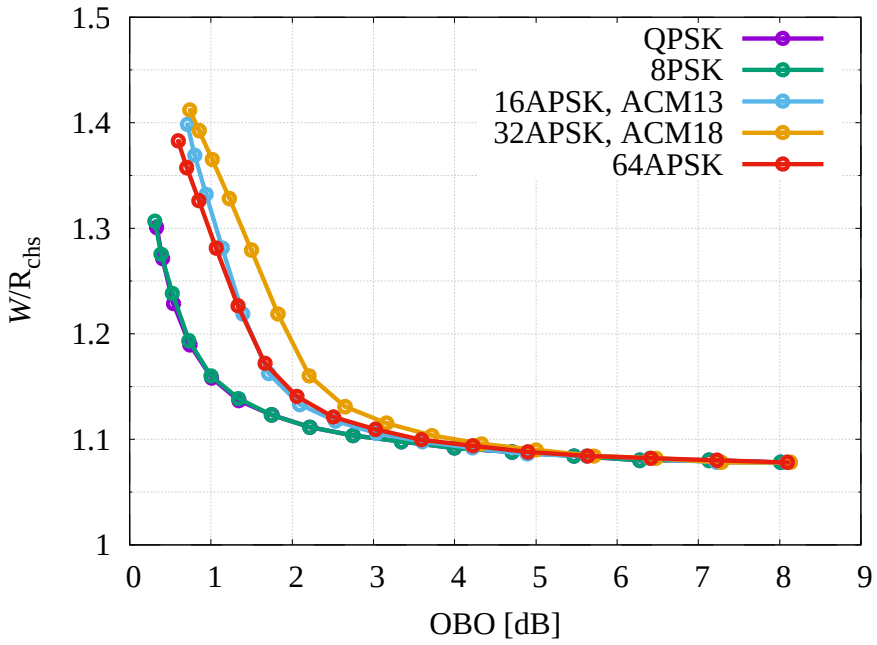

Figure 4-19: Bandwidth after the RF Filter Normalized to the Channel Symbol Rate as a Function of the OBO (SRRC with Roll-Off 0.20)

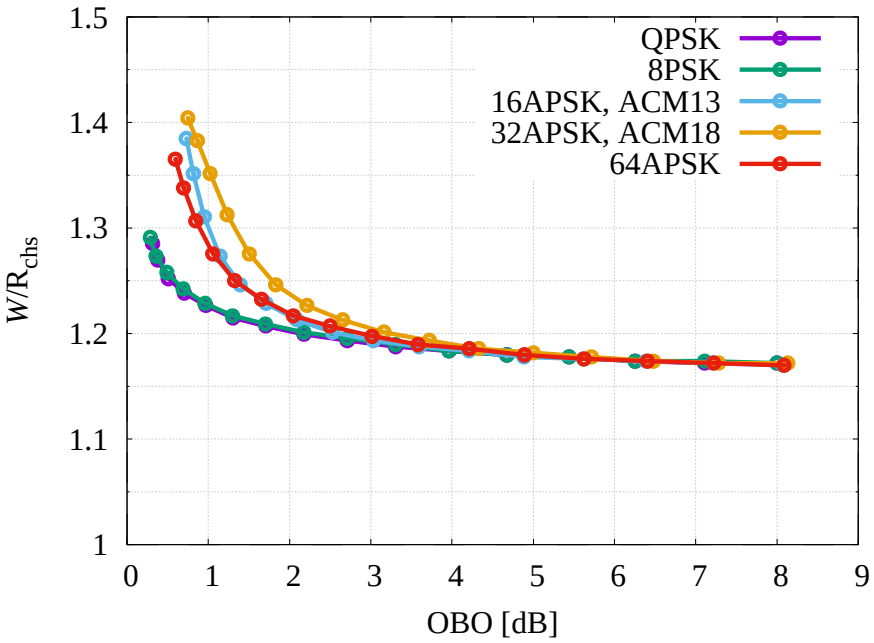

Figure 4-20: Bandwidth after the RF Filter Normalized to the Channel Symbol Rate as a Function of the OBO (SRRC with Roll-Off 0.35)

Table 4-3 shows a summary of the expected bandwidth for some of the ACM formats considered in previous sections when the shaping pulse has roll-off 0.35 and the IBO is selected as the one that minimizes the total degradation. For comparison, table 4-4 shows the bandwidth occupancy with pre-distortion at the transmitter (adopted only for APSK modulations). It can be seen that, if RF filtering is adopted, pre-distortion allows a noticeable decrease of the IBO/OBO, while the bandwidth increase due to spectral regrowth is maintained as acceptable.

Table 4-3: Bandwidth for Different ACM at the Optimal IBO When No Pre-Distortion Is Adopted at the Transmitter (SRRC with Roll-Off 0.35)

ACM	Optimal IBO [dB]	Corresponding OBO [dB]	Bandwidth at optimal IBO before RF filtering	Bandwidth at optimal IBO after RF filtering
4	0	0.32	$2.56 \cdot R_{chs}$	$1.29 \cdot R_{chs}$
10	1	0.36	$2.44 \cdot R_{chs}$	$1.2 \cdot R_{chs}$
14	4	1.34	$2.04 \cdot R_{chs}$	$1.24 \cdot R_{chs}$
20	9	3.68	$1.27 \cdot R_{chs}$	$1.19 \cdot R_{chs}$
25	11	4.89	$1.21 \cdot R_{chs}$	$1.18 \cdot R_{chs}$

Table 4-4: Bandwidth for Different ACM at the Optimal IBO When Pre-Distortion Is Adopted at the Transmitter (SRRC with Roll-Off 0.35)

ACM	Optimal IBO [dB]	Corresponding OBO [dB]	Bandwidth at optimal IBO before RF filtering	Bandwidth at optimal IBO after RF filtering
14	2	1.00	$2.27 \cdot R_{chs}$	$1.31 \cdot R_{chs}$
20	6	2.34	$1.78 \cdot R_{chs}$	$1.22 \cdot R_{chs}$
25	8	3.10	$1.31 \cdot R_{chs}$	$1.20 \cdot R_{chs}$

5 SYNCHRONIZATION

5.1 INTRODUCTION

This section deals with the synchronization for the recommended codes and modulations. In particular, a possible synchronization chain is described and performance evaluated on the AWGN channel when affected by phase noise and Doppler shift. The remainder of this section is organized as follows: Subsection 5.2 describes the adopted channel model with focus on the mathematical models adopted for generating Doppler and phase noise. Subsection 5.3 introduces the synchronization chain that has been adopted for evaluation of the performance. Subsections 5.4 to 5.7 analyze the performance and characteristics of each algorithm adopted in the synchronization chain. Finally, in 5.8, performance results in terms of CER are presented.

5.2 CHANNEL MODEL AFFECTED BY DOPPLER AND PHASE NOISE

The linearly modulated signal of equation (1) is transmitted over an AWGN channel affected by Doppler shift, Doppler rate, and phase noise. Hence, the baseband model of the received is given by

$$y(t) = \sum_{k} x_k p(t - kT) e^{j\phi(t)} + w(t), \tag{4}$$

where x_k are the transmitted channel symbols belonging to a constellation (PSK/APSK) properly normalized such that $E\{|x_k|^2\} = E_s$ (being E_s the energy per channel symbol), and $w(t)$ is AWGN with power spectral density N_0. The SNR is equal to E_s/N_0. Instead, $\phi(t)$ reads

$$\phi(t) = 2\pi \int_0^t f(\tau) d\tau + \theta(t),$$

with $f(t)$ and $\theta(t)$ the Doppler profile and the phase noise, respectively. Once again, all simulations assume a channel symbol rate of R_{chs} = 100 MBaud and SRRC with roll-off 0.35, while for comparison purposes with AWGN results, the E_b/N_0 does not take into account the overhead due to frame header and pilots (for which another ~0.15 dB should be taken into account because of the 3-percent overhead of PL signaling and pilot insertion, see 2.2.2).

For *f*(*t*), two possible profiles were adopted for testing different Doppler shift and rate conditions. Namely, 1) a s*inusoidal profile* having expression and derivative as

$$f(t) = f_{\mathrm{D}} \cos\left(\frac{f_{\mathrm{R}}}{f_{\mathrm{D}}} t\right), \qquad \frac{df(t)}{dt} = -f_{\mathrm{R}} \sin\left(\frac{f_{\mathrm{R}}}{f_{\mathrm{D}}} t\right), \tag{5}$$

where f_{D} is the maximum Doppler shift and f_{R} is the maximum Doppler rate, and 2) a *triangular wave*, having maximum Doppler shift f_{D} and derivative $\pm f_{\mathrm{R}}$. For both the profiles, unless differently specified, f_{D} = 1 MHz and f_{R} = 50 kHz/s were considered.

It should be noted that the sinusoidal profile tries to reproduce the satellite passes. Figure 5-1 shows the Doppler profile sampled at the beginning of each frame when f_{D} = 1 MHz and f_{R} = 50 kHz/s, while figure 5-2 shows the Doppler profile of a satellite at 700 km from Earth, transmitting at 27 GHz, and passing at zenith. It can be observed that the sinusoidal profile is adequate for reproducing the Doppler shift and rate experienced in real passes, and that the adopted values f_{D} and f_{R} are well above the ones that can be experienced in K-Band. In fact, the example in figure 5-2 shows a Doppler shift of 600 kHz and a maximum Doppler rate of 7 kHz/s.

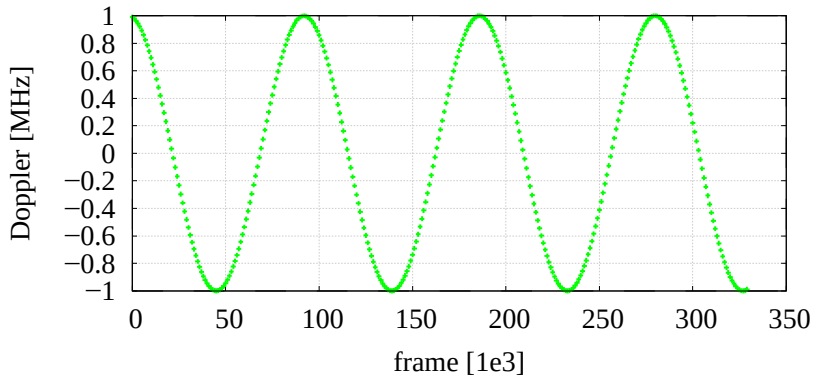

Figure 5-1: Sinusoidal Profile for Doppler Shift and Rate at 1 MHz and 50 kHz/s

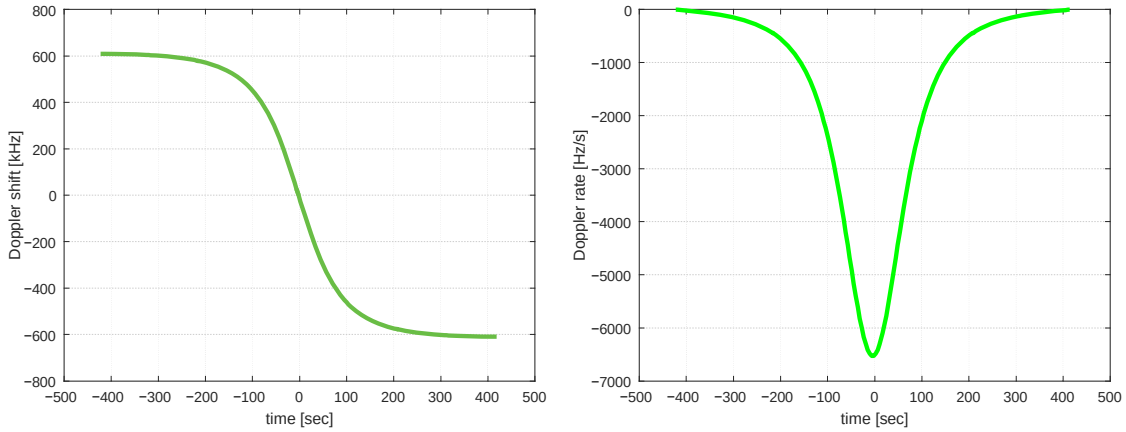

Figure 5-2: Doppler Rate and Shift for an Earth Observation Satellite at 700 km, Passing at Zenith, and Transmitting at 27 GHz

Similarly, the triangular wave tries to model the carrier sweep, and it has been included as the worst case of this Report's simulations. An example is reported in figure 5-3 that shows the triangular wave sampled at begin of each frame when f_D = 1 MHz and f_R = 50 kHz/s.

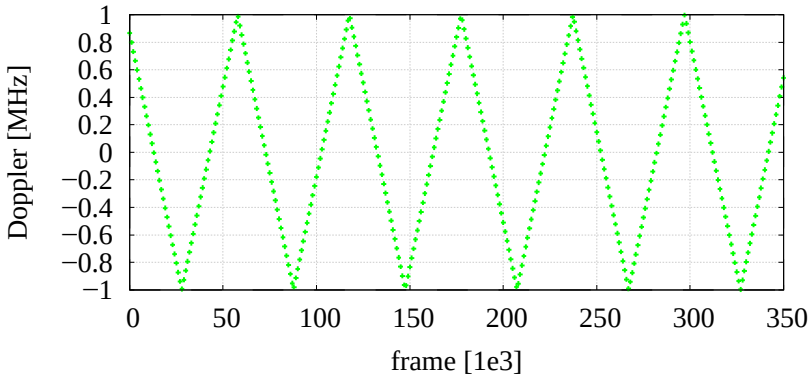

Figure 5-3: Triangular Wave Frequency Profile for Doppler Shift and Rate at 1 MHz and 50 kHz/s

In contrast, the phase noise $\theta(t)$ is a colored Gaussian random process. Its power spectral density is defined by the Fourier transform of $E\{\theta(t+\tau)\theta(t)\}$, which is usually known as *phase noise mask*. For phase noise, all simulations were carried out by using a phase noise mask as shown in figure 5-4, as recommended in reference [7] for channel symbol rates above 1 MBaud. In particular, this phase noise mask has standard deviation σ = 1.45 degrees in the bandwidth $[10^2, R_{chs}/2]$ Hz (being R_{chs} = 100 MBaud the channel symbol rate), and it is slightly worse than the phase noise measured in actual hardware (26 GHz modulator).

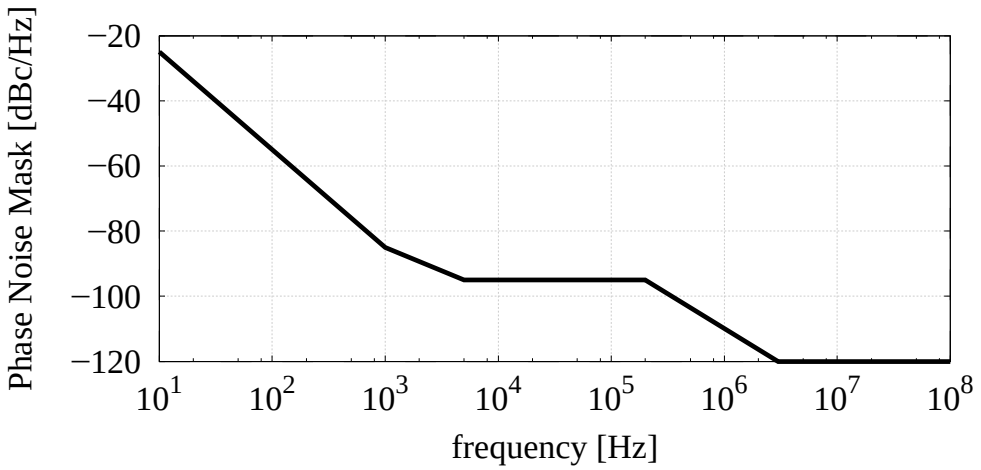

Figure 5-4: Phase Noise Mask Adopted for Simulation of the Phase Noise Experienced in K-Band

5.3 STUDIED SYNCHRONIZATION SCHEME

If the received signal in equation (4) passes through a filter matched to the shaping pulse, the sequence of samples $\{y_k\}$ at its output reads

$$y_k = \sum_i x_{k-i} g_{i,k-i} + w_k,$$

where

$$g_{i,k-i} = \int_{-\infty}^{\infty} e^{j\phi(t+(k-i)T)} p(t) p(t-iT) dt\,,$$

and w_k are independent Gaussian random variables with variance equal to N_0. Under the assumption that $\phi(t)$ is 'slow' with respect the channel symbol time, the expression above simplifies to

$$y_k \cong x_k e^{j\phi_k} + w_k,$$

where $\phi_k = \phi(kT)$. Hence frequency and phase synchronization and SNR estimation can be performed at channel symbol time.

In light of this assumption, the synchronization scheme that has been analyzed in the following sections is the one shown in figure 5-5, where

- frequency synchronization is carried out with a Frequency Locked Loop (FLL) that estimates the frequency on the FM;
- phase synchronization is carried out with a data-aided phase estimator operating on the FM and the pilots, with linear interpolation of the phase between pilot fields; and
- SNR estimation with Digital Automatic Gain Control (DAGC) is based on estimators of the received average power.

Subsections 5.4–5.8 show the design and performance analysis of the adopted algorithms, starting from the final stage continuing to the first stage. At each stage, design and performance analyses are carried out assuming perfect synchronization of the previous stages. Hence 5.4 focuses on the frame descriptor decoding assuming perfect estimation of frequency, phase, and SNR, while 5.8 considers the performance of the full chain.

As illustrated, this receiver is just a reference and is not considered to be optimal. Clock recovery (timing) and FM acquisition have been not considered in the simulation model adopted, since they are believed to be straightforward. For instance, Gardner's timing recovery in reference [5] and the frame synchronization techniques based on correlation shown in reference [6] can be easily adopted.

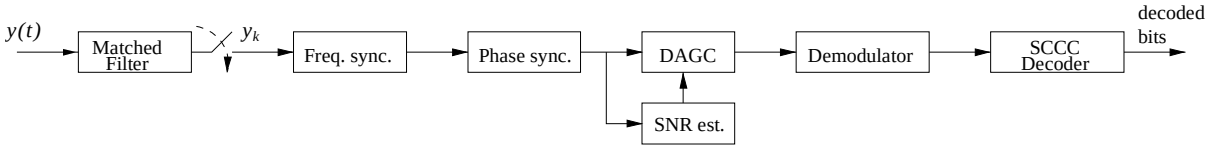

Figure 5-5: Synchronization Scheme Adopted for Performance Evaluation

5.4 FRAME DESCRIPTOR DECODING

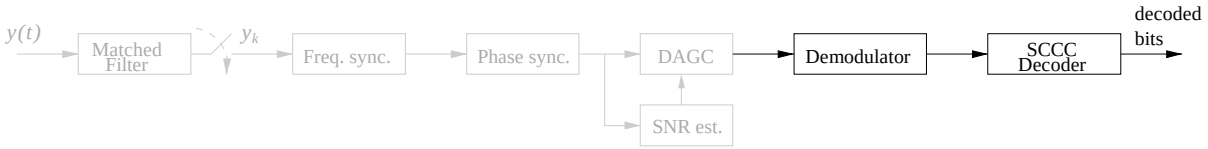

Figure 5-6: Highlight of the Section of the Synchronization Scheme That Is Analyzed for FD Decoding

The synchronization chain is analyzed starting from the last stage as shown in figure 5-6, that is, at the demodulator input that computes LLRs for SCCC turbo decoding. At this stage, FD decoding is performed before constellation de-mapping.

Assuming perfect synchronization in terms of all previous stages, the performance of the FD code described in 2.2.2 has been analyzed for two different implementations of the FD decoder: a Maximum Likelihood (ML) soft decoder versus an ML hard decoder. In turn, for both hard and soft decoding, two cases have been considered:

– a decoding approach, which knows that the 7th information bit b_7 of the FD is '0' (as currently set by the Recommended Standard), or

– a future-proof decoding approach, which assumes b_7 as an extra bit of information to be decoded.

For these four cases, figure 5-7 shows the FD error rate as a function of E_s/N_0. It can be seen that the hard implementation achieves the FD error rate equal to 1e−5 at $E_s/N_0 \cong -2$ dB, that is, 1.4 dB below the minimum E_s/N_0 required for decoding all ACM formats (see table 3-1).

Instead, a soft implementation of the FD decoder allows an extra 2 dB of margin, achieving an FD error rate equal to 1e−5 at $E_s/N_0 \cong -4$ dB. Finally, it can be observed that for both the soft and hard decoding, the knowledge of b_7 allows a small improvement of 0.2 dB.

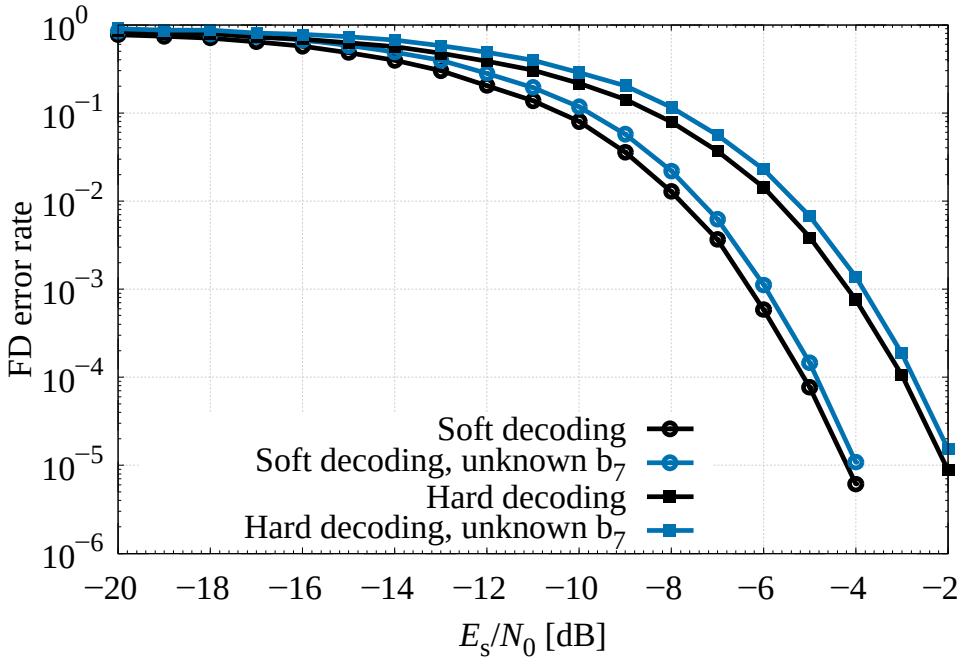

Figure 5-7: FD Error Rate with Hard and Soft Decoding and Whether Bit b7 (Currently Set to '0' in Reference [1]) Is Known at the Receiver

5.5 SNR ESTIMATOR AND DAGC

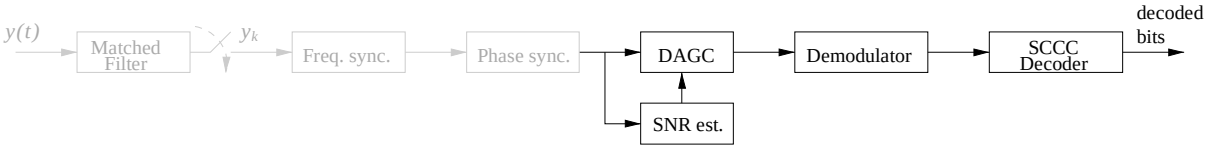

Figure 5-8: Highlight of the Section of the Synchronization Scheme That Is Analyzed for SNR Estimation and DAGC

In this subsection, the synchronization chain is analyzed and simulated starting at the input of the DAGC and the SNR estimator as shown in figure 5-8, assuming perfect frequency and phase synchronization.

The block diagram of this stage is shown in figure 5-9. Its objective is to amplify the signal at the output of the phase synchronization (hereafter denoted by r_k) such that the channel symbols at the demodulator input have power P_{ref}. Without loss of generality, P_{ref} was chosen so that channel symbols at the demodulator input would have unitary power; that is, $P_{\text{ref}} = 1 + 1/(E_s/N_0)$. It should be noted that the SNR estimator and DAGC operate

exclusively on the FM with removed modulation, that is, by performing a multiplication $r_k x^*_{\mathrm{p},k}$, where $x^*_{\mathrm{p},k}$ is the complex conjugate of the *k*th FM channel symbol.

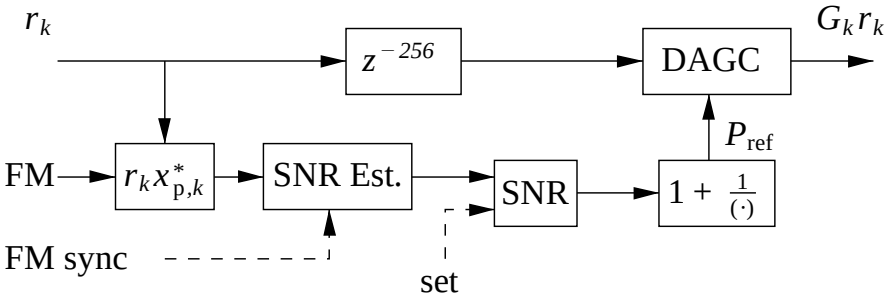

Figure 5-9: Detailed Block Diagram of the Combined Interaction between SNR Estimator and DAGC

For computing the SNR, a simple average power estimator was adopted as shown in figure 5-10. In particular, the average of the in-phase component of $r_k x^*_{\mathrm{p},k}$ (the real part of the complex baseband model) is proportional to the square root of the energy-per-channel-symbol, that is,

$$E\{\mathcal{R}(r_k x^*_{\mathrm{p},k})\} \propto \sqrt{E_{\mathrm{s}}} \ ,$$

while

$$E\{\mathcal{R}^2(r_k x^*_{\mathrm{p},k})\} \propto E_{\mathrm{s}} + N_0/2 \ .$$

Hence, combining the two expressions above, the SNR can be found as

$$SNR = \frac{E_{\mathrm{s}}}{N_0} = \frac{b^2}{2(a - b^2)} \ ,$$

where $a = E\{\mathcal{R}^2(r_k x^*_{\mathrm{p},k})\}$ and $b = E\{\mathcal{R}(r_k x^*_{\mathrm{p},k})\}$.

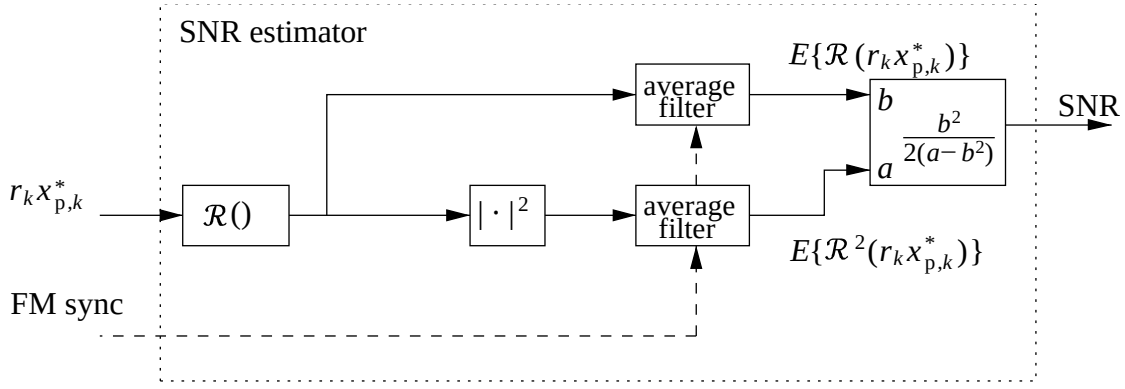

Figure 5-10: Adopted SNR Estimator

For the DAGC, a simple closed-loop algorithm was adopted as shown in figure 5-11. In particular, the gain G_k is updated as

$$G_k = G_{k-1} + e_k \gamma_{\mathrm{DAGC}} ,$$

where γ_{DAGC} is the open-loop gain, while e_k is the error, defined as

$$e_k = |G_k r_k|^2 - P_{\mathrm{ref}} .$$

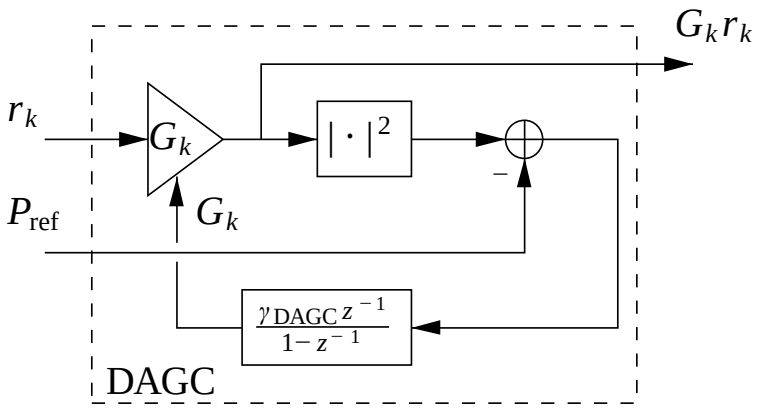

Figure 5-11: Adopted Closed-Loop DAGC

Assuming perfect synchronization of the previous stages, the joint SNR estimator and DAGC have been simulated.

Figure 5-12 shows the convergence of the adopted SNR estimation. The estimated SNR is compared with the real SNR by varying the number of PL frames N_F. It can be seen that, already at the first frame (i.e., by using only the first 256 FM channel symbols), the SNR estimator is able to provide a good estimation if $E_s/N_0 < 8$ dB, while for higher E_s/N_0, the estimation tends to diverge. It can be shown mathematically that this divergence is common to all SNR estimators, since an increase of the SNR makes the noise power level to be estimated more and more as negligible (reference [8]). Hence, for reducing the error, it is sufficient to adopt a higher number of frames, and already at 5-6 frames, the estimation is perfect in the full SNR range for all ACM formats.

Figures 5-13 and 5-14 show instead the convergence of the adopted closed-loop DAGC at low and high SNRs; namely, $E_s/N_0 = -1.4$ dB (equivalent to $E_b/N_0 \cong 0$ for ACM format 1) and $E_s/N_0 = -18.5$ dB (equivalent to $E_b/N_0 \cong 11.2$ for ACM format 27). The convergence has been analyzed for different closed-loop gain γ_{DAGC}. It is well known that for first-type closed-loops, the γ_{DAGC} is be selected as a trade-off between convergence speed and residual error (reference [9]). By means of a preliminary coarse optimization, $\gamma_{\mathrm{DAGC}} = 1/160$ has been found the best for limiting the noise and achieving convergence by means of a single frame (for all ACMs); that is, BER/CER curves show no losses with respect to the case with ideal synchronization.

Figures 5-15 and 5-16 show the CER when using the joint SNR estimator and DAGC. CER is shown as a function of the E_b/N_0 for a subset of the ACM formats, that is, ACM formats 1 and 6 (QPSK modulated), 12 (8PSK), 17 (16APSK), 22 (32APSK), and 27 (64APSK). For comparison, the CER with perfect synchronization is also shown (colored solid lines). It can be seen that the adopted algorithms are able to synchronize almost perfectly, with performance near optimal, while a poor selection of γ_{DAGC} can cause a non-negligible loss.

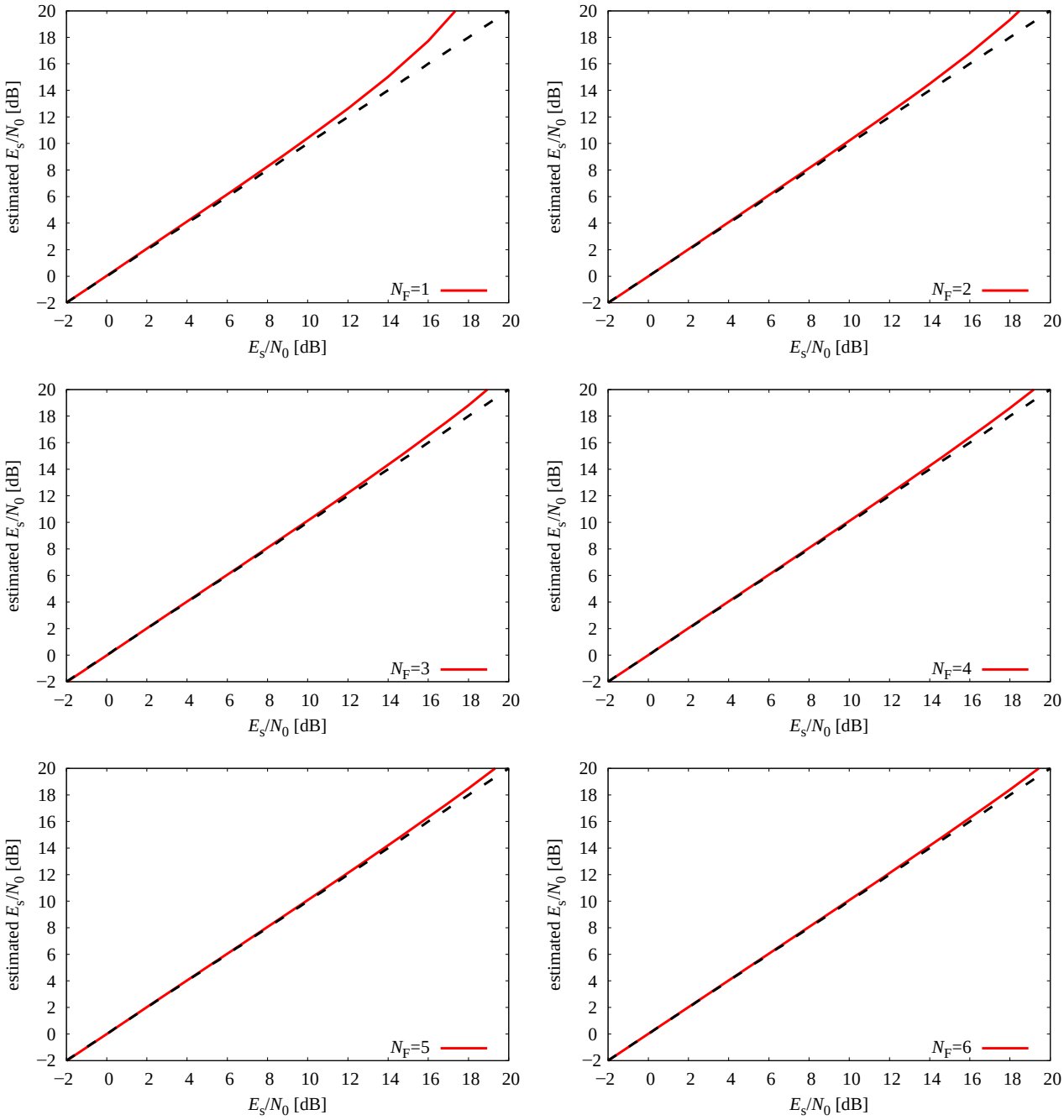

Figure 5-12: Estimated SNR versus Real SNR for Different Number of PL Frames Adopted

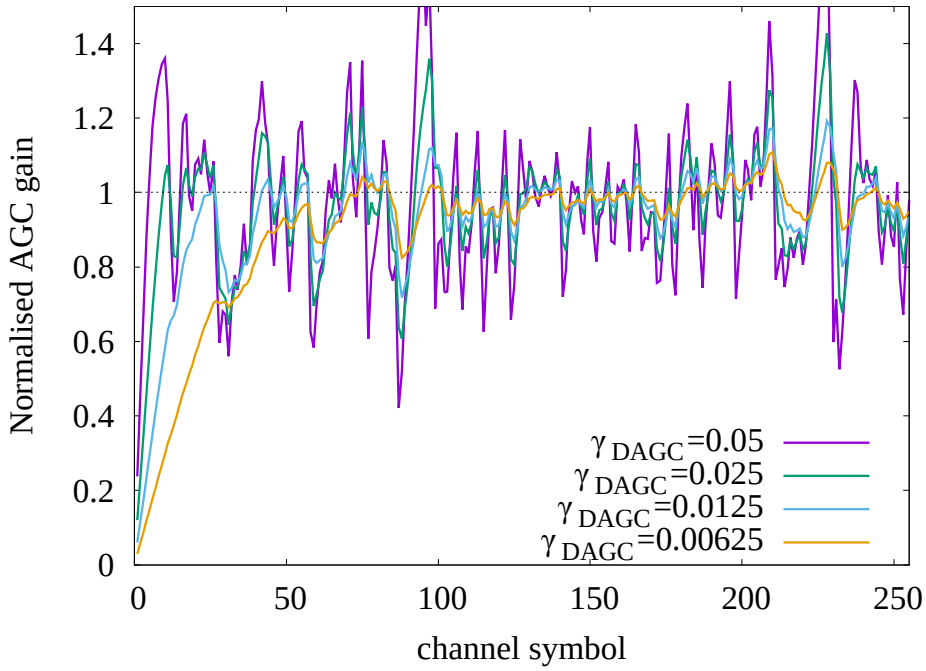

Figure 5-13: Convergence of the DAGC Gain at E_s/N_0 = −1.4 dB (E_b/N_0= 0.0 dB for ACM 1)

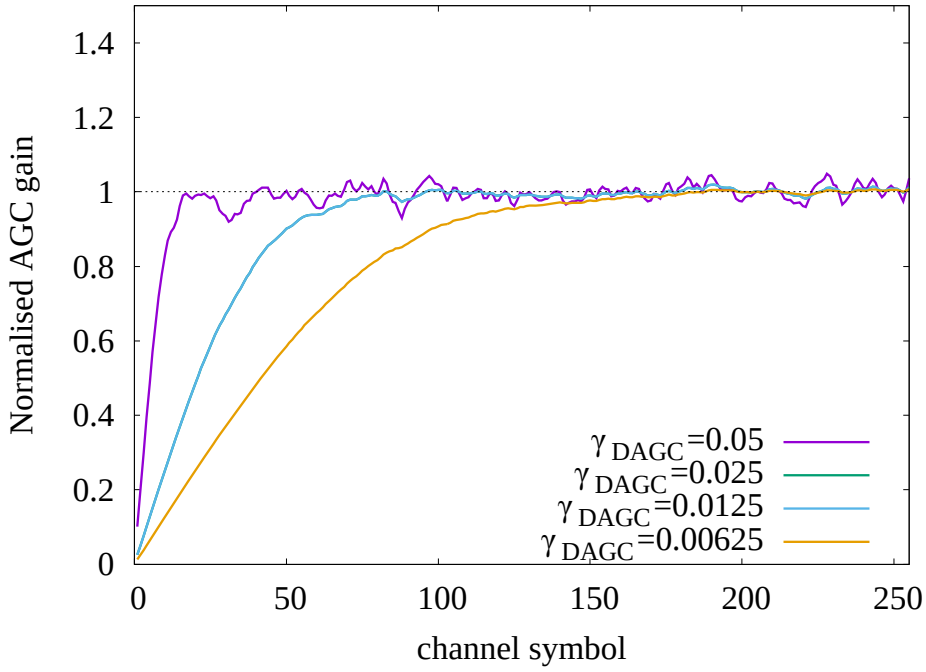

Figure 5-14: Convergence of the DAGC Gain at E_s/N_0= 18.5 dB (E_b/N_0=11.2 dB for ACM 27)

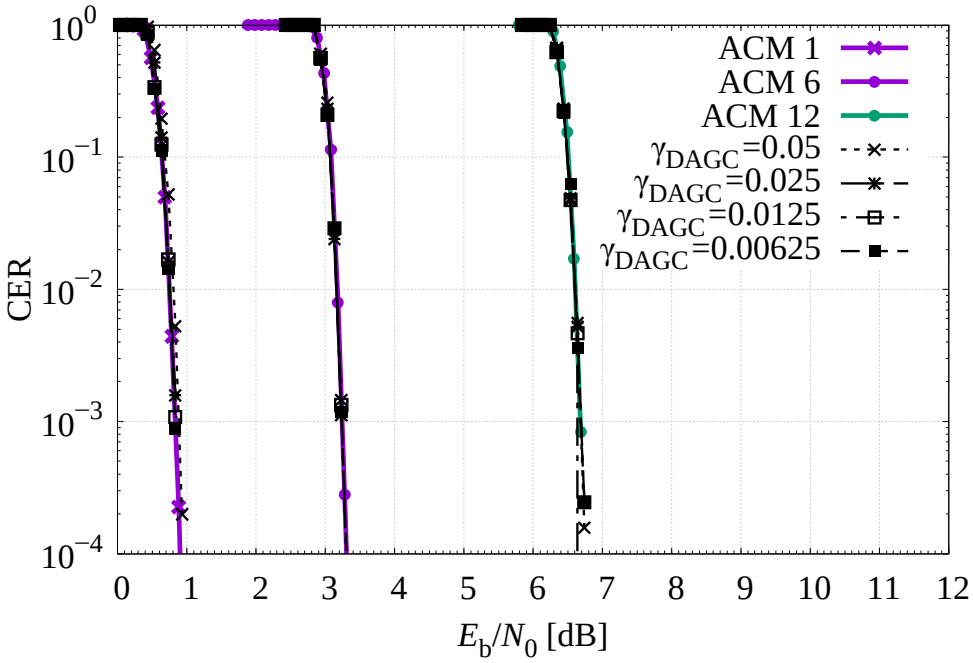

Figure 5-15: CER for ACM 1, 17, and 22 (PSK Modulations), for Different Values of the DAGC Loop Gain

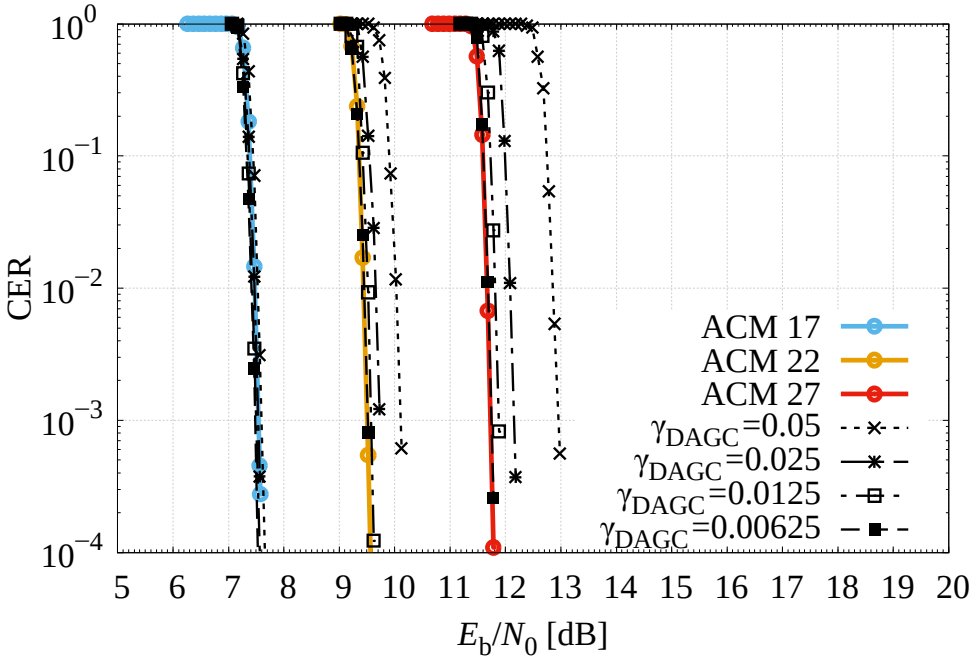

Figure 5-16: CER for ACM 1, 17, and 22 (APSK Modulations), for Different Values of the DAGC Loop Gain

5.6 PHASE SYNCHRONIZATION

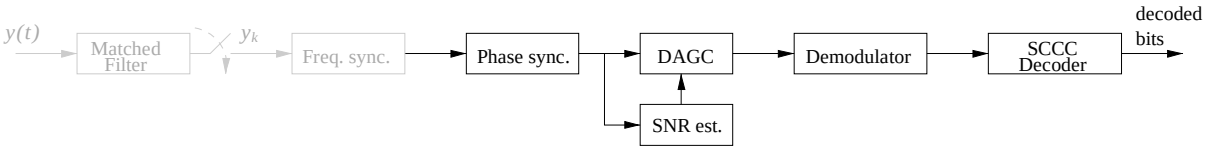

Figure 5-17: Highlight of the Section of the Synchronization Scheme That Is Analyzed for Phase Synchronization

In this subsection, the synchronization chain is analyzed and simulated starting at the input of the phase synchronizer, as shown in figure 5-17, assuming perfect frequency synchronization.

The adopted algorithm is based on a ML estimator operating on the frame marker and pilot fields. The estimated phase values are then linearly interpolated between fields. It is noted that this algorithm operates at PL frame level, and hence it can be carried out independently frame by frame.

Concerning the ML estimation, if $\{r_k\}$ is (with a little abuse of notation) the signal sampled at the input of the phase synchronizer, with $k = 1$ identifying the first channel symbol of the PL frame, the phases on each mth pilot field are estimated as

$$\theta_{\mathrm{p}}^{(m)} = \mathrm{angle}\left(\sum_{i=0}^{15} r_{k+i} x_{\mathrm{p},k+i}^{*}\right), \qquad \begin{matrix} m = 1, \ldots, 16 \\ k = 556m + 305 \end{matrix}.$$

Similarly, the phase estimation on the FM is carried out with the formula above by dividing the FM in blocks of 16 symbols each. This approach has been found to be a good trade-off for limiting the impact of possible residual frequency errors after frequency synchronization on the FM that is then adopted for SNR estimation.

Between two phase estimates (separated by 540 channel symbols), $\theta_{\mathrm{p}}^{(m)}$ and $\theta_{\mathrm{p}}^{(m+1)}$, a linear interpolation is performed. Hence the phase on the channel symbols can be estimated as

$$\theta_{k+\ell} = \frac{(\theta_{\mathrm{p}}^{(m+1)} - \theta_{\mathrm{p}}^{(m)})}{541}\ell + \theta_{\mathrm{p}}^{(m)} \quad , \quad \begin{matrix} k = 556m + 320 \\ \ell = 1, \ldots, 540 \end{matrix} \quad ,$$

where sum and subtraction are performed as modulo operation in the co-domain $(-\pi, \pi]$ for taking into account phase wraps (reference [10]).

Figure 5-18 shows a sketch on how the adopted phase synchronization algorithm works: Assuming a phase noise process as depicted in purple, the estimator provides a constant phase on the pilot fields, that is, $\theta_{\mathrm{p}}^{(1)}$, $\theta_{\mathrm{p}}^{(2)}$, …, which are then linearly interpolated, as shown by the green solid line. On the FM, as mentioned, the estimation is done instead in chunks of

16 channel symbols. Hence only the estimation provided by the last 16 FM channel symbols is then interpolated with $\theta_{\mathrm{p}}^{(1)}$.

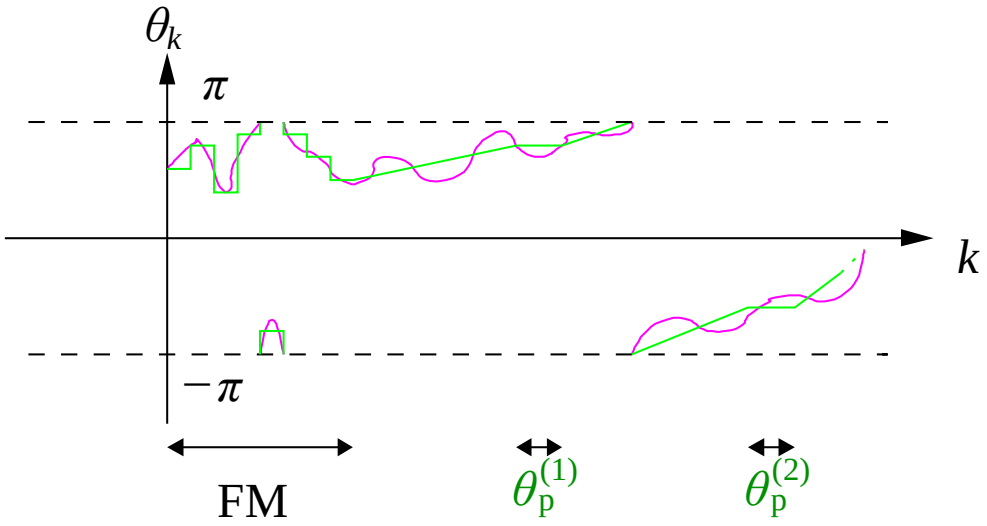

Figure 5-18: Sketch of the Phase Linear Interpolation

Figures 5-19 and 5-20 show the CER when using the phase synchronization algorithm discussed. CER is shown as a function of the E_b/N_0 for a subset of the ACM formats, that is, ACM formats 1 and 6 (QPSK modulated), 12 (8PSK), 17 (16APSK), 22 (32APSK), and 27 (64APSK). It can be seen that the adopted algorithm is able to synchronize with a loss between 0.2-0.4 dB with respect to AWGN with ideal synchronization.

It is interesting to note that by increasing the SNR, the loss from AWGN curves does not tend to decrease. In fact, although at higher SNR the phase estimation improves, the adopted ACM formats rely on high-cardinality APSK constellations and on SCCC with high-rate, thus providing less tolerance to phase errors. On the other hand, at low SNR, the adopted phase estimator provides a noisy estimation that is mitigated only thanks to low cardinality and low rate SCCC. This can be better seen from figures 5-21 to 5-24. In these figures, a realization of the phase noise is shown versus the phase estimated by the proposed algorithm at low SNR (E_b/N_0 = 1.3 dB for ACM format 1) and high SNR (E_b/N_0 = 12.3 dB for ACM format 27), and with and without a frequency shift (250 Hz, arbitrary value just for illustration purposes). At low SNR, the phase-estimator performance is very poor and tends to follow only low-frequency components, but as mentioned, the ACM format is well protected by QPSK with low rate SCCC. At high SNR, the phase estimator performance improves, but, as shown by CER curves, the ACM format is more sensitive to the residual phase error.

As already pointed out in previous sections, the phase synchronization can be improved; hence the proposed algorithm is not considered to be optimal. For instance, a possible alternative that could improve results for certain ModCods is the use of a Phase-Locked Loop (PLL) that is data-aided on FM and pilot fields and decision-directed on the other channel symbols.

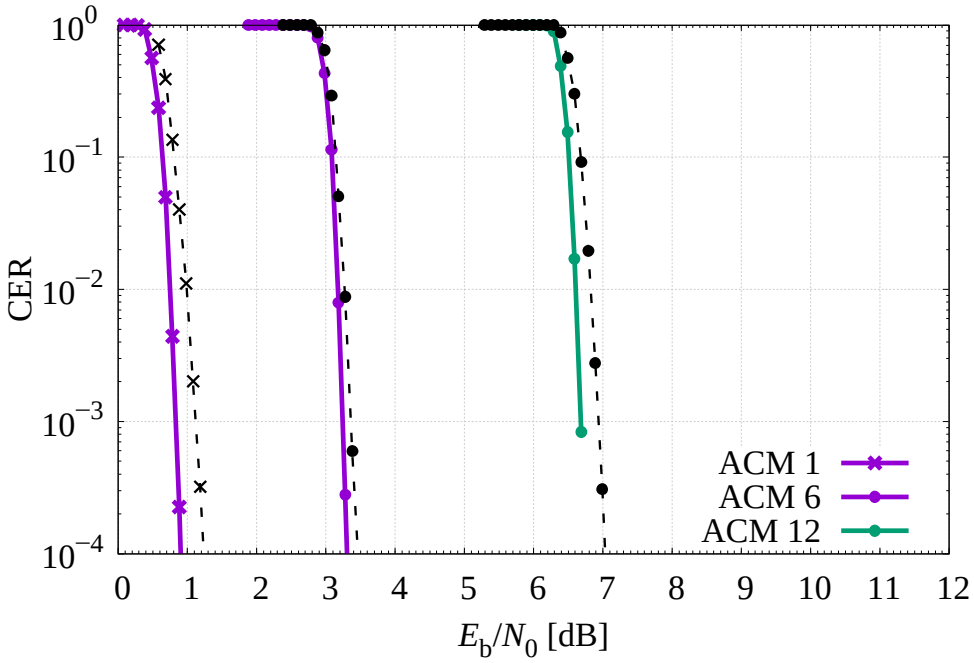

Figure 5-19: CER for ACM Format 1, 6, and 12 (PSK Modulations) in Presence of Phase Noise and Using a Phase Synchronizer with Linear Interpolation

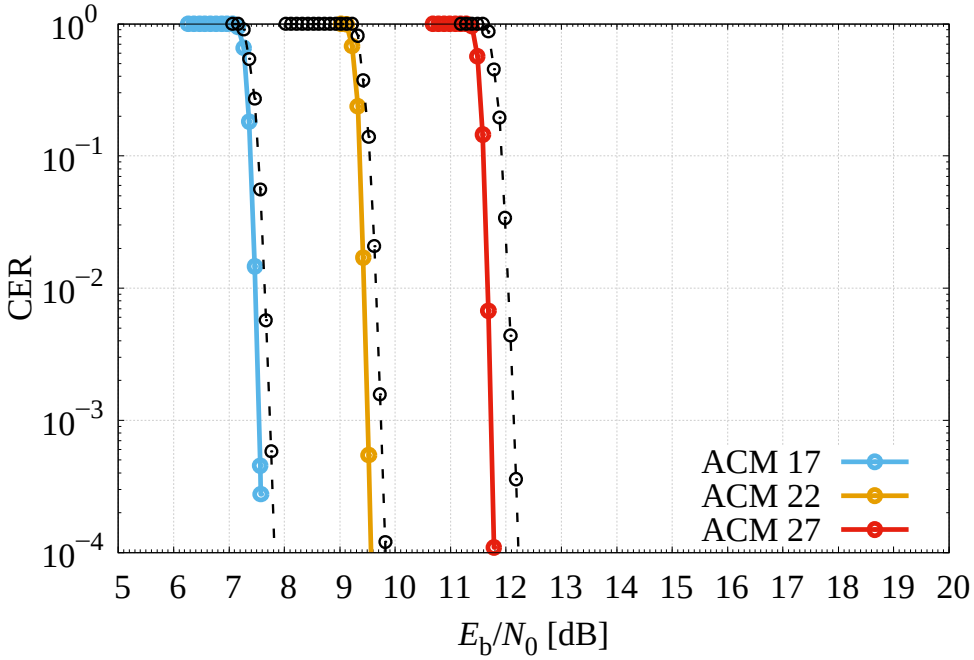

Figure 5-20: CER for ACM Format 17, 22, and 27 (APSK Modulations) in Presence of Phase Noise and Using a Phase Synchronizer with Linear Interpolation

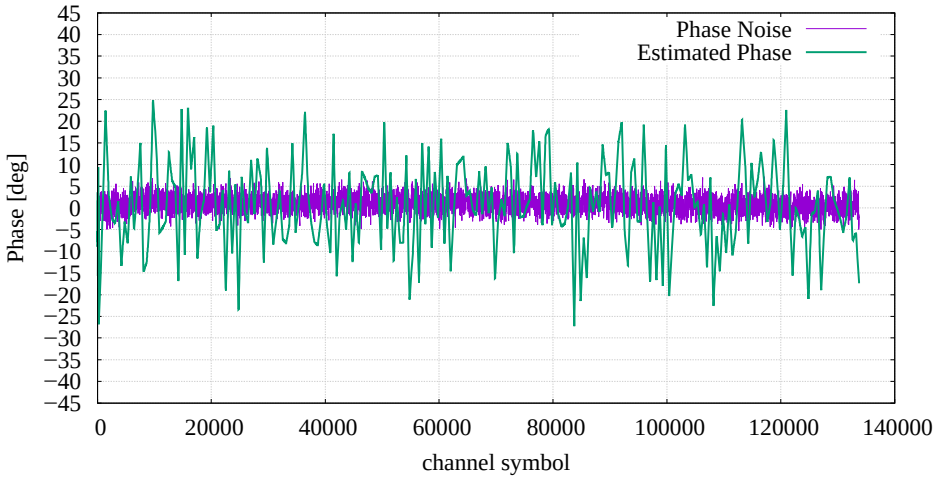

Figure 5-21: Phase Noise versus Tracked Phase for ACM 1 at E_b/N_0=1.3 dB

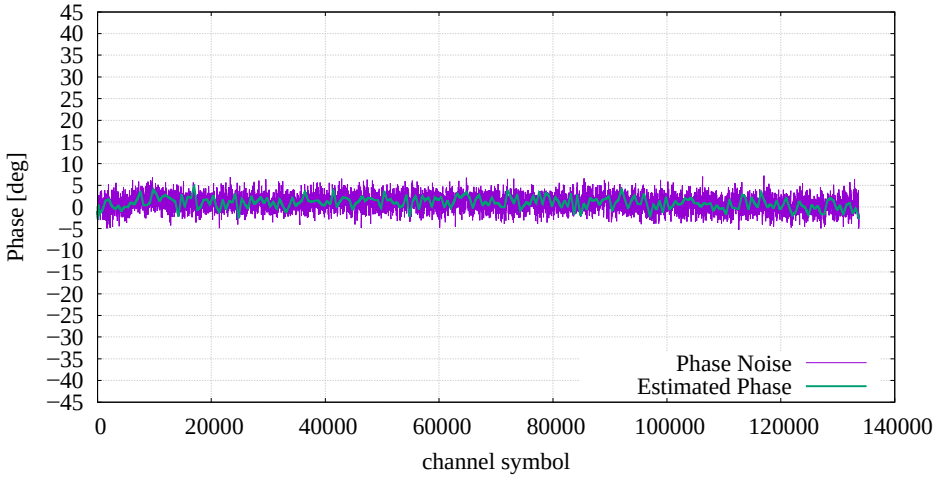

Figure 5-22: Phase Noise versus Tracked Phase for ACM 27 at E_b/N_0=12.3 dB

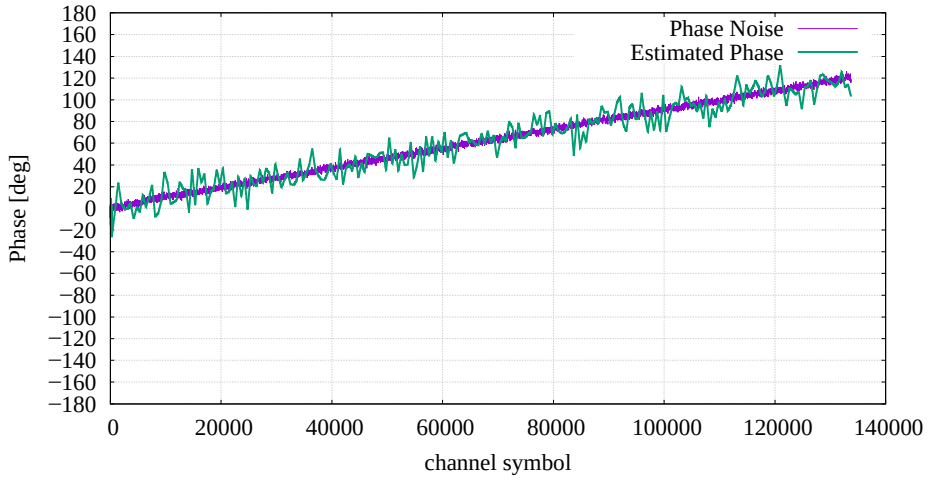

Figure 5-23: Phase Noise with Frequency Shift of 250 Hz, versus Tracked Phase for ACM 1 at E_b/N_0=1.3 dB

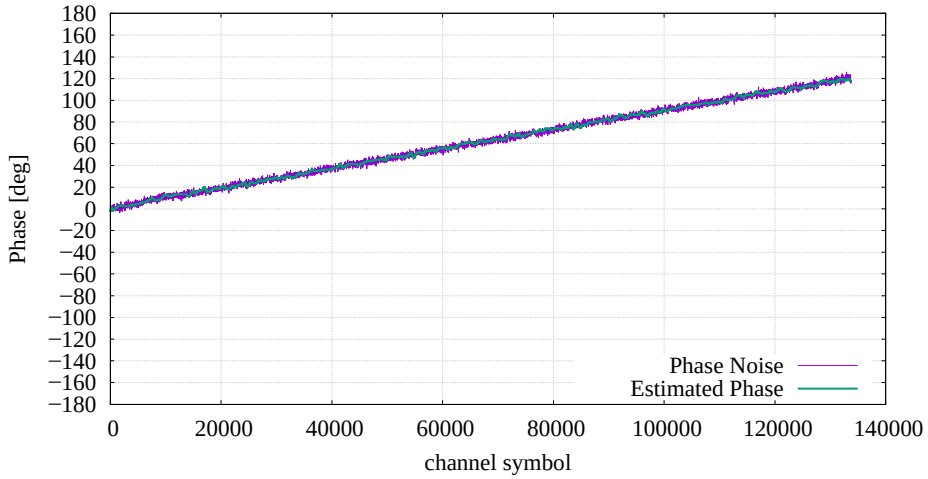

Figure 5-24: Phase Noise with Frequency Shift of 250 Hz, versus Tracked Phase for ACM 27 at E_b/N_0=12.3 dB

5.7 FREQUENCY SYNCHRONIZATION

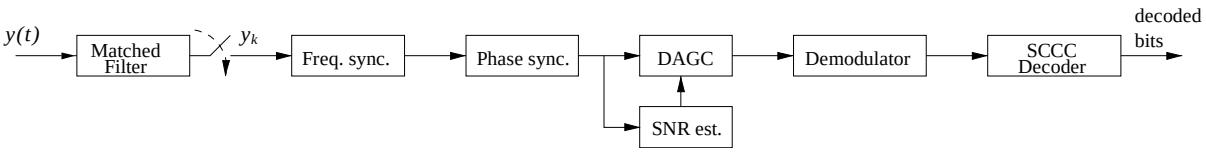

Figure 5-25: Synchronization Scheme That Is Analyzed for Frequency Synchronization

In this subsection, the frequency synchronization is analyzed for the chain shown in figure 5-25, in which all the following stages are the ones studied in previous sections.

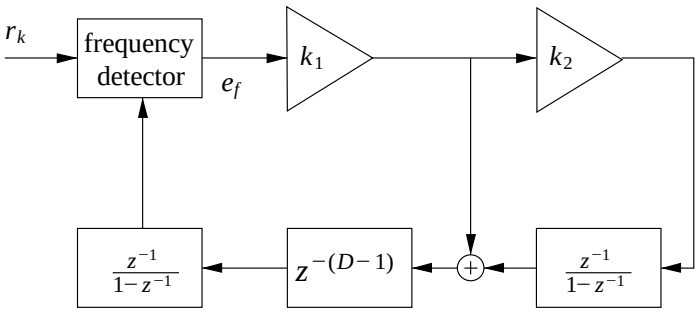

Figure 5-26: Adopted FLL

The adopted frequency synchronization algorithm is based on a digital second-type FLL working at frame level, as shown in figure 5-26. The frequency detector computes the error e_f between real and estimated frequency. The error is then fed to a loop filter, characterized by the gains k_1 and k_2 and excess delay equal to $D = 2$ (for taking into account a possible process delay of real implementations; see reference [9]). It should be noted that when $k_2 = 0$, the FLL is reduced to the first type.

With regard to the frequency detector, a Fast Fourier Transform (FFT) approach has been adopted. Namely, a FFT with 1024 points was done on the 256 channel symbols of the FM. With abuse of notation, if $\{r_k\}$ is defined as the sequence of samples at the input of the frequency synchronizer (with $k = 1$ identifying the first channel symbol of the PL frame under processing), the FFT operation reads

$$R_\ell = \sum_{k=1}^{256} r_k x_{\mathrm{p},k}^{*}\, e^{-j2\pi(k-1)\frac{\ell}{1024}} \quad , \qquad \ell = -511, \ldots, 0, \ldots, 512,$$

where $x_{\mathrm{p},k}^{*}$ is the complex conjugate of the kth FM channel symbol. The magnitude of R_ℓ provides information about the frequency bin cantered in $\ell R_{chs}/1024$. Hence the frequency error can be estimated as

$$e_f = \mathrm{argmax}_\ell |R_\ell|.$$

However, this method is limited by the resolution of the FFT. Hence, for improving the resolution of e_f, Newton interpolation is done around the maximum.

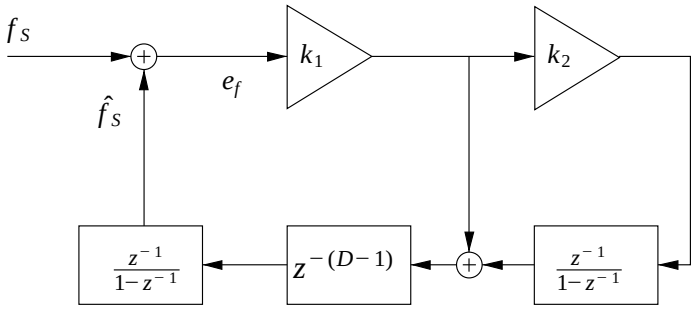

Figure 5-27: Linearized Scheme of the Adopted FLL

For this FLL, it can be demonstrated that the linearized equivalent scheme is the one shown in figure 5-27. Such FLL has a noise bandwidth B_L well approximated by the following formula (reference [9]):

$$B_{\mathrm{L}} \cong \frac{R_{\mathrm{FM}}}{4}(k_1 + k_2),$$

where R_{FM} is the number of FM (or PL frames) per second, that is, $R_{FM} = \mathrm{R_{chs}}/133760$ (when using pilot fields), while the SNR in the loop is given by

$$\mathrm{SNR_{FLL}} = \frac{E_{\mathrm{s}} R_{\mathrm{FM}} 256}{N_0 B_{\mathrm{L}}}.$$

Considering that for stability reasons, $(k_1 + k_2) < 1$, and that $E_s/N_0 > -0.6$ dB for all ACM formats (see AWGN results in 3.3), at 100 MBaud it holds that $B_L < 186.9$ Hz, hence

$$\mathrm{SNR_{FLL}} > 29.5 \text{ dB},$$

or in other terms, the adopted FLL works in almost noiseless conditions. This can be easily seen by the following figures. Figure 5-28 shows the theoretical convergence of the frequency error of the FLL linearized scheme for different k_1 ($k_2 = 0$ for the sake of simplicity), for constant Doppler shift. Figure 5-29 shows instead the convergence of the frequency error for the adopted FLL with an FFT-based frequency detector and when simulating the ACM format in noisy conditions ($E_s/N_0 = -0.9$ dB, that is, $E_b/N_0 = -0.6$ dB for ACM format 1). It can be seen that the real convergence has a perfect match with the theoretical convergence, proving that noise has no impact.

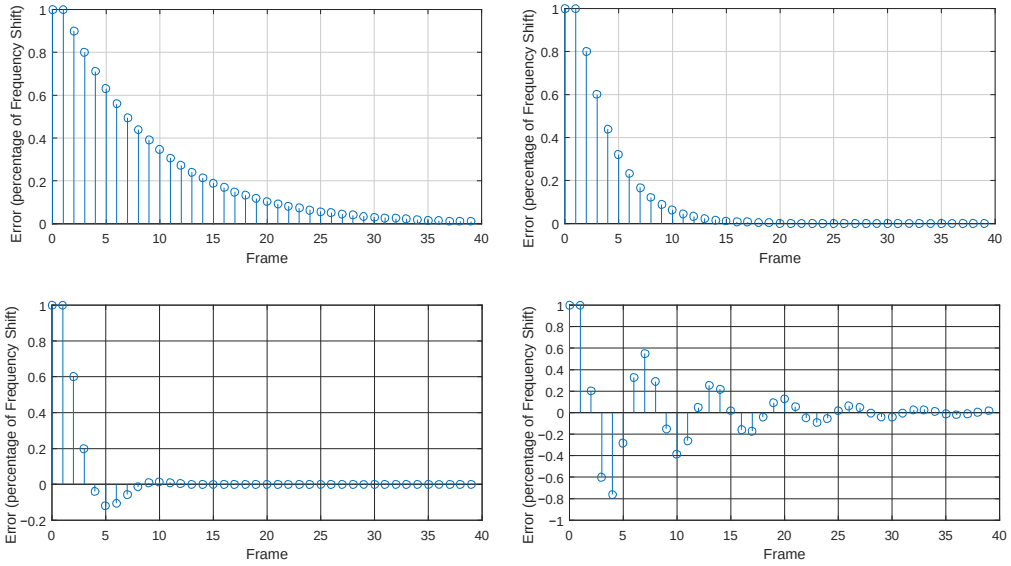

Figure 5-28: Theoretical Frequency Error Convergence (in Absence of Thermal Noise) for the Linearized Scheme When (Left to Right) k_1 is 0.1, 0.2, 0.4, and 0.8

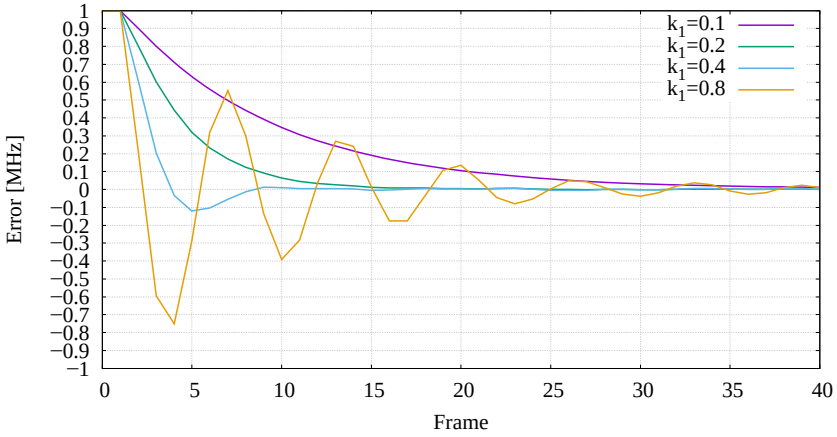

Figure 5-29: Simulated Frequency Error Convergence E_s/N_0 = −0.9 dB (E_b/N_0 = 0.6 dB for ACM1)

For tuning the FLL coefficients k_1 and k_2, the FLL has been tested with the Doppler profiles described in 5.2. For Doppler shifts up to 1 MHz, and Doppler rate 50 kHz/s, it has been found that an FLL of the first type $k_1 = 0.2$, $k_2 = 0$ is more than sufficient, since the residual error due to Doppler rate is compensated by the phase synchronizer. Hence, the FLL can be simplified in favor of the adopted phase synchronization algorithm. For the reader's reference, the detailed analysis of the FLL tuning is reported in annex A.

5.8 NUMERICAL RESULTS

The performance results of the Recommended Standard's modulation and coding scheme has been evaluated over the AWGN channel affected by the phase noise and Doppler of 5.2, and with the synchronization chain described in previous sections.

Figures 5-30 and 5-31 show the CER as function of the E_b/N_0 for a subset of the ACM formats, that is, ACM formats 1 and 6 (QPSK modulated), 12 (8PSK), 17 (16APSK), 22 (32APSK), and 27 (64APSK). For comparison, the CER with perfect synchronization is also shown (colored solid lines). It can be seen that the adopted algorithms are able to synchronize with a performance loss between 0.2-0.4 dB (at CER=1e−4) with respect to AWGN with ideal synchronization. Finally, it is noted that CER has been computed also adopting the triangular Doppler profile, and identical results were found.

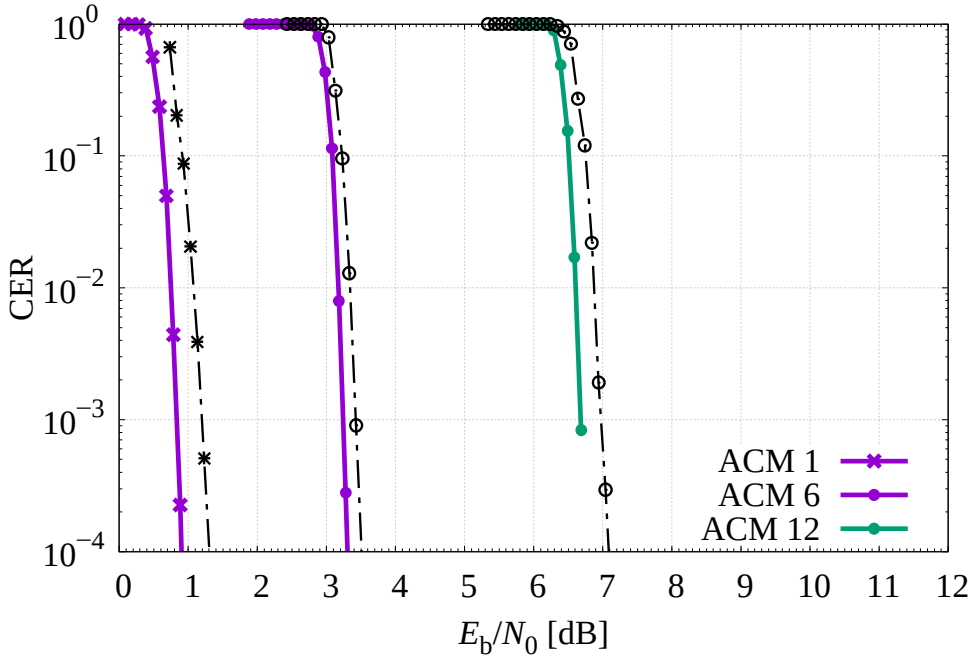

Figure 5-30: CER for ACM Format 1, 6, and 12 (PSK Modulations) in Presence of Sinusoidal Doppler Profile (f_D = 1 MHz, f_R = 50 kHz/sec) and Phase Noise When Using the Described Synchronization Chain

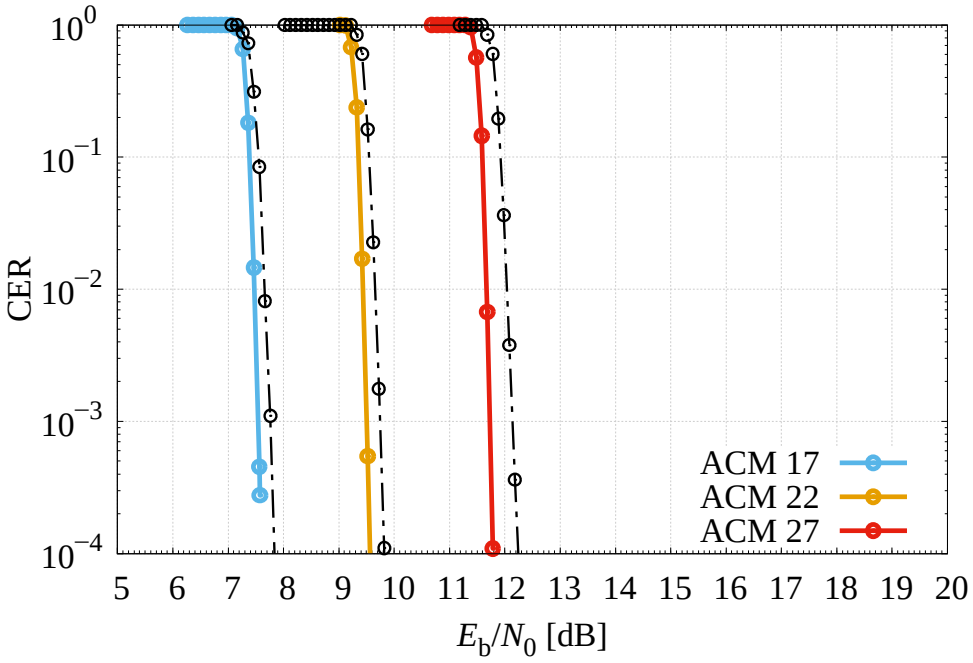

Figure 5-31: CER for ACM Format 17, 22, and 27 (APSK Modulations) in Presence of Sinusoidal Doppler Profile (f_D = 1 MHz, f_R = 50 kHz/sec) and Phase Noise When Using the Described Synchronization Chain

6 END-TO-END SIMULATIONS

6.1 INTRODUCTION

In this section, the performance of the recommended codes and modulations is evaluated by means of end-to-end simulations. In particular, this section considers the nonlinear channel of section 4 and the synchronization chain of section 5. The optimal Input and IBO/OBO is re-verified by means of the total degradation provided in 6.2. This is done to verify the possible increase of the required back-off for making the synchronization chain work in the presence of nonlinear distortions. Then, performance is assessed for all 27 ACM formats in 6.3, where it is also shown how pre-distortion can improve the performance, especially for ACMs 13-27, which use APSK modulations.

6.2 TOTAL DEGRADATION

As in section 4, the adopted total degradation definition for end-to-end simulations is defined as

$$\mathrm{TD} = \left(\frac{E_\mathrm{b}}{N_0} + \mathrm{OBO}\right)_{\mathrm{E2E}} - \left(\frac{E_\mathrm{b}}{N_0}\right)_{\mathrm{AWGN}} \quad [\mathrm{dB}],$$

where $\left(\frac{E_\mathrm{b}}{N_0} + \mathrm{OBO}\right)_{\mathrm{E2E}}$ is the SNR and OBO required for obtaining a specific target CER with the assumed channel model and receiver. The value $\left(\frac{E_\mathrm{b}}{N_0}\right)_{\mathrm{AWGN}}$ instead represents the SNR required on the ideal AWGN channel with ideal synchronization to achieve the same target CER. A target CER equal to 10^{-4} has been adopted. It should be noted that, differently from in section 4, TD provides a useful representation of the overall losses experienced by the link in terms of distortion as well as reduced available power due not only to the back-off but also the synchronization in the presence of phase noise and Doppler. Hence, the optimal IBO/OBO is found as the value that minimizes TD (see 4.3 for optimization examples).

6.3 NUMERICAL RESULTS

6.3.1 TOTAL DEGRADATION AND ERROR RATE CURVES

Figure 6-1 shows the total degradation for a subset of the ACM formats as a function of the IBO, in particular, ACM formats 1 and 6 (QPSK modulated), 12 (8PSK), 17 (16APSK), and 22 (32APSK). For comparison, the total degradation with ideal synchronization (results of 4.4.1) has been reported. From the figure, it can be seen that optimal IBO/OBO is approximately still the same as the one found when using ideal synchronization. On the other hand, a performance loss between 0.2 dB and 0.8 dB is found resulting from the synchronization in the presence of phase noise, Doppler, and nonlinear distortions.

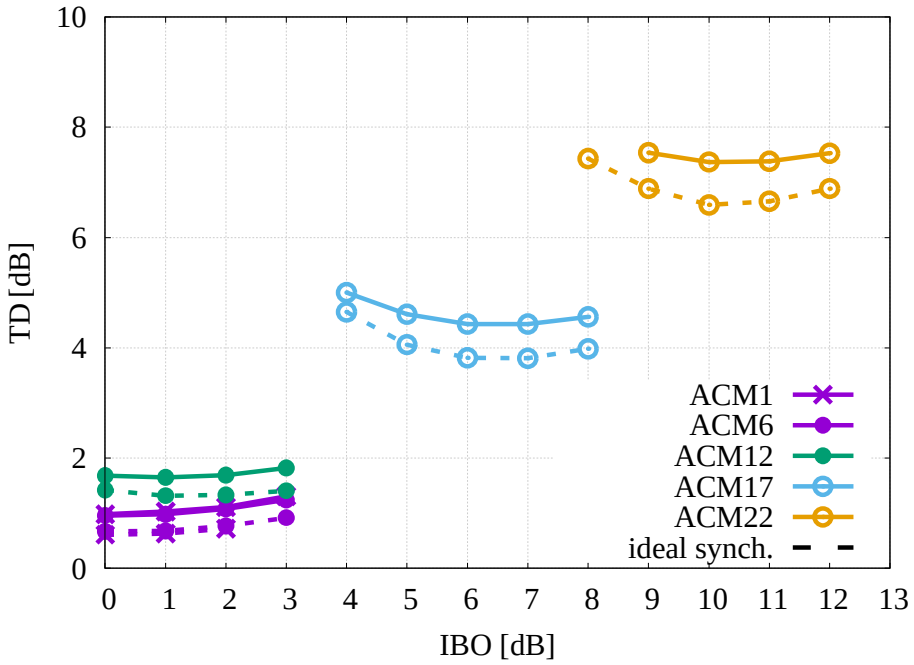

Figure 6-1: TD (End-to-End) for ACM Formats 1, 6, 12, 17, and 22

Different conclusions were found for the ACM formats from 23 to 27, which are based on the 64APSK. Figure 6-2 shows the total degradation as a function of IBO compared with ideal synchronization (results of 4.4.1). It can be seen that the synchronization chain for the 64APSK is highly penalized by nonlinear effects, and that even increasing the back-off, losses as high as 2 dB can be experienced. The reason for such a penalty has been found in the phase synchronizer. In particular, the adopted phase synchronization algorithm relies on the estimation done on the FM and pilots whose I/Q amplitude with respect to 64APSK channel symbols is as shown in figure 6-3. Hence after phase synchronization, the I/Q samples (see figure 6-3) of the intermediate circles will be well aligned with respect the original constellation, while the external circle (representing 43 percent of the probability) will be misaligned. As further evidence, the CER for the ACM format 27 has been computed in figure 6-4 when different impairments are enabled step by step. It can be seen that the figure confirms that the loss is mostly due to the phase synchronization in presence of nonlinearities, while the fraction of loss due to phase noise is similar to the one seen in the linear channel in 5.6. Hence for 64APSK, the use of pre-distortion at the transmitter (discussed in next section) appears almost mandatory.

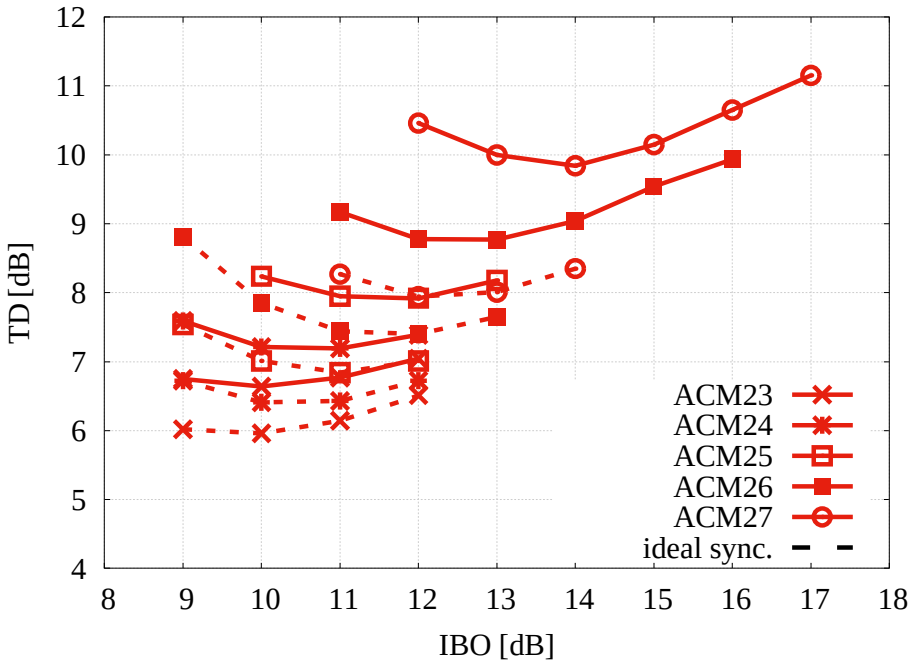

Figure 6-2: TD (End-to-End) for ACM Formats from 23 till 27 (64APSK)

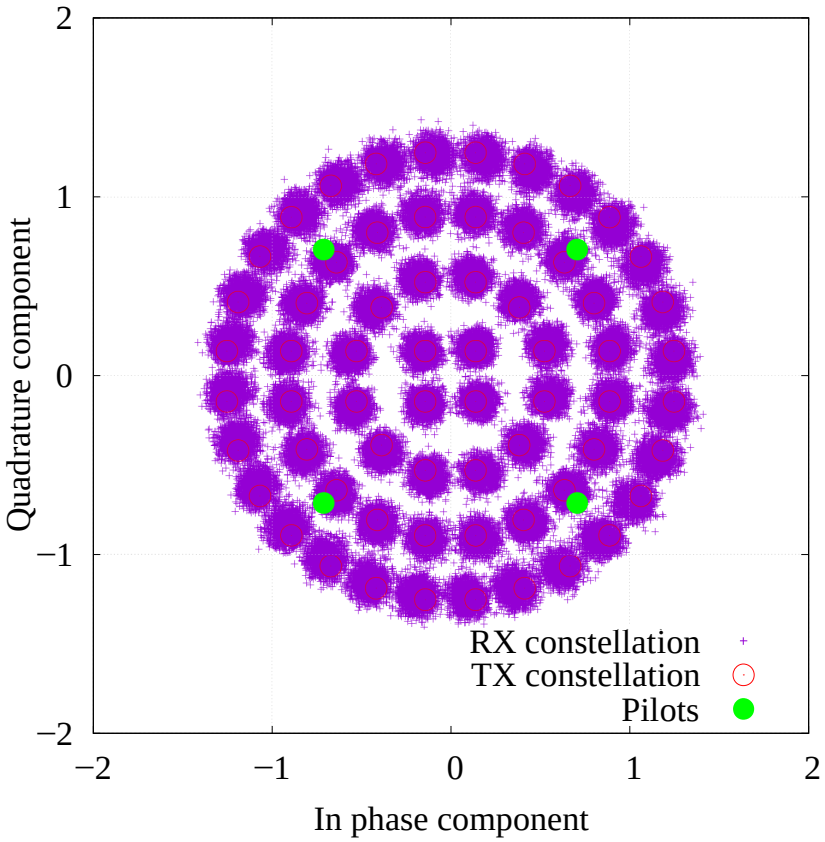

Figure 6-3: Scattering at the Demodulator Input for ACM27 at E_b/N_0=17.5 dB, IBO=14 dB

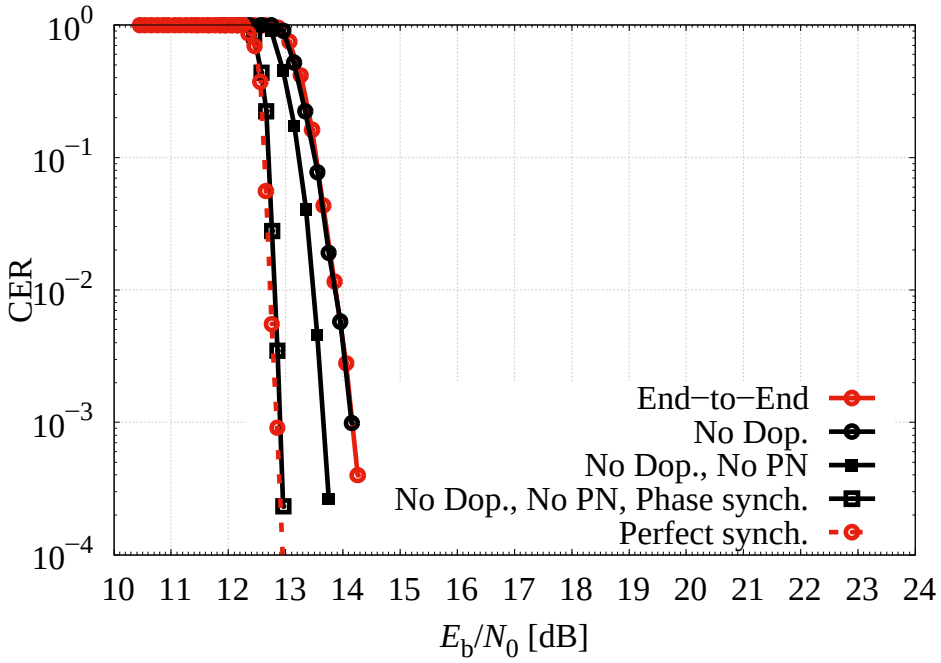

Figure 6-4: CER for ACM Format 27, IBO=14 dB, for Different Impairments

In figures 6-5 to 6-8, the BER and CER are shown for all the possible ACM formats using the optimal IBO found by means of the total degradation analysis. The corresponding SNR thresholds for CER equal to 10^{-4} and OBO for each individual ACM mode (to be taken into account when performing system level design) can be found in table 6-1.

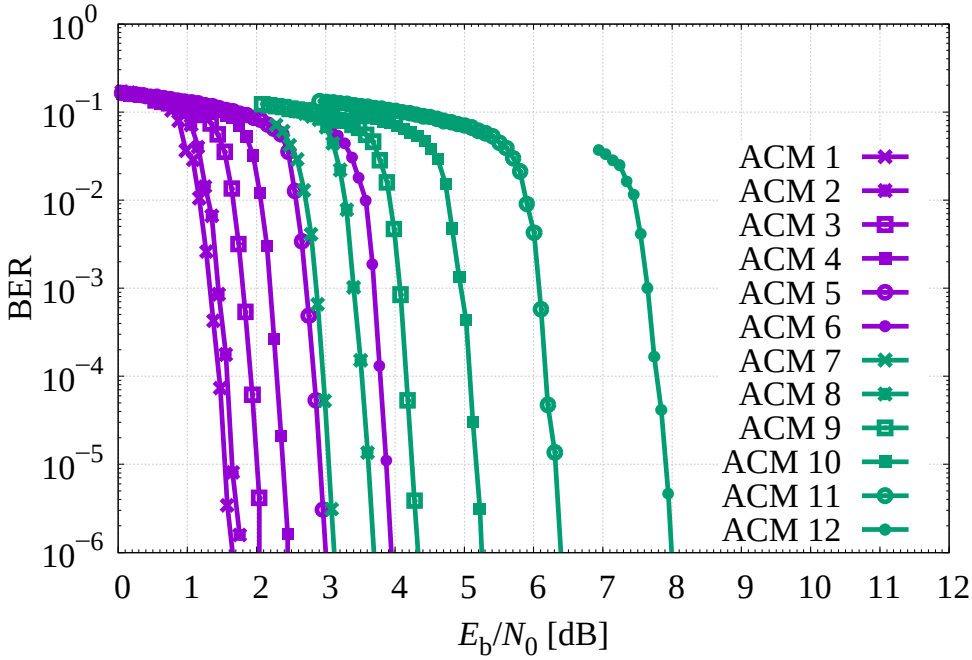

Figure 6-5: BER (End-to-End) for ACM Formats from 1 to 12 (PSK Modulations) with the Optimal IBO

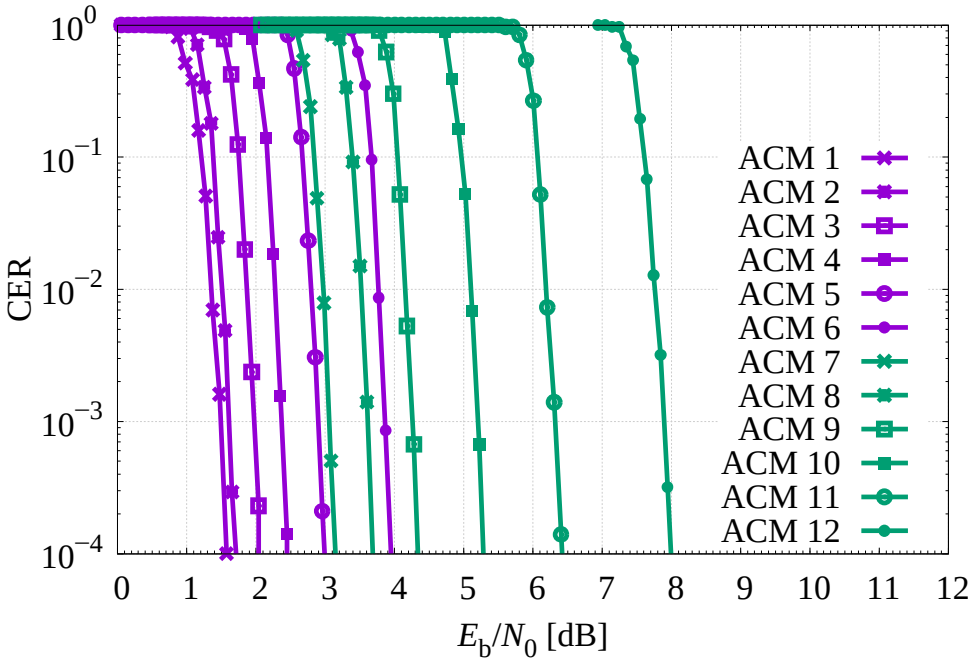

Figure 6-6: CER (End-to-End) for ACM Formats from 1 to 12 (PSK Modulations) with the Optimal IBO

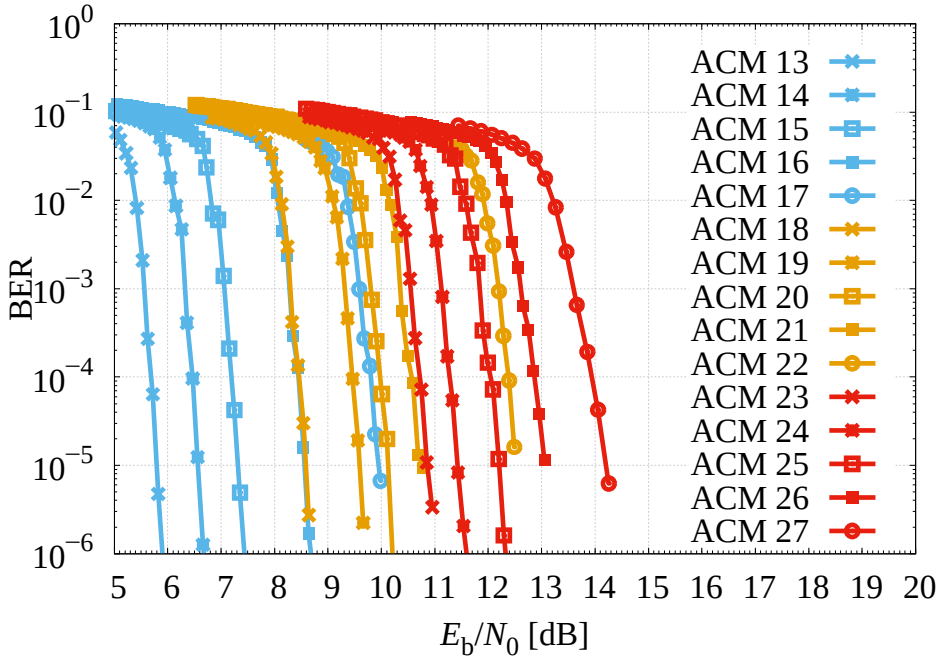

Figure 6-7: BER (End-to-End) for ACM Formats from 13 to 27 (APSK Modulations) with the Optimal IBO

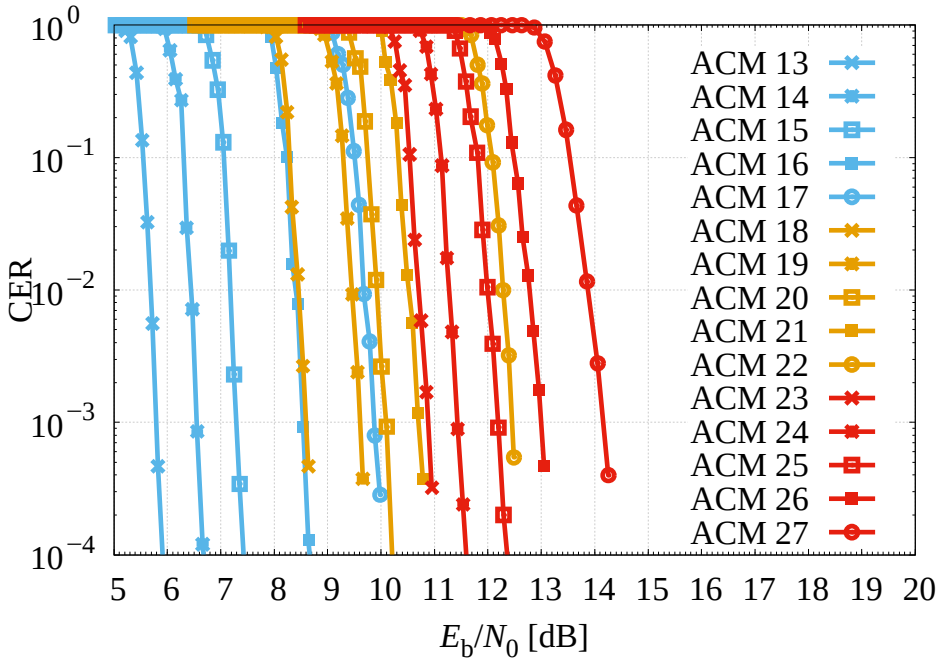

Figure 6-8: CER (End-to-End) for ACM Formats from 13 to 27 (APSK Modulations) with the Optimal IBO

Table 6-1: SNR Thresholds for CER=1e−4 and Corresponding OBO, TD, and Bandwidth (for SRRC Roll-Off 0.35 after RF Filtering), Achieved by the Recommended ACM Formats with SRRC Roll-Off 0.35 in End-to-End Simulations and without Pre-Distortion

	ACM	E_s/N_0 [dB]	E_b/N_0 [dB]	OBO [dB]	TD [dB]	Bandwidth
QPSK	1	0.08	1.57	0.32	0.98	$1.29 \cdot R_{chs}$
	2	1.04	1.70	0.32	0.94	$1.29 \cdot R_{chs}$
	3	2.22	2.05	0.32	0.94	$1.29 \cdot R_{chs}$
	4	3.29	2.47	0.32	0.90	$1.29 \cdot R_{chs}$
	5	4.42	2.99	0.32	0.91	$1.29 \cdot R_{chs}$
	6	6.06	3.94	0.32	0.96	$1.29 \cdot R_{chs}$
8PSK	7	4.57	3.14	0.29	0.95	$1.29 \cdot R_{chs}$
	8	5.80	3.68	0.29	0.99	$1.29 \cdot R_{chs}$
	9	6.97	4.32	0.29	1.01	$1.29 \cdot R_{chs}$
	10	8.50	5.28	0.36	1.11	$1.27 \cdot R_{chs}$
	11	10.15	6.41	0.36	1.30	$1.27 \cdot R_{chs}$
	12	12.19	7.97	0.36	1.65	$1.27 \cdot R_{chs}$
16APSK	13	9.62	5.87	1.34	2.78	$1.24 \cdot R_{chs}$
	14	10.87	6.65	1.34	2.97	$1.24 \cdot R_{chs}$
	15	12.01	7.39	1.63	3.30	$1.23 \cdot R_{chs}$
	16	13.68	8.63	1.63	3.76	$1.23 \cdot R_{chs}$
	17	15.46	10.02	1.99	4.43	$1.21 \cdot R_{chs}$
32APSK	18	13.77	8.72	3.12	5.43	$1.20 \cdot R_{chs}$
	19	15.15	9.71	3.12	5.75	$1.20 \cdot R_{chs}$
	20	16.00	10.18	3.68	6.19	$1.19 \cdot R_{chs}$
	21	17.04	10.90	4.27	6.69	$1.18 \cdot R_{chs}$
	22	19.14	12.66	4.27	7.37	$1.18 \cdot R_{chs}$
64APSK	23	17.17	11.02	4.21	6.64	$1.18 \cdot R_{chs}$
	24	18.05	11.57	4.88	7.19	$1.18 \cdot R_{chs}$
	25	19.14	12.36	5.61	7.92	$1.17 \cdot R_{chs}$
	26	20.22	13.17	6.40	8.77	$1.17 \cdot R_{chs}$
	27	21.72	14.40	7.22	9.84	$1.17 \cdot R_{chs}$

6.3.2 STATIC PRE-DISTORTION

The total degradation can be effectively decreased by means of pre-distortion for those ACM formats using APSK modulations (17-27). A static data pre-distorter (at the transmitter), as the one in reference [3], was assumed for the simulations presented in this section. Such pre-distortion is basically a simple look-up table that transmits the constellation symbols with a fixed correction of the radii amplitudes and phases (computed off-line).

Figure 6-9 shows the total degradation for a subset of the ACM formats as a function of the IBO, in particular ACM formats 17 (16APSK), 22 (32APSK), and 27 (64APSK). For comparison, the total degradation with ideal synchronization (results of 4.4.2) and without pre-distortion (previous section) have been reported. From the figure, it can be seen that when using pre-distortion, the optimal IBO/OBO is approximately the same derived for ideal synchronization. In particular, an increase of 0.6 dB in OBO has been found as worst case. On the other hand, a performance loss between 0.7 dB and 1.0 dB has been found resulting from the synchronization when in presence of phase noise, Doppler, and nonlinear distortions.

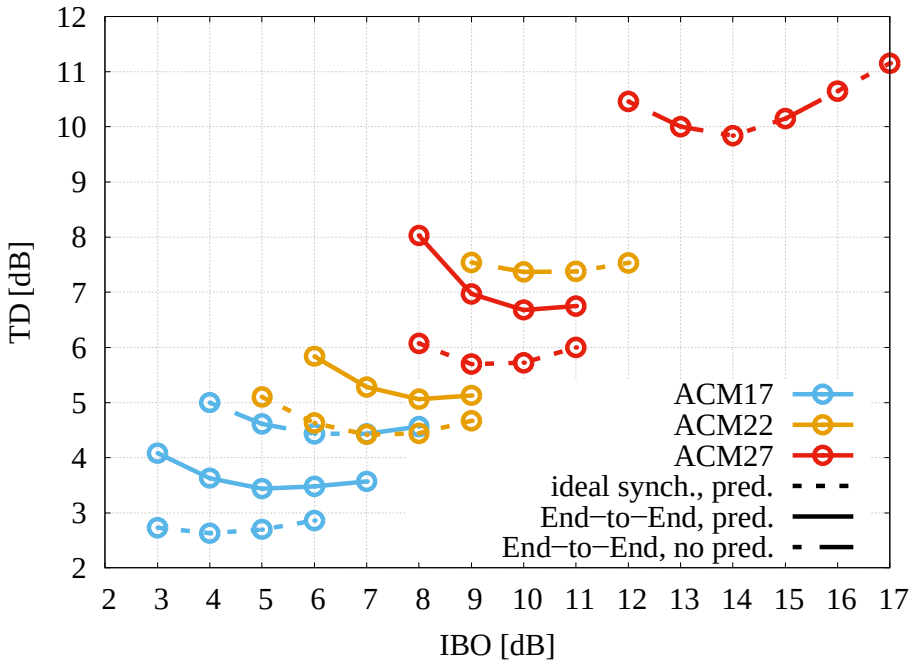

Figure 6-9: TD (End-to-End) for ACM Formats 17, 22, and 27, with Pre-Distortion

Similarly to the previous subsection, the loss from ideal synchronization was investigated in detail. In particular, the loss with respect to ideal synchronization has been found to be due to two main components, the presence of phase noise and the use of a phase synchronizer operating on the FM and pilots (see previous section for detailed discussion on the phase synchronizer). This is proven by the example in figure 6-10 that shows the CER for ACM format 27 when the different impairments are enabled one by one.

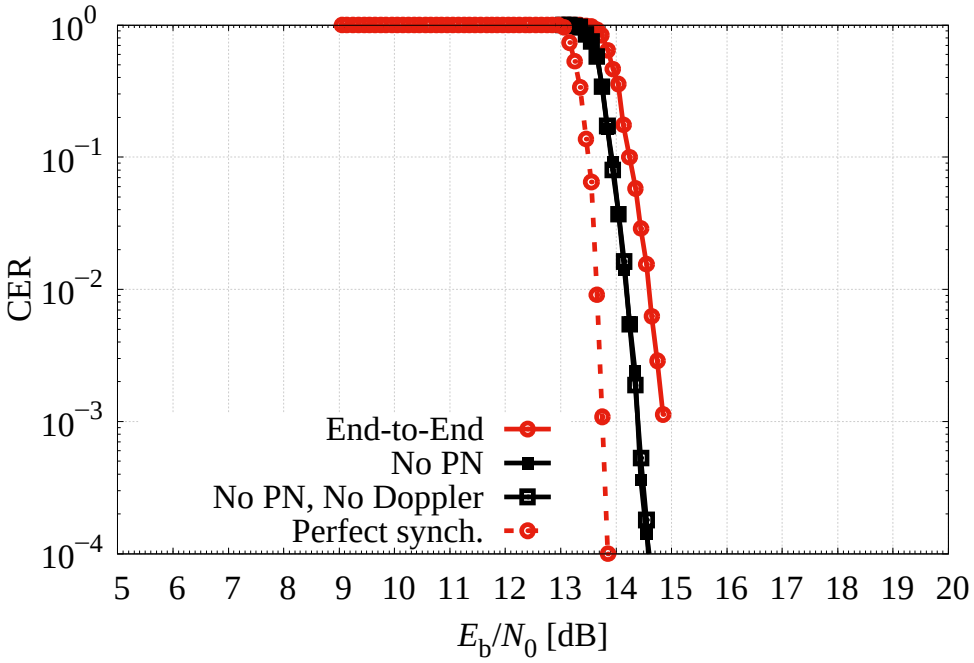

Figure 6-10: CER for ACM Format 27, with Static Pre-Distortion, IBO=9 dB, for Different Impairments

Figures 6-11 and 6-12 and show the BER and CER for all the possible ACMs using the optimal IBO found by means of the total degradation analysis. Finally, the SNR values for APSK modulations that allow a CER equal to 10^{-4} when static pre-distortion is adopted are summarized in table 6-2. Also reported in the table are the corresponding OBO, total degradation TD, and its gain with respect to the scenario without pre-distortion (i.e., table 6-1).

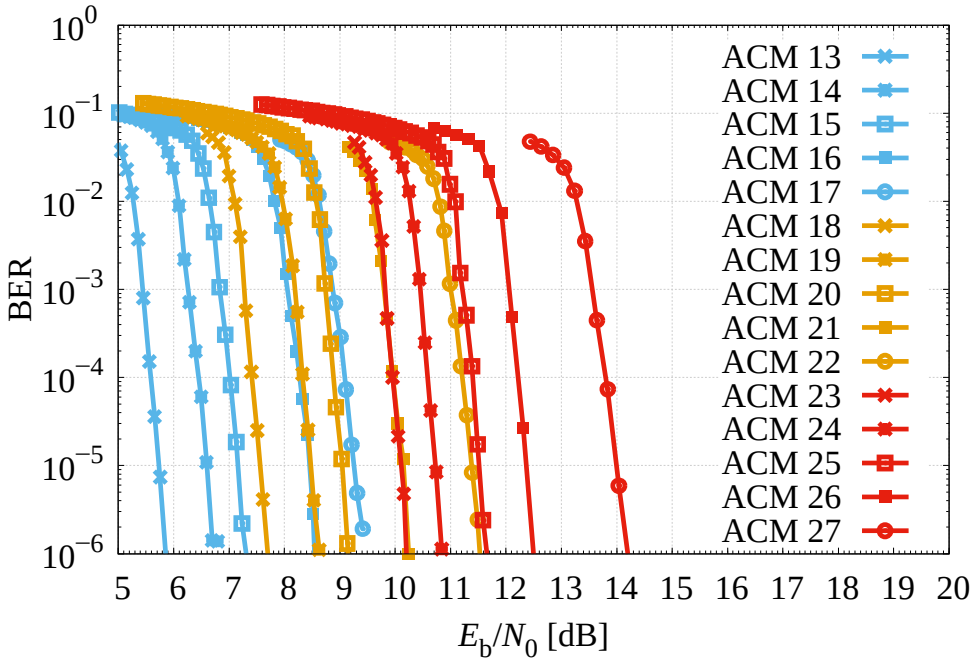

Figure 6-11: BER (End-to-End), with Static Pre-Distortion, for ACM Formats from 13 to 27 (APSK Modulations) with the Optimal IBO

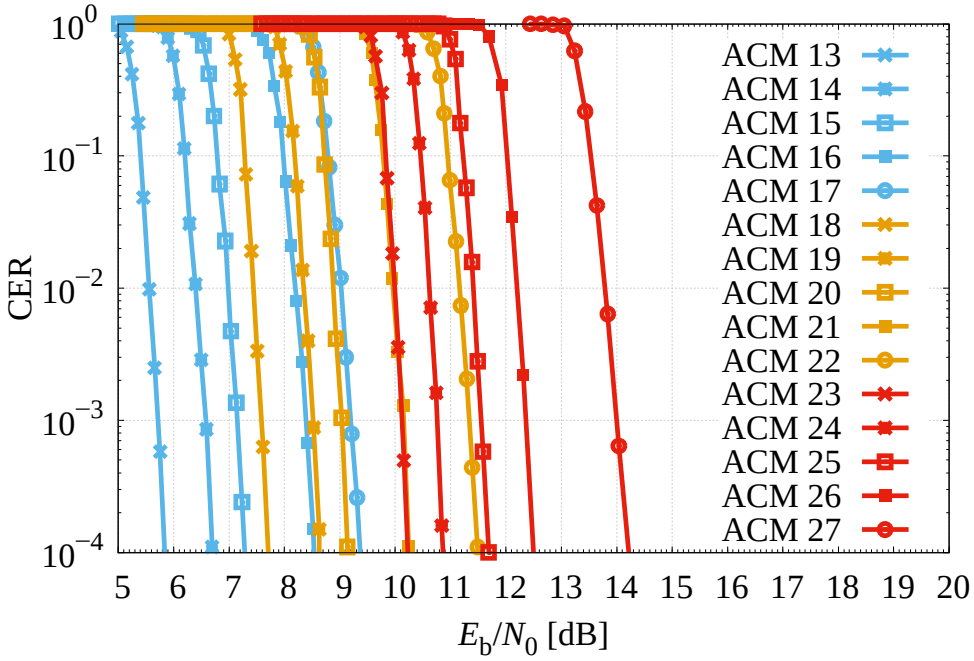

Figure 6-12: CER (End-to-End), with Static Pre-Distortion, for ACM Formats from 13 to 27 (APSK Modulations) with the Optimal IBO

Table 6-2: SNR Thresholds for CER=1e−4, and Corresponding OBO, TD, and Bandwidth (for SRRC Roll-Off 0.35 after RF Filtering), Achieved by the Recommended ACM Formats with SRRC Roll-Off 0.35 in End-to-End Simulations and with Pre-Distortion

	ACM	E_s/N_0 [dB]	E_b/N_0 [dB]	OBO [dB]	TD [dB]	TD Gain [dB]	Bandwidth
16APSK	13	9.59	5.84	0.99	2.40	0.38	$1.31 \cdot R_{chs}$
	14	10.92	6.70	0.99	2.67	0.30	$1.31 \cdot R_{chs}$
	15	11.91	7.28	1.14	2.71	0.59	$1.27 \cdot R_{chs}$
	16	13.14	8.08	1.36	2.95	0.82	$1.24 \cdot R_{chs}$
	17	14.81	9.37	1.65	3.44	0.99	$1.23 \cdot R_{chs}$
32APSK	18	12.75	7.70	2.34	3.63	1.79	$1.22 \cdot R_{chs}$
	19	14.08	8.64	2.34	3.90	1.85	$1.22 \cdot R_{chs}$
	20	14.97	9.15	2.74	4.22	1.97	$1.21 \cdot R_{chs}$
	21	16.36	10.21	2.74	4.48	2.21	$1.21 \cdot R_{chs}$
	22	17.96	11.49	3.14	5.06	2.30	$1.20 \cdot R_{chs}$
64APSK	23	16.39	10.24	2.59	4.25	2.39	$1.20 \cdot R_{chs}$
	24	17.34	10.87	3.08	4.68	2.50	$1.20 \cdot R_{chs}$
	25	18.48	11.69	3.62	5.27	2.65	$1.19 \cdot R_{chs}$
	26	19.56	12.52	4.23	5.94	2.83	$1.18 \cdot R_{chs}$
	27	21.54	14.22	4.24	6.68	3.16	$1.18 \cdot R_{chs}$

7 TEST RESULTS

In this section, results of the compatibility testing between one transmitter and one receiver implementing CCSDS 131.2-B are reported. Out of the transmitter/receiver models developed under ESA contracts or other means, the tests reported herein refer to an Engineering Model transmitter (see figure 7-1) developed by Tesat Spacecomm (DE) and one receiver developed by Konsberg Spacetec (NO) (reference [11]).

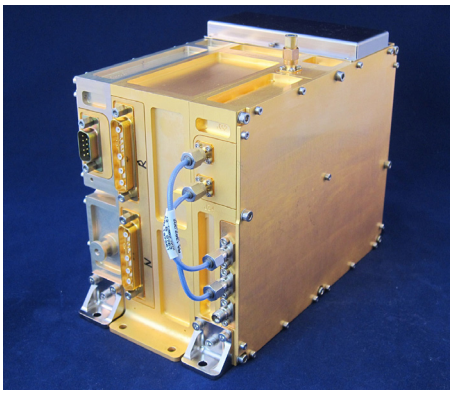

Figure 7-1: Tesat Transmitter EM

The test setup used in the measurement campaign is shown in figure 7-2 and includes a K-band TWTA (EM model) as well as a noise source and other elements, as appropriate. The tests were performed at K-band (26.25 GHz), with a 500 MBaud signal generated by the EM transmitter, amplified by the TWTA, down-mixed to IF (1.2 GHz, where noise was added), and demodulated and decoded by the receiver.

The setup was used extensively for the verification of the EM transmitter and the receiver. A minimal subset of results is reported here, for information.

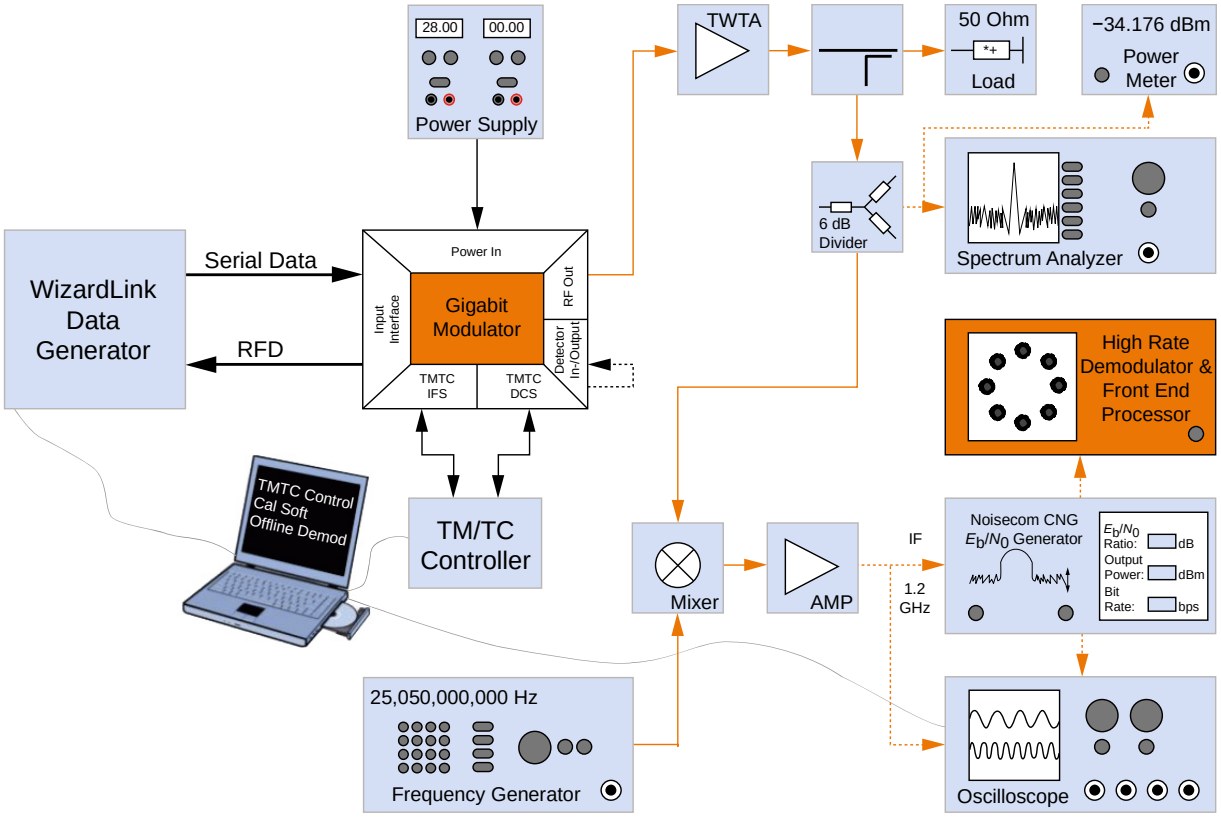

Figure 7-2: End-to-End Test Setup

A scatter plot obtained with 64APSK modulation is shown in figure 7-3, comparing the results over a linear channel (w/o TWTA) with the measurement taken with the TWTA (back-off of 2.8 dB). The modulator employed a digital pre-distortion technique with better performance than the one used for the simulations shown in the previous section.

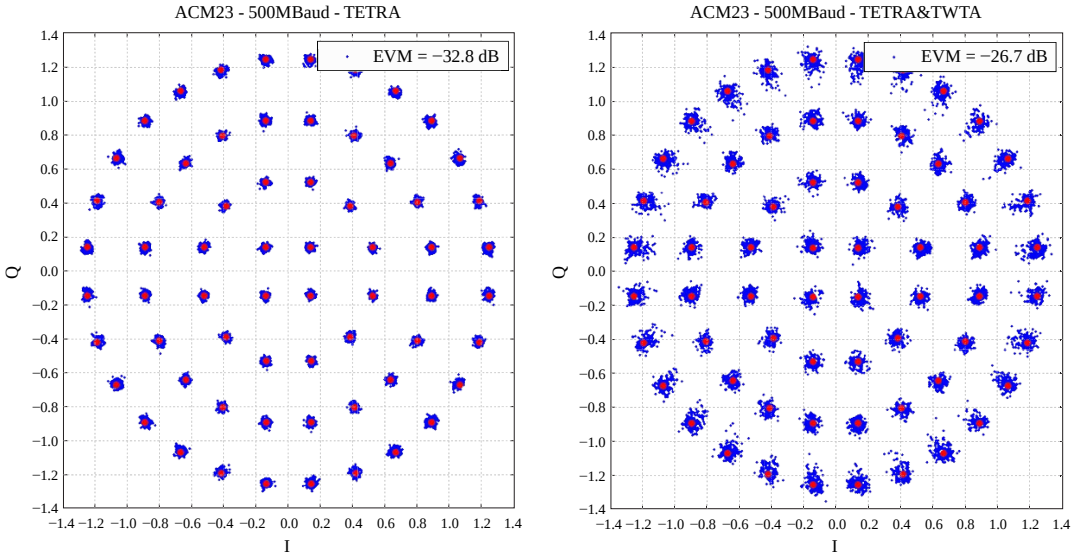

Figure 7-3: Modulator in 64APSK Mode, without TWTA (Left-Side) and with TWTA (2.8 dB Back-Off)

The modulator phase noise was measured in different configurations (e.g., central frequencies) always resulting lower than 1 deg rms when integrated between 10 kHz and 250 MHz. As an example, a snapshot of the phase noise measurement taken for a central frequency of 26.25 GHz is shown in figure 7-4.

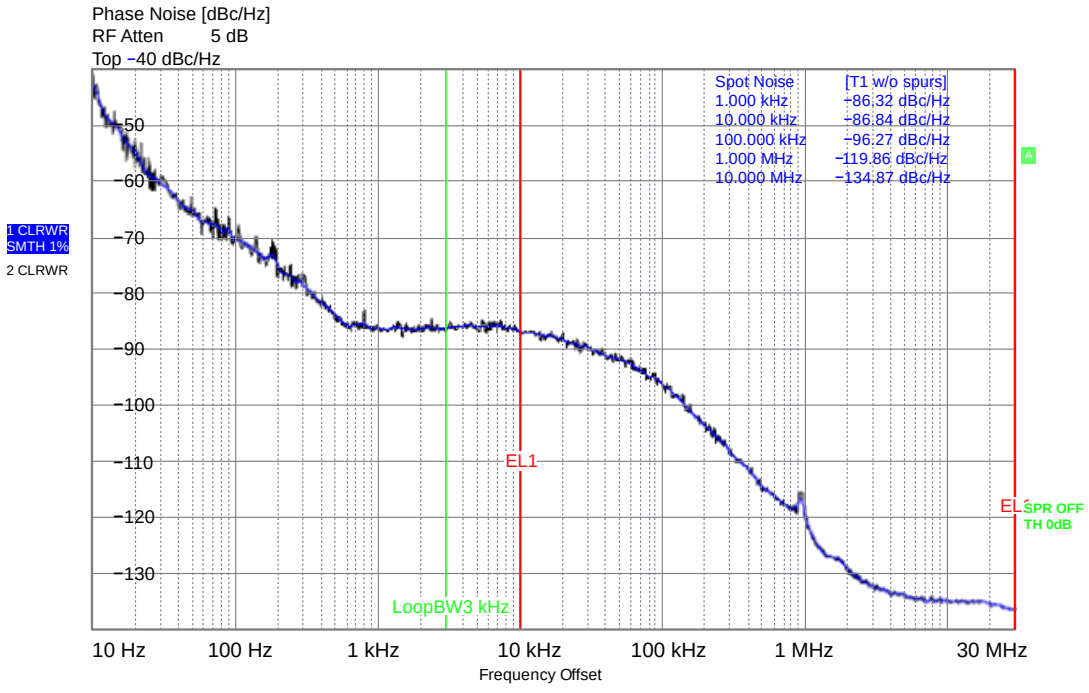

Figure 7-4: Modulator Phase Noise (26.25 GHz, Ambient)

BER measurement results are shown in figure 7-5, where one ModCod for each modulation order is included, with channel symbol rate set at 500 MBaud. Different back-off values are used for the different modulations, with a maximum of 2.8 dB for the 64APSK case.

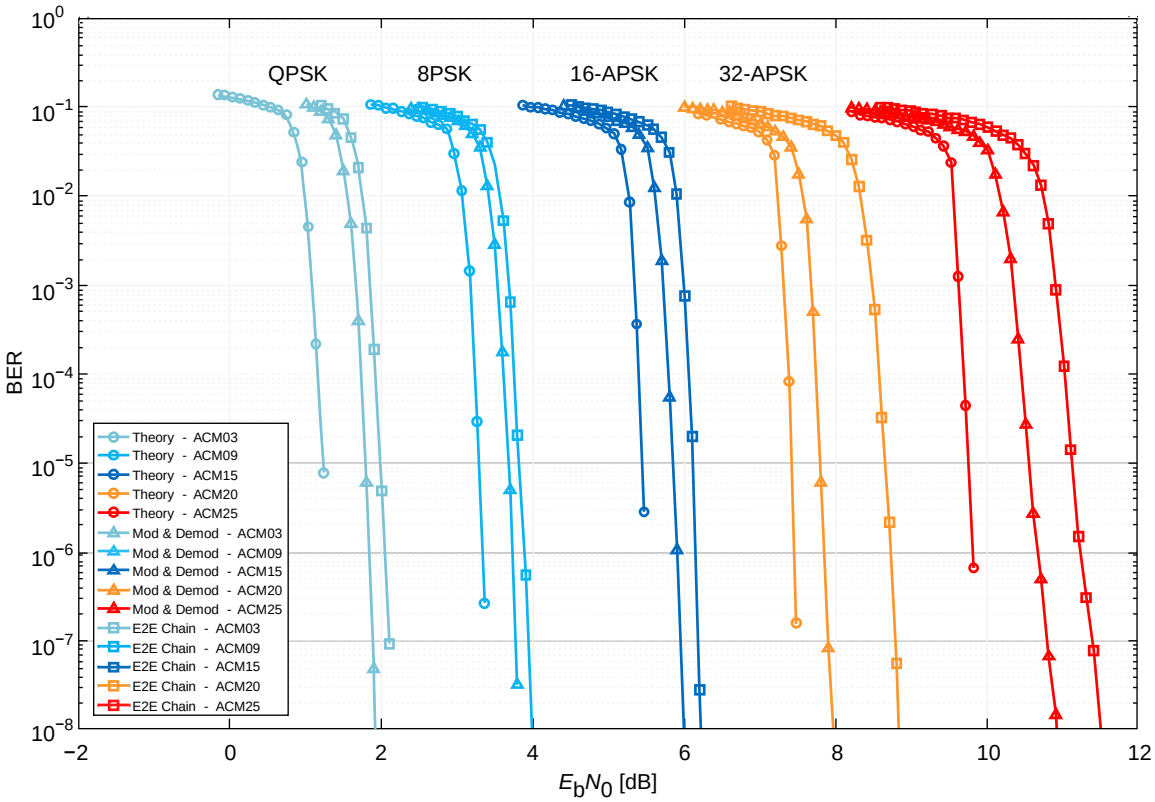

Figure 7-5: BER Performance

Reference results[5] (without impairments other than Gaussian noise) are compared with the actual measurement taken with or without the TWTA in the chain. The latter case shows the overall (transmitter/receiver) implementation losses as well as the impact of phase noise and other imbalances, while the former shows the degradation introduced by the non-linear amplification (the back-off should be added to this to obtain the total degradation, as in previous section).

[5] Tesat proprietary simulation model.

8 CONCLUSIONS

This Report provided additional informative material for reference [1].

Section 2 covered a tutorial overview of CCSDS specification in reference [1] with a description of the main functions and parameters.

Section 3 assessed the performance of the recommended codes and modulations by means of BER/CER curves on the AWGN channel, assuming ideal synchronization.

Section 4 provided the performance of the recommended codes and modulations in presence of a nonlinear distortions, aimed at modelling nonlinear effects due to amplification. A preliminary optimization of the IBO/OBO and assessment of occupied bandwidth (99 percent of the signal power) were carried out and performance reported by means of BER/CER curves. The same section also showed that pre-distortion at the transmitter can noticeably improve the performance for those ACM formats using APSK modulations.

Section 5 focused on the synchronization for the recommended codes and modulations. A possible synchronization chain was provided and performance evaluated on the linear AWGN channel in presence of phase noise, Doppler shift, and Doppler rate. The section showed that synchronization can be achieved with a loss less than 0.4 dB with respect to AWGN results.

Finally, section 6 provided performance of the full chain (end-to-end) when the channel is nonlinear, as in section 4, and the synchronization chain adopted is the one in section 5. The section showed that in the absence of pre-distortion, the AM/PM effect can impair the phase synchronization, causing huge performance losses on the ACM formats using APSK modulations (especially 64APSK). Differently, if pre-distortion at the transmitter was adopted, the performance analysis showed on the nonlinear channel a loss (worst case) limited to 1 dB with respect to ideal synchronization. Hence the use of pre-distortion at the transmitter appeared mandatory. As a validation of the simulation campaign, section 7 reported a subset of the results obtained with an extensive test campaign performed for the performance validation of one transmitter model and one receiver developed under ESA contracts.

ANNEX A

FLL TUNING FOR THE REFERENCE RECEIVER

This annex shows the detailed analysis that has been carried out for tuning the FLL presented in 5.7; the linearized model of which is shown again, for the reader's convenience, in figure A-1.

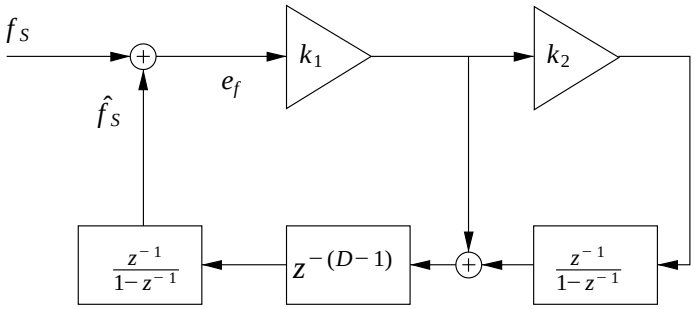

Figure A-1: Linearized Scheme of the Adopted FLL

The FLL has been first tested considering $k_2 = 0$, that is, a FLL of the first type, to see if the residual frequency error due to Doppler rate is still acceptable. As mentioned, the FLL operates in near noise-free conditions; hence, when considering a FLL of the first type, the coefficient k_1 can be selected as the value providing the best convergence and stability. This can be easily done by means of the root locus, as shown in figure A-2, where it is shown that for $k_1 \in [0,0.25]$, the roots are real and they provide a damped convergence, while for $k_1 \in [0.25,1.0)$, the roots are a complex conjugate, and the response is undamped. Figure A-3 shows exactly this behavior when the FLL with FFT-based frequency detector is simulated for the ACM format 1 at low SNR ($E_s/N_0 = -0.9$ dB, that is, $E_b/N_0 = 0.6$ dB for ACM format 1). Hence for tuning the first-type FLL, $k_1 = 0.2$ was selected.

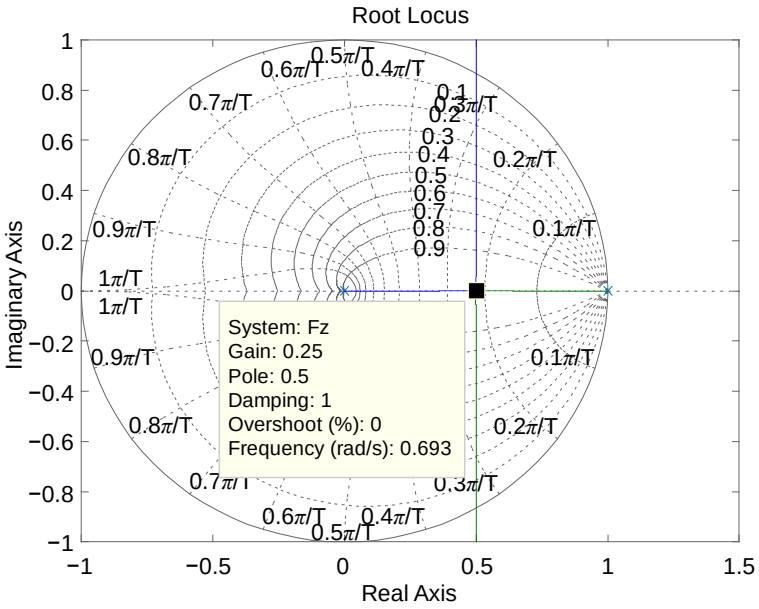

Figure A-2: Root Locus for the First-Type FLL

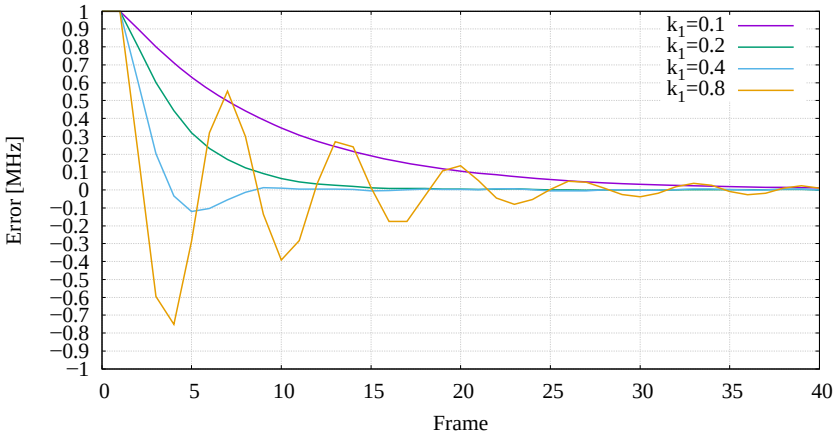

Figure A-3: Simulated Frequency Error Convergence at $E_s/N_0 = -0.9$ dB ($E_b/N_0 = 0.6$ dB for ACM1)

Once the FLL first-type has been tuned, the residual error due to Doppler rate is assessed. It can be shown that for this FLL the error is given by

$$e_f = \frac{f_{\mathrm{R}}}{k_1 R_{\mathrm{FM}}} \quad ,$$

where R_{FM} is the number of FM per second, that is, $R_{\mathrm{FM}} = \mathrm{R_{chs}}/133760$ (when using pilot fields), and f_{R} is the Doppler rate. Hence, when considering a Doppler rate (worst case) of 50 kHz/s, and channel symbol rate $\mathrm{R_{chs}} = 100$ MBaud, it holds that the residual error e_f when using a FLL of the first type is

$$e_f < 334.4 \text{ Hz}.$$

Normally this could require the use of second-type FLL. However, the adopted phase estimator (see 5.6), because of the linear interpolation, can correct a residual frequency error as long as this is under the maximum slope of the linear interpolation. As already discussed, the linear interpolation is able to interpolate a maximum phase variation of ±π over 540 channel symbols. Hence the maximum residual frequency error acceptable at the phase synchronizer is given by

$$\frac{1}{2\pi} \cdot \frac{\pi R_{chs}}{540} = 92.6 \text{ kHz}.$$

It should be noted that this value is well above the residual error e_f = 334.4 Hz, meaning that a first-type FLL with k_1 = 0.2 and k_2 = 0 is sufficient for the considered scenarios.

As further proof, simulations of the full synchronization chain were done for checking the maximum acceptable Doppler rate. Figure A-4 shows the measured residual frequency error as a function of the time (reported as PL frame number) at E_s/N_0 = −0.9 dB, when using a triangular Doppler profile (see 5.2) with Doppler shift f_D = 1 MHz and increasing Doppler rate f_R. For comparison, the figure also shows the maximum residual frequency error by the phase synchronizer that has been formulated as 92.6 kHz. From the figure, it can be seen that Doppler rates even up to 7 MHz/s are well inside the theoretical limit, whereas only Doppler rate values as high as 12 MHz/s could cause a loss of synchronization. This has been confirmed by means of CER curves, as shown in figures A-5 and A-6 for ACM formats 1 and 27, respectively.

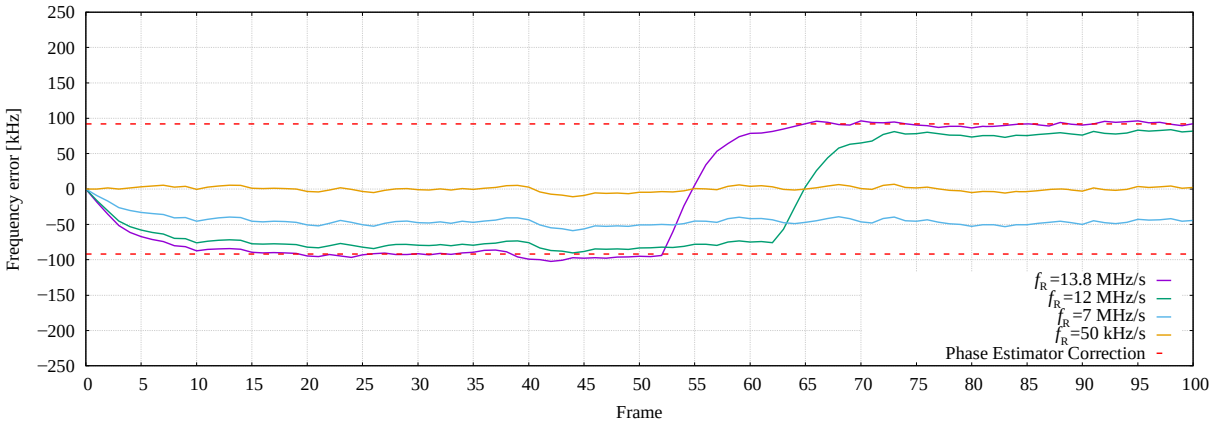

Figure A-4: Frequency Error Convergence for First-Type FLL (k_1 = 0.2), at E_s/N_0=−0.9 dB, and Triangular Doppler Profile with f_D = 1 MHz and Increasing Doppler Rate f_R

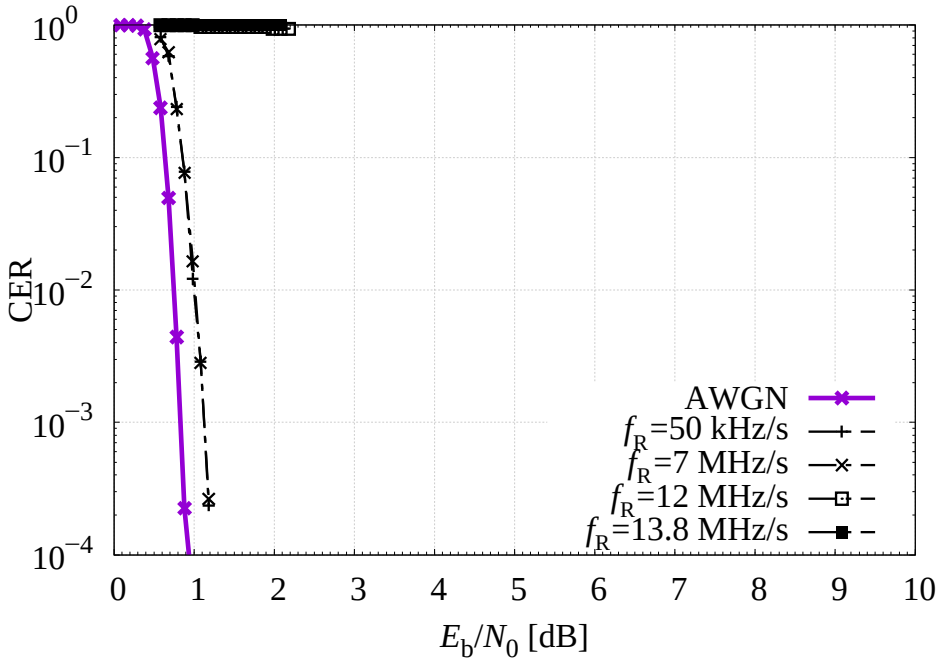

Figure A-5: CER for ACM Format 1, Triangular Doppler Profile with f_D = 1 MHz and Increasing Doppler Rate f_R, First-Type FLL (k_1 = 0.2)

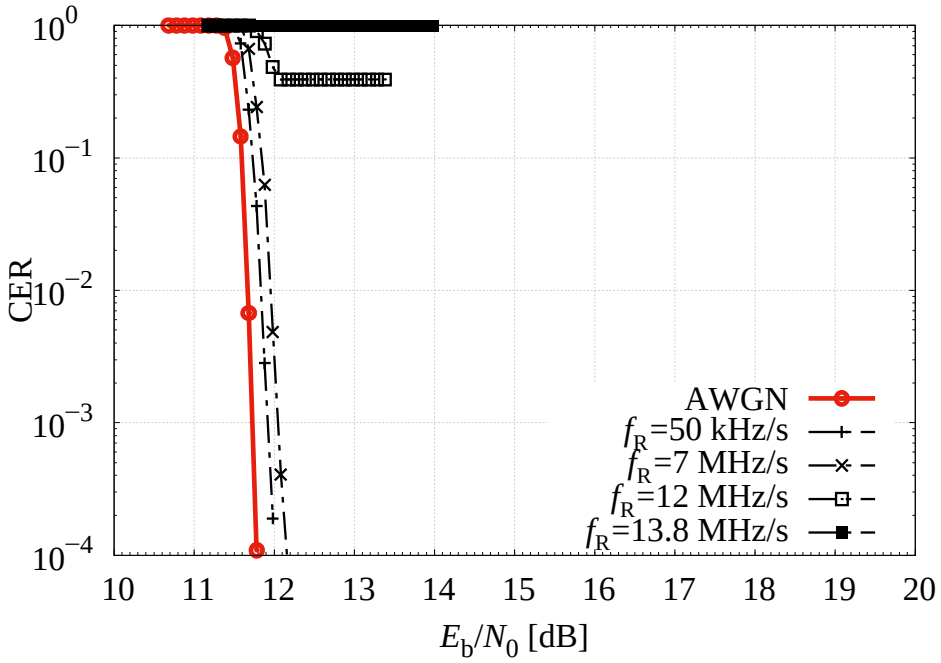

Figure A-6: CER for ACM Format 27, Triangular Doppler Profile with f_D = 1 MHz and Increasing Doppler Rate f_R, First-Type FLL (k_1 = 0.2)

The simulation has also been repeated with the sinusoidal Doppler profile (see 5.2) with Doppler shift f_D = 1 MHz and increasing Doppler rate f_R, and results are shown in figures A-7, A-8, and A-9. It can be seen that similar a conclusion holds.

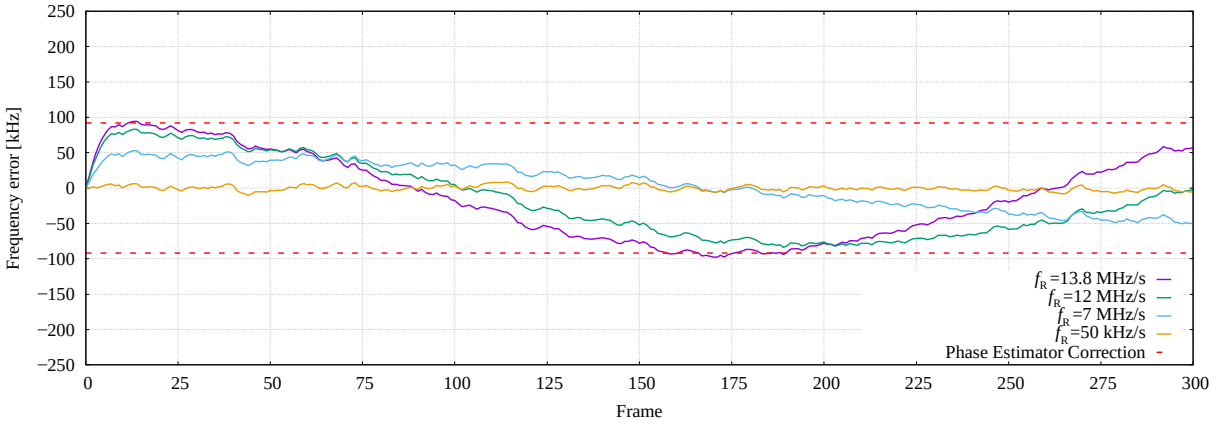

Figure A-7: Frequency Error Convergence for First-Type FLL (k_1 = 0.2), at E_s/N_0=-0.9 dB, and Sinusoidal Doppler Profile with f_D = 1 MHz and Increasing Doppler Rate f_R

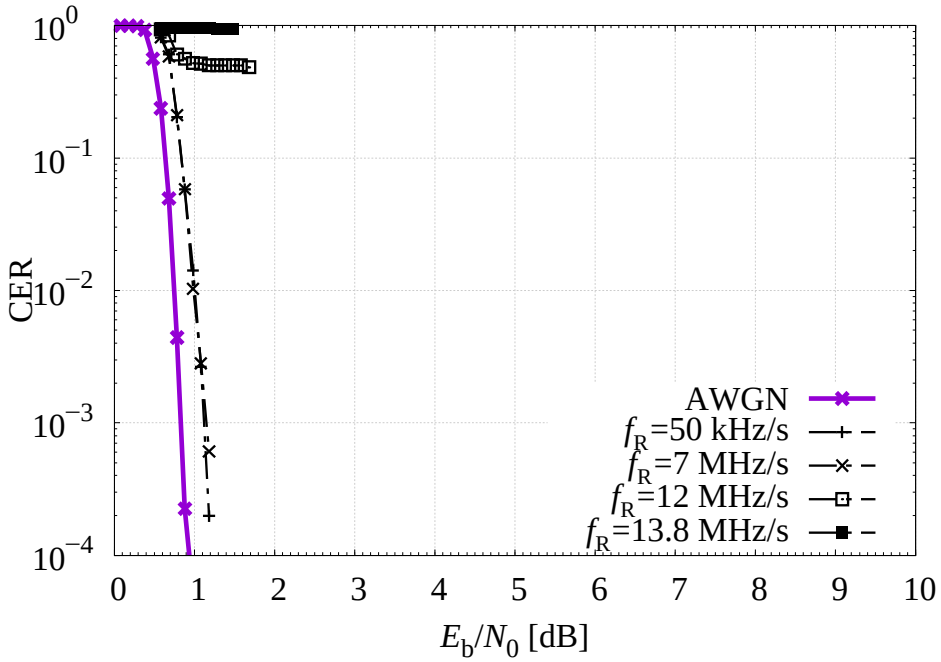

Figure A-8: CER for ACM Format 1, Sinusoidal Doppler Profile with f_D = 1 MHz and Increasing Doppler Rate f_R, First-Type FLL (k_1 = 0.2)

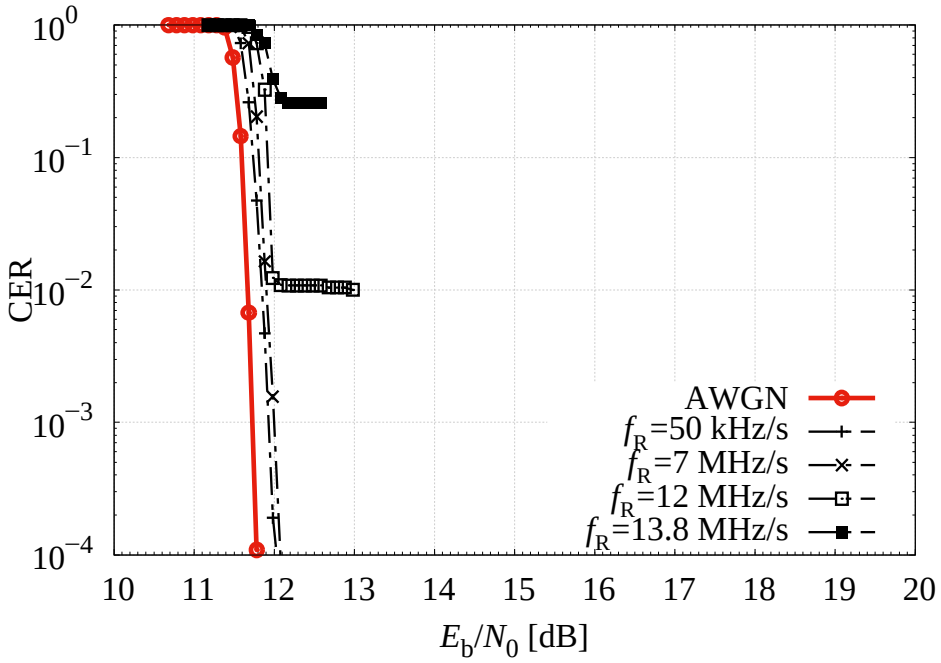

Figure A-9: CER for ACM Format 27, Sinusoidal Doppler Profile with f_D = 1 MHz and Increasing Doppler Rate f_R, First-Type FLL (k_1 = 0.2)

As a final cross-check (reported for reader's reference), simulation by using a second-type FLL has also been carried out. Figure A-10 shows the measured residual frequency error as function of the time (reported as PL frame number) at $E_s/N_0 = -0.9$ dB when using a sinusoidal Doppler profile, while figures A-11 and A-12 show the corresponding CER curves. It can be seen that the use of a second-type FLL, as expected, decreases the residual frequency error due to the Doppler rate improving resilience, although this improvement is not required for the considered scenarios.

In conclusion, it has been found analytically and by simulations that for the considered scenarios, a first-type FLL is more than sufficient, even in the presence of a Doppler rate of 50 kHz/s. This is possible thanks to the adopted phase synchronizer that is able to correct residual frequency errors well above the maximum residual error estimated for the adopted FLL.

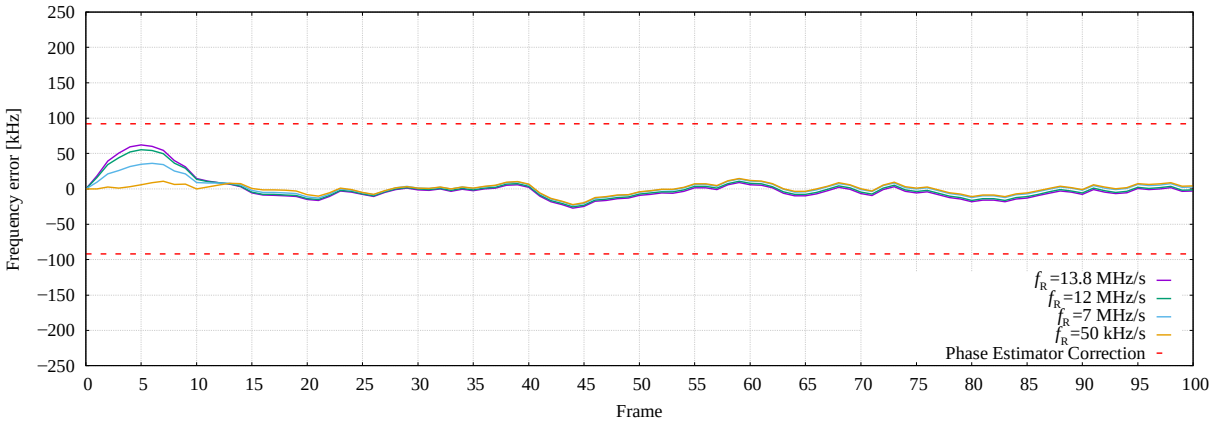

Figure A-10: Frequency Error Convergence for Second-Type FLL (k_1 = 0.32, k_2 = 0.16), at E_s/N_0=−0.9 dB, and Sinusoidal Doppler Profile with f_D = 1 MHz and Increasing Doppler Rate f_R

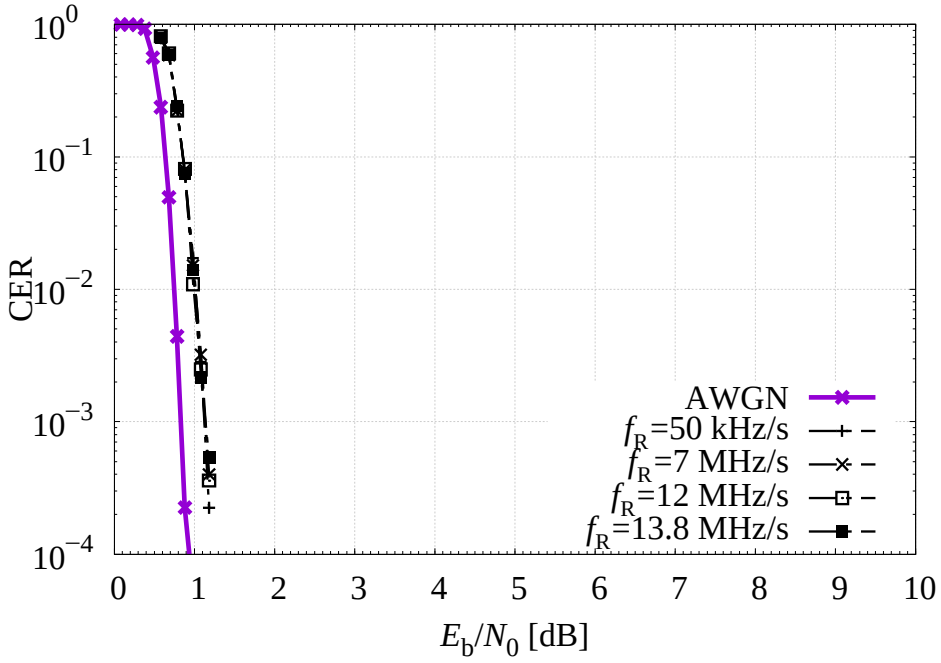

Figure A-11: CER for ACM Format 1, Sinusoidal Doppler Profile with f_D = 1 MHz and Increasing Doppler Rate f_R, Second-Type FLL (k_1 = 0.32, k_2 = 0.16)

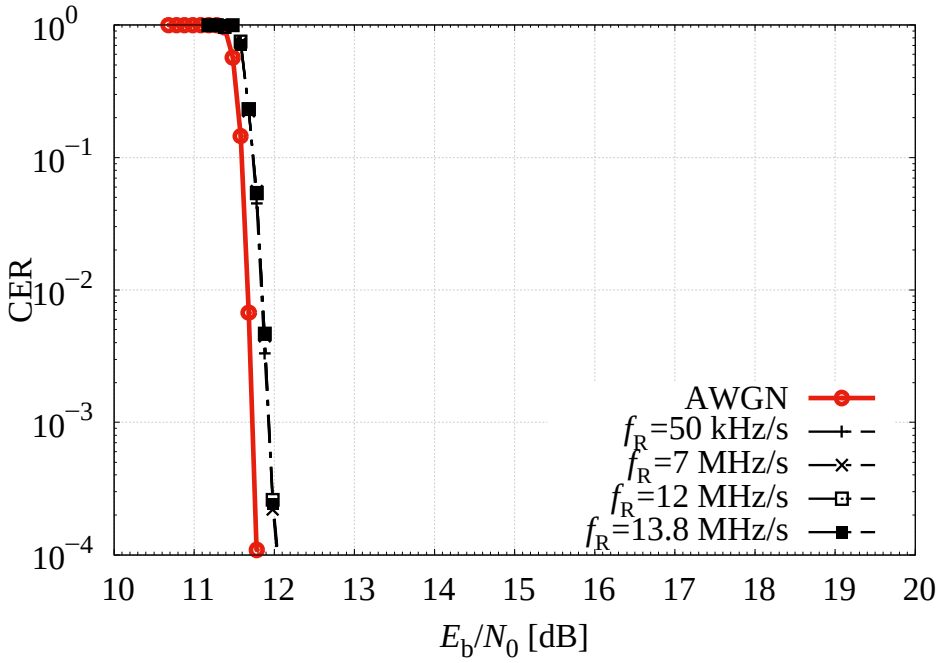

Figure A-12: CER for ACM Format 27, Sinusoidal Doppler Profile with f_D = 1 MHz and Increasing Doppler Rate f_R, Second-Type FLL (k_1 = 0.32, k_2 = 0.16)

ANNEX B

ABBREVIATIONS AND ACRONYMS

Term	Meaning
ACM	adaptive coding and modulation
AOS	Advanced Orbiting Systems (space data link protocol)
APSK	amplitude phase shift keying
ASM	attached synchronization marker
AWGN	additive white Gaussian noise
BER	bit error rate
BPSK	binary phase shift keying
CER	codeword error rate
DAGC	digital automatic gain control
DVB-S2	Digital Video Broadcasting—Second Generation
EESS	Earth Exploration Satellite Service
FD	frame descriptor
FER	frame error rate
FFT	fast Fourier transform
FLL	frequency locked loop
FM	frame marker
IBO	input back-off
LLR	log-likelihood ratio
ML	maximum likelihood
OBO	output back-off
PL	Physical Layer

PLL	phase-locked loop
PSK	phase shift keying
QPSK	quadrature phase shift keying
SCCC	serial concatenated convolutional code
SMTF	synch marked transfer frame
SNR	signal-to-noise ratio
SRRC	square root raised cosine
TD	total degradation
TWTA	traveling wave tube amplifier